U.PORTO
FEUP FACULDADE DE ENGENHARIA
UNIVERSIDADE DO PORTO

SEISMIC ANALYSIS OF A STEEL ARCH BRIDGE USING THE PUSHOVER METHOD

MARYANA BEREZYAK

Dissertação submetida para satisfação parcial dos requisitos do grau de

MESTRE EM ENGENHARIA CIVIL — ESPECIALIZAÇÃO EM ESTRUTURAS

Orientador: Elsa de Sá Caetano

Coorientador: Rafael Cabral (PEDELTA)

JUNHO DE 2019

MESTRADO INTEGRADO EM ENGENHARIA CIVIL 2018/2019

DEPARTAMENTO DE ENGENHARIA CIVIL

Tel. +351-22-508 1901

Fax +351-22-508 1446

✉ miec@fe.up.pt

Editado por

FACULDADE DE ENGENHARIA DA UNIVERSIDADE DO PORTO

Rua Dr. Roberto Frias

4200-465 PORTO

Portugal

Tel. +351-22-508 1400

Fax +351-22-508 1440

✉ feup@fe.up.pt

🌐 http://www.fe.up.pt

Reproduções parciais deste documento serão autorizadas na condição que seja mencionado o Autor e feita referência a *Mestrado Integrado em Engenharia Civil - 2018/2019 - Departamento de Engenharia Civil, Faculdade de Engenharia da Universidade do Porto, Porto, Portugal, 2019*.

As opiniões e informações incluídas neste documento representam unicamente o ponto de vista do respetivo Autor, não podendo o Editor aceitar qualquer responsabilidade legal ou outra em relação a erros ou omissões que possam existir.

Este documento foi produzido a partir de versão eletrónica fornecida pelo respetivo Autor.

Aos meus avós,

"A good plan violently executed now is better than a perfect plan executed next week."

George S. Patton

AGRADECIMENTOS

A todos os professores que conheci durante estes 5 anos que mostraram um amor profundo e dedicação total ao trabalho que desenvolvem no dia-a-dia. Agradeço pela disponibilidade, simpatia e dedicação.

À Professora Elsa Caetano, minha orientadora, a oportunidade de desenvolver uma tese no meio empresarial, sem esquecer a revisão atenta da tese.

Agradeço a empresa PEDELTA, onde realizei a tese, pela simpatia e disponibilização de informações fulcrais ao desenrolar desta tese.

Ao Rafael Cabral, meu coorientador e engenheiro na PEDELTA, pelo todo apoio, disponibilidade, interesse, paciência e ajuda que foram essenciais para o bom desenvolvimento da tese.

Aos Professores Miguel Castro e Humberto Varum, pela disponibilidade para esclarecer as dúvidas que surgiram no desenrolar da tese e interesse em ajudar.

A empresa BENTLEY pela disponibilização do software RM Bridge para fins educativos e ao seu apoio técnico, especialmente ao Afshin Hatami e Jeff Kroon.

Aos amigos e colegas que durante este percurso estiveram comigo.

À Olga Vyshynska pela amizade contínua, independentemente da distância.

Reservo um especial agradecimento à Humberto Lopes, por todo o apoio, motivação e carinho ao longo destes anos.

Por último, tenho de agradecer aos meus pais, meu irmão e aos meus avós, por todo apoio, sem os quais nada disto seria possível.

Muito obrigada!

ABSTRACT

Arch bridges are among the first to be built and their use has been continuous up to this day. There are bridges that date back to the 8th century BC and that continue operational until today, resisting time and the increase of loads that they have to withstand. Essentially, arch bridges can be divided in three types, according to the relative position of the deck. In this analysis, specific attention will be given to the upper deck arch, since it is the one corresponding to the case study.

The occurrence of natural phenomena, such as an earthquake, has encouraged their study and a continuous search for a better understanding of the response and behavior of the structures when subjected to these phenomena, in order to improve the design of the structures and guarantee the protection of human lives.

The methodologies used in the seismic design vary as to whether the nonlinearity of the materials is considered and can be static or dynamic. From these methodologies, the non-linear static analysis (pushover) will be put into practice in the case of a bridge study located in Guatemala. The remaining analyzes (fundamental mode method, response spectrum method and time history) will be briefly described in order to identify the main differences.

For the pushover analysis, different methodologies are presented: EC-N2, FEMA440-Capacity Spectrum Method and FEMA 440- Displacement Coefficient Method.

The modeling of the structure is presented, using RM Bridge software (Bentley). Other aspects associated to the analysis are explored, such as the modeling of the inelastic behavior of structural elements, mass and static load pattern adopted.

The ductile capacity of the structure will be analyzed in the form of the capacity curve, which reproduces the variation of deformability with the increment of lateral load, exploring the behavior of the structure. From this plot, conclusions will be drawn regarding the possible oversizing of the structure.

With the response spectrum, defined according to the Guatemala regulation, and the capacity curve, the performance point and the performance level of the structure are obtained. In addition, adequacy of the behavior factor adopted in the project is analyzed.

Finally, three complementary analysis will be carried out, in order to verify the influence of the seismic importance category and the cross-section dimensions in the structural performance. The last analysis is developed in order to study the capacity curve.

KEYWORDS: Arch Bridge, Earthquake, Pushover, Guatemala, RM Bridge.

RESUMO

As pontes em arco foram das primeiras a serem construídas e a sua utilização tem sido efetuada correntemente até aos dias de hoje. Existem pontes que datam ao século VIII a.C. e que continuam em funcionamento até aos dias hoje resistindo ao tempo e ao aumento das cargas que se tem verificado. Essencialmente, existem três tipos de ponte em arco, que se diferenciam pela posição relativa do tabuleiro. Nesta dissertação, será estudada uma ponte em arco com tabuleiro superior.

A ocorrência de fenómenos naturais, como é o caso do sismo, impulsionou o estudo dos mesmos e uma busca contínua por uma melhor compreensão da resposta e do comportamento das estruturas quando sujeitas a estes fenómenos com o objetivo de melhorar o projeto das estruturas e garantir a proteção das vidas humanas.

As metodologias empregues no dimensionamento sísmico variam quanto à consideração ou não da não linearidade dos materiais, podendo ser divididas em metodologias estáticas e dinâmicas. Na presente dissertação será realizada uma análise não linear estática (pushover) de uma ponte em arco a construir na Guatemala, a qual constitui o caso de estudo. As restantes análises (análise por forças laterais, modal por espetro resposta e dinâmica temporal não linear) serão descritas brevemente de modo a identificar as principais diferenças.

Para a análise pushover, diferentes metodologias são apresentadas: EC-N2, FEMA440- Capacity Spectrum Method and FEMA 440- Displacement Coefficient Method.

A capacidade dúctil da estrutura é então expressa sob a forma da curva de capacidade, que reproduz a variação de deformabilidade com o incremento da carga lateral, explorando o comportamento da estrutura. A partir deste traçado são tiradas conclusões quanto à possível sobreresistência da estrutura.

Com o espetro de resposta, definido de acordo com o regulamento de Guatemala, e a curva de capacidade é obtido o "performance point" e o nível de desempenho da estrutura. Adicionalmente, procede-se a avaliação da adequabilidade do coeficiente de comportamento adotado no projeto.

Por fim, são realizadas três análises complementares de modo a identificar a influência da classe de importância sísmica e da secção no desempenho da estrutura. A terceira análise visa estudar a curva de capacidade.

PALAVRAS-CHAVE: Ponte em Arco, Sismo, Pushover, Guatemala, RM Bridge.

INDEX

Agradecimentos i
Abstract iii
Resumo v
1. INTRODUCTION 1
1.1. Preamble 1
1.2. Objectives 1
1.3. Thesis Outline 2
2. INTRODUCTORY NOTE ARCH 3
2.1.Arch Bridge - History 6
2.2. Arch bridge – Structural Behavior 11
2.2.1. FORM AND FUNCTION 12
2.2.1.1 Position of the Deck 12
2.2.1.2 Structural Form 13
2.2.1.3 Slenderness 14
2.2.2 CONCEPTUAL DESIGN AND CONSTRUCTION ELEMENTS 16
2.2.2.1 Load Paths 16
2.2.2.2 Imposed Deformations 17
2.2.2.3 Asymmetric loads 18
2.2.2.4 Concentrated Loads 19
2.2.3 CONSTRUCTION 19
2.2.3.1 Centring 19
2.2.3.2 Successive cantilever advance method 24
2.2.3.3 Lowering Method 27
3. INTRODUCTORY NOTE EARTHQUAKE 31
3.1 Types of Analysis 35
3.1.1 ELASTIC ANALYSIS 35
3.1.2 NONLINEAR ANALYSIS 36
3.2 Earthquake Ground Motion 37
3.2.1 RESPONSE SPECTRA 37
3.2.1.1 Elastic Response Spectrum 37
3.2.1.2 Elastic Design Spectrum 38
3.2.1.3 Inelastic Response Spectrum 39
3.3 Nonlinear Static Analysis – Pushover Analysis 40
3.3.1 LATERAL LOAD 41

3.3.2 NONLINEAR STATIC SEISMIC ANALYSIS- METHODOLOGIE PROPOSED IN FEMA440 42
3.3.2.1 Capacity Spectrum Method (Equivalent Linearization) 42
3.3.2.2 Coefficient Method 50
3.3.3 THE N2 METHOD 51
3.3.3.1 Definition of the Capacity Curve 54
3.3.3.2Target Displacement Calculation 54
4. CASE STUDY 61
4.1 Geological and Geotechnical Environment 62
4.2 Seismicity of the Zone 63
4.3 Structural Solution 64
4.3.1 SUPERSTRUCTURE 64
4.3.2 SUBSTRUCTURE AND FOUNDATIONS 65
4.3.3 MATERIALS 66
5 MODELING 67
5.1 Quantification of Structure Weight 70
5.1.1 SLAB WEIGHT 70
5.1.2 SUBSTRUCTURE WEIGHT 71
5.1.3 DECK WEIGHT 71
5.1.4 REMAINING ELEMENTS 72
5.1.5 LIVE LOAD 73
5.2 Verification of the Model 76
5.3 Obtaining Natural Modes and Frequencies 82
5.3 Response Spectra 84
5.3.1 RESPONSE SPECTRUM OBTAINED FROM STRUCTURAL SAFETY RULES OF GUATEMALA (NSE 2 DE AGIES) 84
5.3.2 EN1998-1: 2004 SPECTRUM 87
5.3.3 BEHAVIOUR COEFFICIENT 89
6. NONLINEAR ANALYSIS PUSHOVER 91
6.1 Classification of cross-sections 91
6.2 Non-linear behavior of material 92
6.2.1 MODELING OF NON-LINEAR BEHAVIOR 96
6.2.2 GEOMETRIC NONLINEAR EFFECTS 96
6.3 Calculation Example with a Cantilever Beam 97

6.4 Pushover Analysis of the Case Study 100

6.4.1 CAPACITY CURVE 101

6.4.2 PERFORMANCE POINT 111

6.4.2.1 Modal Displacement 111

6.4.2.2 Uniform Displacement 113

6.4.2.3 Comparison of the pushover analysis results. 115

6.4.3 BEHAVIOUR FACTOR/RESPONSE MODIFICATION FACTOR 116

6.4.4 ANALYSIS OF A STRUCTURE CONSIDERING DIFFERENT IMPORTANCE CATEGORY 118

6.4.5 ANALYSIS OF A STRUCTURE WITH REDUCED SECTION 122

6.4.6 ANALYSIS OF A STRUCTURE IN ORDER TO ANALYZE THE CAPACITY CURVE 128

7 CONCLUSIONS 131

7.1 Discussion 131

7.2 Recommendations for Future Developments 132

References 133

ANNEX A - CALCULATING T_{eff} and β_{eff} (FEMA 440)

ANNEX B-SIMPLIFIED EQUATIONS FOR CALCULATING T_{eff} and β_{eff} (FEMA 440)

ANNEX C – SPECIFIC RULES FOR THE PUSHOVER ANALYSIS OF BRIDGES (EUROCODE EN 1998-2:2005)

ANNEX D – TRANSFORMATION OF THE RESPONSE SPECTRUM IN THE FORMAT (SA, T) TO FORMAT (SA, SD).

ANNEX E – INELASTIC RESPONSE SPECTRUM FOR THE CANTILEVER EXAMPLE

ANNEX F – MANUAL CLASSIFICATION OF THE SECTION ACCORDINGLY TO EN 1993-1-1:2005

ANNEX G – MODIFICATION OF THE MATERIAL CURVE TAKING INTO ACCOUNT LOCAL BUCKLING

ANNEX H – CALCULATION OF COMPOSED STRESSES USING - VON MISES

ANNEX I –REPRESENTATION OF MOMENT CURVATURE FOR THE ORIGINAL CASE STUDY

ANNEX J– PERFORMANCE POINT OF A STRUCTURE CONSIDERING DIFFERENT CLASS (UNIFORM DISTRIBUTION)

ANNEX K – PERFORMANCE POINT OF A STRUCTURE CONSIDERING REDUCED SECTION (MODAL AND UNIFORM DISTRIBUTION)

INDEX OF FIGURES

Figure 2.1 Aqueduct Águas Livres (Lisbon) [2]. ... 3
Figure 2. 2 Lleida Pedestrian Footbridge in Lleida (Spain) [4] ... 4
Figure 2. 3 Double skin tubular arch bridge [6]. ... 5
Figure 2. 4 3D-printed bridge in Shanghai [7]. ... 6
Figure 2. 5 3D-printing of components [7]. ... 6
Figure 2. 6 Arkadiko Bridge (1300-1190 BC) [8]. ... 7
Figure 2. 7 Arch Bridge Trajano (Chaves,Portugal) [10]. ... 7
Figure 2. 8 Bridge in Turkey (VIII b.c) [8]. ... 8
Figure 2. 9 Danhe Bridge (China) [11]. ... 8
Figure 2. 10 First metal bridge (Coalbrookdale, England) [8]. ... 9
Figure 2. 11 Craigellechie Bridge (Scotland) [12]. ... 9
Figure 2. 12 Bridge d´lena [8]. ... 10
Figure 2. 13 Plougastel Bridge (France) [3]. ... 10
Figure 2. 14 Arrábida Bridge (Porto, Portugal) [9]. ... 11
Figure 2. 15 Cracked section and structural analysis of the dome of Saints Peter´s [13]. ... 11
Figure 2. 16 Upper deck bridge- The Garabit Viaduct (France) [15]. ... 12
Figure 2. 17 NYC's Hell Gate Bridge [16]. ... 13
Figure 2. 18 River Usk Crossing (Newport) [17]. ... 13
Figure 2. 19 Structural forms for arches [14]. ... 14
Figure 2. 20 Comparison of internal forces taking into account slenderness [18]. ... 15
Figure 2. 21 "Static coefficient" of world arch bridges with long spans [9]. ... 15
Figure 2. 22 Ideal form for an arch, depending on the loads [14]. ... 16
Figure 2. 23 Normal compression force in a parabolic arch that is pinned at both ends and subject to uniform vertical load [14]. ... 17
Figure 2. 24 Internal forces due imposed deformations (arch fixed at both ends, pinned at both ends and three pinned arch) [18]. ... 17
Figure 2. 25 Effect of symmetric and asymmetric uniform loads on deformation, normal force, and bending moment [14]. ... 18
Figure 2. 26 Influence of the stiffness of the arch relative to that of the deck, for symmetric uniform load [14]. ... 18
Figure 2. 27 Maria Pia Bridge- Portugal, 160 m span (designed by Théophile Seyrig and built by Gustave Eiffel) [3]. ... 19
Figure 2. 28 Timber centring for stone arches from the book by M.Gauthey. ... 20
Figure 2. 29 High-speed train Beipanjiang Bridge- China (445 m span,2016) [9]. ... 20
Figure 2. 30 Albert Louppe Bridge - France (3 spans of 186 m, 1930) [19]. ... 21
Figure 2. 31 Bridge over river Cávado (1954) [20]. ... 21
Figure 2. 32 Centring of Foz do Sousa Bridge (1950) [21]. ... 22
Figure 2. 33 Detail of a bridge support [21]. ... 22
Figure 2. 34 Central scaffolding in the three Guaira Viaducts – Venezuela [22]. ... 23
Figure 2. 35 Arrábida Bridge (Porto) [8]. ... 23
Figure 2. 36 Closing of scaffolding with the central part [8]. ... 23
Figure 2. 37 St. Louis Bridge (The Eads Bridge) construction [3]. ... 24
Figure 2. 38 Sydney Harbour Bridge (503 m span) [3]. ... 25
Figure 2. 39 Construction of foundations (arch supports and piers) [23]. ... 25
Figure 2. 40 Construction of the deck and arch [23]. ... 26
Figure 2. 41 Launching method for deck construction [8]. ... 26
Figure 2. 42 Ballast in order to reduce asymmetry of loads [8]. ... 27

Figure 2. 43 Lussia Footbridge [25]. 27
Figure 2. 44 Construction process of the Bridge over the Tagus River in the Alcántara [26]. 28
Figure 2. 45 All the construction phases of the Bridge over the river Tagus at Alcántara [26]. 29

Figure 3. 1 Major earthquakes and advances that resulted from them [27]. 32
Figure 3.2 Example of unseated span due to insufficient support length and superstructure damage due to inadequate load path [27]. 33
Figure 3. 3 Example of pier damage due to lack of ductile detailing and structural damage due to ground Failure [27]. 33
Figure 3. 4 The road map for the seismic design of a bridge [27]. 35
Figure 3.5 Calculation of Design Force Level [27] 36
Figure 3. 6 Response spectrum of an elastic structural system [29]. 38
Figure 3. 7 Project-specific acceleration response spectra for the California Sonoma Creek Bridge [29]. 38
Figure 3. 8 Transformation of elastic design spectrum into inelastic [29]. 39
Figure 3. 9 General flowchart for Nonlinear Static Procedure [31]. 41
Figure 3. 10 Response Spectrum Conversion [30] 43
Figure 3. 11 Capacity Curve [30]. 43
Figure 3. 12 Idealized Force-Displacement Curves [34]. 44
Figure 3. 13 Capacity Curve transformed into a Capacity Spectrum [30]. 45
Figure 3.14 Equal Displacement Approximation [30]. 45
Figure 3.15 Bilinear representation of capacity spectrum [32]. 46
Figure 3.16 Bilinear representation of capacity spectrum [32]. 47
Figure 3.17 Modified acceleration-displacement response spectrum (MADRS) for use with secant period, Tsec [32]. 48
Figure 3.18 Bilinear representation of capacity spectrum [32]. 49
Figure 3. 19 Locus of possible performance points using MADRS [32]. 49
Figure 3.20 Idealized force-displacement curve for nonlinear static analysis [32]. 50
Figure 3.21 Cross-section and representation of a cantilever in software RM Bridge. 52
Figure 3.22 Pushover representation. 53
Figure 3. 23 Elastic response spectrum used for the cantilever beam example. 53
Figure 3. 24 Capacity curve obtained for the cantilever beam example. 54
Figure 3.25 Idealized bilinear force-displacement curve [33]. 55
Figure 3.26 Short Period Range [33]. 57
Figure 3. 27Medium and Long Period [33]. 58
Figure 3. 28 Calculation of target displacement (EN). 59

Figure 4.1 Bridge No.6 location (Google Earth), Google Earth. 61
Figure 4. 2 Geological map of the zone where the Bridge No.6 will be built (Red Point), National Geographic Institute. 62
Figure 4.3 Open Drillings (Wells), PEDELTA. 63
Figure 4. 4 Seismic zones in the Republic of Guatemala [35]. 63
Figure 4. 5 Bridge elevation view, PEDELTA. 64
Figure 4. 6 Typical Section of the Deck, PEDELTA. 65
Figure 4.7 Pier Section, PEDELTA. 65
Figure 4. 8 Transverse Section of an Arch, PEDELTA. 65
Figure 4. 9 Location of the transverse section in the arch, PEDELTA. 66
Figure 4. 10 Foundation plan-view of arch start, PEDELTA. 66

Figure 5.1 3-D View of the Model, RM BRIDGE. 67
Figure 5.2 Frontal View of the Model, RM BRIDGE. 67
Figure 5.3 Modelled foundation with SAP2000. 68
Figure 5. 4 Permanent Load of Slab, RM BRIDGE. 71
Figure 5.5 Permanent Load of the Substructure (Arch, Transverse Beam, Pier), RM BRIDGE. 71
Figure 5. 6 Permanent Load of the Deck, RM BRIDGE. 72
Figure 5. 7 Permanent Load (SIDL), RM BRIDGE. 72
Figure 5. 8 Multiple Presence Factors,m. (AASHTO 3.6.1.1.2-1) 73
Figure 5. 9 Characteristics of the Design Truck. (AASHTO 3.6.1.2.2-1). 73
Figure 5. 10 Characteristics of the special permit vehicle (NSE Guatemala). 74
Figure 5. 11 Dynamic Load Allowance. 74
Figure 5. 12 Live Load- Design Truck, RM BRIDGE. 75
Figure 5. 13 Live Load-Lane Load, RM BRIDGE. 75
Figure 5. 14 Deflected structure due to uniform permanent load (15.83 kN/m). 76
Figure 5. 15 Deflected structure due to antisymmetric load (15.83 kN/m). 77
Figure 5. 16 Deflected structure due load at the ends of structure (15.83 kN/m). 77
Figure 5. 17 Support reactions due to permanent load, 15.83kN/m. (Arch nº1). 78
Figure 5. 18 Support reactions due to permanent load, 15.83kN/m. (Arch nº2). 78
Figure 5. 19 Moments Mz due to permanent loads (deck load=15.83 kN/m). 78
Figure 5.20 Moments Mz due to antisymmetric load (15.83 kN/m) 79
Figure 5. 21 Moments Mz due to loads at the ends of the structure (15.83 kN/m) 80
Figure 5. 22 Forces Nx due to permanent load (15.83 kN/m) 80
Figure 5. 23 Stresses in the arch. 81
Figure 5. 24 Mode 1, f=0.801. 83
Figure 5. 25 Mode 4, f=1.311. 83
Figure 5. 26 Seismic zoning of Guatemala [27]. 84
Figure 5. 27 Site coefficient Fa [35]. 85
Figure 5. 28 Site coefficient Fv [35]. 85
Figure 5. 29 Response Spectrum made accordingly with Guatemalan Regulations (NSE 2 DE AGIES). 86
Figure 5. 30 Response Spectrum EN for the case study. 87
Figure 5. 31 Response Spectrum (Guatemala vs EN). 88
Figure 5. 32 Response Spectrum taking into account change in Tc. (Representing Guatemalan vs EN) 88

Figure 6. 1 Material curve for steel. 92
Figure 6. 2 Material curve (Arch-Section 4-4). 94
Figure 6. 3 Material curve (SHS650*25.4). 95
Figure 6. 4 Idealized models of beam-column elements [38]. 96
Figure 6. 5 Cantilever case study. 97
Figure 6.6 Virtual deformation of the structure. 97
Figure 6. 7 Capacity curve obtained in RM Bridge for a steel cantilever (IPE-200). 98
Figure 6. 8 Capacity Curve obtained in RM Bridge for the concrete cantilever example. 98
Figure 6. 9 Performance point obtained in RM Bridge for the concrete cantilever example. 99
Figure 6. 10 Load Combinations and Load Factors (AASHTO LRFD, 2014-3-14). 101
Figure 6.11 Modal shape load distribution for the case study. 102

Figure 6. 12 Lateral modal shape load distribution for the case study. 102
Figure 6. 13 Uniform load distribution for the case study. 102
Figure 6. 14 Capacity curve obtained for the modal shape distribution. 103
Figure 6. 15 Capacity curve obtained for the uniform shape distribution. 103
Figure 6.16 Comparation between two capacity curves for the uniform and modal shape distribution. 104
Figure 6. 17 Change in Stiffness (Blue-Modal, Orange-Uniform) 104
Figure 6. 18 Identification of elements in the normal stresses diagram. 105
Figure 6. 19 Normal stresses for the modal load distribution in step 53. 106
Figure 6. 20 Normal stresses for the uniform load pattern and step 25. 106
Figure 6. 21 Force in the abutments (modal distribution). 107
Figure 6. 22 Normal stresses (modal distribution, last increment). 107
Figure 6. 23 Representation of normal stresses (modal distribution, last increment). 108
Figure 6. 24 Normal stresses (uniform distribution, last increment). 108
Figure 6. 25 Representation of normal stresses (uniform distribution, last increment). 109
Figure 6. 26 Moment-curvature relation for arch (right and left, last iteration). 110
Figure 6. 27 Moment-curvature curve for the outer pier (right side pier-blue and left side-green)..... 110
Figure 6. 28 Moment-curvature for the transverse beam situated near foundation. 111
Figure 6. 29 Performance point (EC-N2) for the modal distribution. 112
Figure 6. 30 Performance point (FEMA 440-Equivalent Linearization) for the modal distribution. 112
Figure 6. 31 Performance point (FEMA 440- Displacement modification) for the modal distribution. 113
Figure 6. 32 Performance point (Uniform load, EC-N2) for the uniform distribution. 113
Figure 6. 33 Performance point (Uniform load, FEMA 440-Equivalent Linearization) for the uniform distribution. 114
Figure 6.34 Performance point (Uniform load, FEMA 440- Displacement modification) for the uniform distribution. 114
Figure 6. 35 Capacity curve and representation of behavior factor. 116
Figure 6. 36 Capacity curve and representation of the correspondent forces. 117
Figure 6. 37 Minimum level of seismic protection and probability of design earthquake [35]. 118
Figure 6. 38 New Response Spectrum made accordingly with Guatemalan Regulations for the case considering different importance category (essential). 119
Figure 6. 39 Response Spectrum (EN) for the case considering different importance category (essential). 119
Figure 6. 40 Performance point (Modal distribution-EC N2) for the case considering different importance category (essential). 120
Figure 6. 41 Performance point (Modal distribution-FEMA 440 Equivalent Linearization) for the case considering different importance category (essential). 120
Figure 6. 42 Performance point (Modal distribution -FEMA 440- Displacement modification) for the case considering different importance category (essential). 121
Figure 6. 43 Capacity curve for the reduced section scenario (modal). 123
Figure 6. 44 Capacity curve for the reduced section scenario (uniform). 123
Figure 6. 45 Comparison between capacity curves in original case and in the case with reduced section. 124
Figure 6. 46 Performance point (EC-N2- modal distribution) for the reduced section scenario..... 125
Figure 6. 47 Performance point (EC-N2 - uniform distribution) for the reduced section scenario. 125
Figure 6. 48 Detail extracted from the Figure 6.45. 126
Figure 6. 49 Comparison between the capacity curve obtained for the original case and for the case with free abutments. 128

Figure 6. 50 Change in stiffness in the original case and in the case with free abutments. 129

Figure 7. 1 Localization of the performance point (case study) accordingly to performance level [30]. 131

INDEX OF TABLES

Table 3. 1 Response spectrum data. 53
Table 3. 2 First Iteration in order to calculate displacement target. 59
Table 3. 3 Third iteration in order to calculate displacement target. 59

Table 5.1 Characteristics of the profiles in the deck. 69
Table 5. 2 Equivalent Profile used in model. 69
Table 5. 3 Eigenvalue analysis results. 82
Table 5. 4 Information used for the transformation of Guatemalan spectrum into spectrum accordingly to EN. 87
Table 5. 5 Information used for the transformation nº2 to spectrum accordingly to EN (Tc=0.4 s). 88

Table 6. 2 Classification of three representative sections according to EN 1993-1-1:2005 table 5.2… 92
Table 6. 3 Classification of three representative sections according to EN 1993-1-1:2005 table 5.2… 92
Table 6.4 Data obtained from Pushover (RM Bridge) for the concrete cantilever example. 99
Table 6.5 Main results from the two analysis (modal and uniform load distribution). 115
Table 6. 6 Information used for the transformation to equivalent response spectrum. 119
Table 6. 7 Main results for the modal and uniform distribution for the case with different class of the structure (essential). 122
Table 6. 8 Sections in the original case. 122
Table 6. 9 Change of the section in the structure. 122
Table 6. 10 Change of the sections in the structure. 123
Table 6. 11 Main results for the modal and uniform distribution for the reduced section scenario. 127
Table 6. 12 Sections used for the analysis of a structure in order to analyse the capacity curve. 128

1. INTRODUCTION

1.1. PREAMBLE

Bridges are perhaps some of the most emblematic structures that have been built. Through their main function of connecting civilizations and communities, they impelled their development and, in some cities, became iconic images. This is the case, for example, of Porto, with the bridge D. Luís, or Venice with the Rialto Bridge.

One of the major concerns of today's society is the preservation of human life and, consequently, the integrity of the structures sustaining them.

As such, due to the great importance of bridges, it is essential to ensure that they can resist seismic actions, absorbing the energy that is transmitted through the ground without collapsing and allowing damages to be easily repaired.

Seismic design underwent a great evolution over time. Currently, there are different analysis methodologies that differ in the consideration of the nonlinearity of the material and on the static or dynamic approach.

Non-linear static analysis using pushover curves has become an increasingly used tool in seismic study and adopted in design offices. Its goal is to evaluate the resistant capacity of the structure for a certain level of desired performance of the structure, performing a non-linear static analysis.

Essentially, pushover analysis consists of "pushing" the structure up to a target displacement, using for that purpose, a uniformly distributed load or a load proportional to the first mode of vibration, considering the nonlinear material behavior of the structural elements.

1.2. OBJECTIVES

In this dissertation, the goal is to understand the behavior of an arch bridge under seismic loads using a pushover analysis. For this purpose, it is necessary to learn and understand this kind of analysis, and identify the potentialities of pushover analysis as well as possible limitations.

The case study is an arch bridge - designed by PEDELTA for construction in Guatemala City.

In addition, Bentley's RM Bridge software was studied, and its advantages and limitations identified.

Finally, it is intended to conclude on the behavior of the structure, its level of performance for the design seismic event and ascertain its behavior factor.

1.3. THESIS OUTLINE

This dissertation is organized in seven chapters. The first chapter presents an introduction to arch bridges and seismic engineering and the definition of the main objectives to be fulfilled in the development of this thesis.

In chapter 2, arch bridges are presented, and their history and their structural behavior described, the form, function and constructive method.

In the third chapter, different types of analyses (elastic and nonlinear analysis) to deal with the seismic action are presented, in particular the non-linear static analysis.

In Chapter 4, a description of the case study is made, in terms of the adopted structural solution for the superstructure and substructure, and the geographic, seismic and geological-geotechnical contextualization of Guatemala City.

Based on the information from chapter 4, chapter 5 describes the numerical model of the bridge, including a discussion on the mass, a modal analysis and the construction of the response spectrum.

In the 6th chapter, the pushover analysis is carried out with the modeling of the nonlinearities of the materials, obtaining the capacity curve and the performance point for the design seismic event. These results are analyzed and discussed. In addition, two variants of the analysis are presented, which consist of a spectrum modification and section reduction. The behavior factor is also described in this chapter.

Finally, Chapter 7 summarizes the conclusions that have been drawn from the developed studies and suggestions are proposed for future developments in this area.

2.
INTRODUCTORY NOTE ARCH

According to the Cambridge dictionary, a bridge is: "*a structure that is built over a river or road so that people can go across it*" [1]. It connects the roadways when there is a separation and withstands different kinds of loading, starting with its self-weight, and, during its service lifetime, traffic loads, wind loads and, possibly, an earthquake. There are many different types of bridges and which to use depends on the environment, ground conditions, aesthetics, price and many other variables. A bridge not only serves to carry the traffic load but can also serve for the passage of water pipes or canals. As an example, the Águas Livres Aqueduct in Lisbon, represented in the fig.2.1, with its pointed arches achieving a 28-metres span and 65-metres high piers.

Figure 2.1 Aqueduct Águas Livres (Lisbon) [2].

The construction of a bridge is not an individual process, it involves people from different professions. Starting with the designers and finishing with those who manually build it, they all contribute to make an idea real. The design includes organization and formalization of the bridge, calculations and everything that incorporates it. The construction process must be taken in account a priori during the design phase.

Depending on the function and surroundings, the material, typology, construction process and cross section of a bridge is chosen. The way bridges are built, and which materials are used have advanced much to the present day, which allows us to build bigger bridges with a more aesthetic and lighter design. Safety in construction is also a point with a high importance nowadays.

There are mainly four types of materials that have been used in bridge construction, some more than others. Stone and timber, natural materials as they are obtained from nature and don't need special treatment besides shaping, were used in the first period of bridge construction. Timber bridges are hard to find nowadays as the material is really vulnerable to fire and river floods. On the other side, a stone bridge is made of durable material, and there are many examples in all parts of the world, some of them still in service. In the second period appeared a new artificial material, cast iron that was an authentic revolution in bridges. Cast iron progressed to steel, stronger and with better mechanical properties. Concrete, an artificial material, appeared at the end of nineteenth century and gave rise to the reinforced concrete, junction between iron and concrete. This system permitted the construction of arch bridges with bigger spans. Later, the introduction of prestressed concrete permitted to achieve longer spans [3].

Nowadays, other materials are being studied and there are attempts to apply them, like the aluminum, glass-fiber reinforced plastic (GFRP) and others.

Lleida pedestrian footbridge, represented in the fig.2.2, is a tied-arch bridge with a span of 32 m and 6.2 rise crossing the Madrid—Barcelona high-speed rail link. The bridge was designed by the Spanish engineering company PEDELTA and entirely made out of GFRP (except the joints). The material was chosen because it is light and easy to transport and also as electrical insulator, eliminating magnetic interference with the electrified railway. The bridge was assembled lineside and lifted into position by crane in 3 hours. It was open in 2001 and it´s completely functional until today [4].

Figure 2. 2 Lleida Pedestrian Footbridge in Lleida (Spain) [4]

This year 2019, the WIBE Prize *("The award, attributed by a Jury made up of renowned Engineers from entities of the utmost importance in the world of Bridge Engineering, distinguishes the greatest contribution to innovation in this area on a global level."* [5]) was attributed to an Australian team that proposed a novel bridge system for durable, low cost and rapid construction.

This system is a hybrid double skin tubular arch bridge, represented in fig.2.3, with an outer tube of fiber reinforced polymer (FRP), an inner steel tube, and a layer of concrete filled between them.

This bridge is sustainable, lightweight, durable, low cost and of fast construction [6].

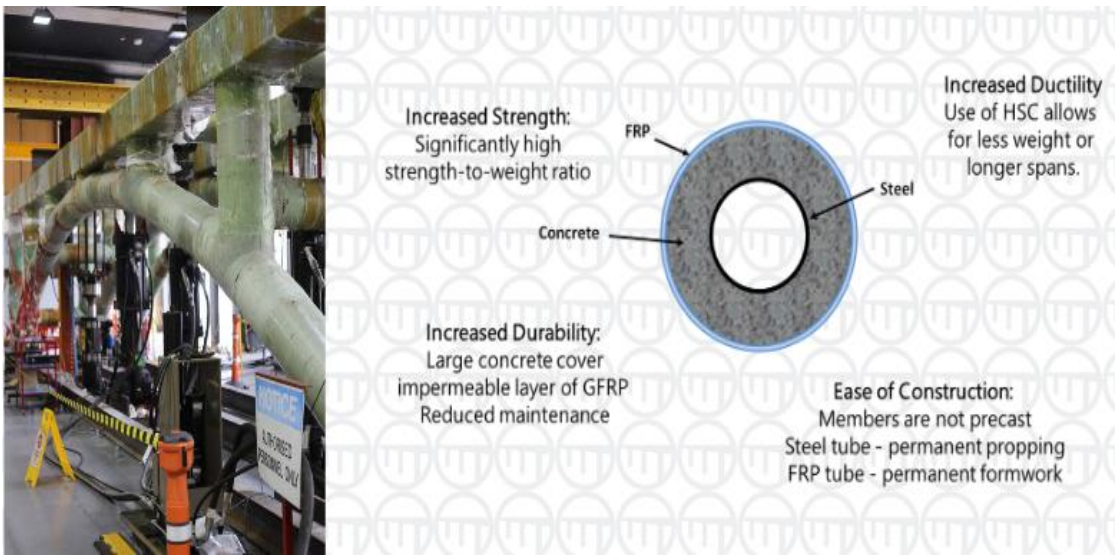

Figure 2. 3 Double skin tubular arch bridge [6].

There is a new wave and completely innovative process in the construction of bridges that is through the use of 3D printing, fig.2.4-2.5. It is not very popularized, but it is evolving and there already exist real examples of its application, in concrete and steel. A 3D-printed concrete pedestrian arch bridge has been completed in Shanghai. The bridge with a span of 26.3 meters includes 44 hollowed-out 3D printed concrete units, while the handrails are divided into 68 units. The bridge was built using composite materials, containing polyethylene fiber concrete to match the structural performance of conventional materials [7].

Figure 2. 4 3D-printed bridge in Shanghai [7].

Figure 2. 5 3D-printing of components [7].

Arch bridges can reach a span between 100-400m for the concrete ones and 530 m for the metallic ones. Spans between 80 and 200 m are usually more frequent and competitive compared to other structural forms.

2.1. ARCH BRIDGE - HISTORY

Arch bridges play a large role in the history of bridges. They were first built in stone by the Sumerians and the Egyptians, but it was the Romans who massified the construction of bridges using the stone as a result of the needs and opportunities of maintaining an empire. The Romans developed several techniques, such as the addition of lime and pozzolana, which prevented the disintegration of mortar when exposed to water, developed a record of incidents and accidents that were stored in Rome and the technique of the wood cofferdams filled with clay what allowed constructing in watercourses [8].

They were built to last as permanent constructions and immortalize the names of ones that have built them. Many stone bridges are still standing, and most are in service withstanding the passage of time and increase in loads due to the evolution. Nowadays, stone bridges are no longer being built.

The oldest bridge, according to several sources, that has survived to the present day is located in Ancient Greece, Arkadiko Bridge, ca. 1300-1190 BC and represented in fig.2.6.

Figure 2. 6 Arkadiko Bridge (1300-1190 BC) [8].

The Roman bridges were mostly semicircular (fig.2.7); it is in the age of the Renaissance that the bridges with arches more slaughtered appeared, ogives. This type of arch bridges are not so effective carrying the bridge´s loads as the semicircular one because its shape doesn't match the load antifunicular polygon. However, considering that a stone bridge is heavy, the bending moments that appears on the arc are not high enough to generate some kind of problem [9].

During this time, the technique to construct stone arch remained practically unchanged. There are some architectural variations in them; we can speak about Roman, Romanesque, Gothic, Renaissance and Baroque arch bridges. These variations are mostly formal.

Figure 2. 7 Arch Bridge Trajano (Chaves,Portugal) [10].

In the fig.2.8 is represented the Bridge over the Meles River, Turkey. This bridge with only one arch is the oldest one that is still in service. VIII b.c [8].

Figure 2. 8 Bridge in Turkey (VIII b.c) [8].

China continued to build stone bridges even in the second half of the twentieth century. The largest of stone arch bridges (fig.2.9) in existence till now is situated in China, the 146-m span Danhe Bridge that was open in 2001 [11].

Figure 2. 9 Danhe Bridge (China) [11].

With the Industrial Revolution in the 19th century, the railroad network emerged as a means of communication and there was a strong development of iron and steel. After this pause in the development of the bridges, the metallic bridges appear, replacing stone, and great scientific and technological advances occur.

In England, still in the eighteenth century, the Darby family built the first iron bridge over the Severn at Coalbrookdale, fig.2.10. The bridge comprises five arches of 30 m span [8].

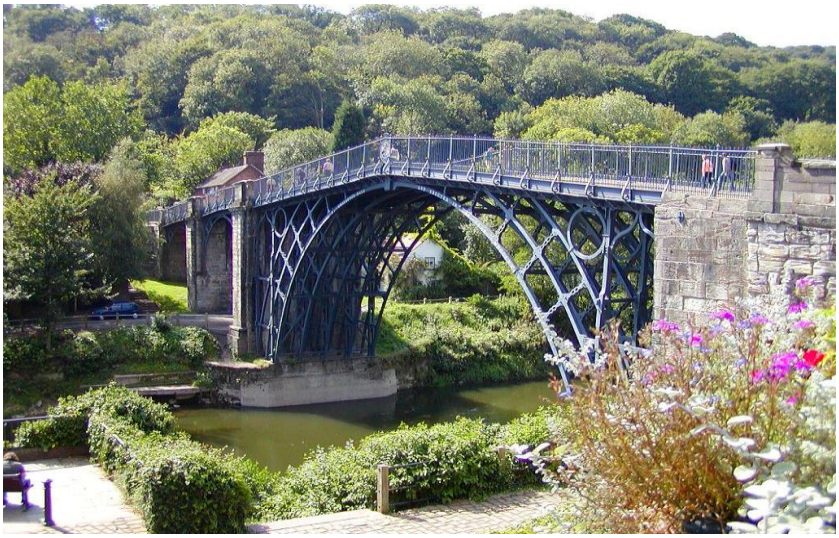

Figure 2. 10 First metal bridge (Coalbrookdale, England) [8].

Thomas Telford, British Engineer, contributed to the development of metal bridges reflecting a constant concern about aesthetic issue in all of his works, fig.2.11.

Figure 2. 11 Craigellechie Bridge (Scotland) [12].

France contributed a lot to the development of bridges. Corps des Ponts and Chaussées created by Luís XIV for maintaining the roads and bridges of the kingdom was the basis for creating the first world's top civil engineering college (*École nationale des ponts et chaussées*), in the eighteenth century. This school evidenced and contributed to the great evolution of the urban arcs in the French streets, fig.2.12 [8].

Figure 2. 12 Bridge d´lena [8].

Robert Maillart was one of the initiators of the reinforced concrete and used this material in his works leaving an extensive range of notorious bridges. Maillart had a strong technological preparation and an intuitive understanding of the bridge. The new material partially pushed metal out of the way for small and medium sized spans. The first concrete bridges were arches because it was a material suited to resisting compression forces, although the cost of large arch centering is too expensive the use of this material in this type of arch was temporarily discontinued. However, new construction systems as cantilever methods appeared avoiding the use of centering and turning this material a valid solution for medium and large spans in arch bridges. The first bridge in concrete is situated in Souillac, France [3].

Freyssinet, representative of French engineering, who contributed as Maillart to the use and study of reinforced concrete and invented prestressed concrete, was also a great bridge builder and one of his masterpieces is the three arch, 186 m span Plougastel Bridge shown in fig.2.13.

Figure 2. 13 Plougastel Bridge (France) [3].

Portuguese Engineer Edgar Cardoso was recognized not only nationally but also internationally due to his unique and magnificent works. To illustrate this there is the Arrabida bridge (fig.2.14) that held a world record as the concrete-arch bridge with the largest span (270 m) [9].

Figure 2. 14 Arrábida Bridge (Porto, Portugal) [9].

2.2. ARCH BRIDGE – STRUCTURAL BEHAVIOR

Until the seventeenth century the understanding of an arch bridge behavior was purely intuitive. Robert Hooke was the first to study the catenary, the curve that originates when we take a flexible wire subject to its own weight, in 1675 [3]. After him, Poleni studied a crack in Rome´s dome in 1748. He divided the dome in several arches and experimentally obtained the perfect shape of a dome using flexible wire loaded with the loads proportional to their weight. With his study he concluded that vertical cracks where no harmful for the stability of a dome because they divided the dome in arches that were stable even working on their own, fig.2.15 [13].

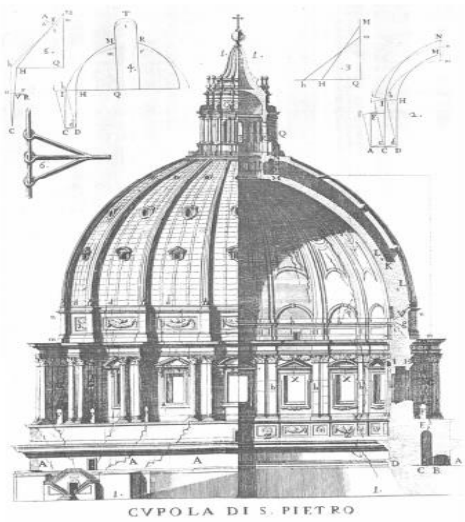

Figure 2. 15 Cracked section and structural analysis of the dome of Saints Peter´s [13].

La Hire developed the idea of funicular polygon that is a shape taken by the flexible wire subjected to a series of forces, such as self-weight or others. The ideal shape of an arch subjected to the same forces will be the antifunicular curve.

Coloumb, Bresse and Culmann contributed to the study of the arch and the last one developed elastic centre method.

Nowadays, the most used model is the computer-calculated straight bar. The arch is transformed into a linear member discretized as straight bars [3].

2.2.1. FORM AND FUNCTION

2.2.1.1 Position of the Deck

The first bridges were all built with the deck in an upper position due to the material that was used, stone or masonry. With the appearance of iron and later steel it became possible to make cable hangers that could take loads in tension, which permitted to build bridges with intermediate or lower position [14].

Which type of bridge to choose depends on local environment. Upper deck bridges are more advantageous for the mountain valleys where the bridge can be supported; for places that are plainer the option of lower deck is more suitable.

Nowadays, concrete arch bridges usually have upper deck and the metal ones intermediate or lower deck.

In the fig.2.16-2.18 are represented three type of arch bridges differing in the deck position.

Figure 2. 16 Upper deck bridge- The Garabit Viaduct (France) [15].

Figure 2. 17 NYC's Hell Gate Bridge [16].

Figure 2. 18 River Usk Crossing (Newport) [17].

2.2.1.2 Structural Form

There are 4 most usual structural forms for an arch bridge (fig.2.19). The arch can be fixed at both ends, pinned at both ends, three-pin arch or be a tied arch. Arches that have an upper deck are usually fixed at both ends because the joints are expensive and need maintenance beside the fact that they introduce great deformability. These arches have three degrees of redundancy. The indeterminate load effects are the horizontal thrust and the fixed end moments. The arches that are pinned at both ends have one degree and a three-pinned arch has no redundancy.

When we increase the redundancy, we decrease the magnitude of vertical deformation but increase the moments and forces in bending.

For all of these structural forms beside the tied arch, a large horizontal support reaction must be provided by the foundation ground that's why an arch bridge is not a frequent solution for week soils [18].

Tied arch, or bowstring arch, has a particular advantage in comparison to others because it has a tie that connects two ends of abutments what contributes to balance the horizontal support reaction and permits to choose this type of arch for weaker soils transmitting only the vertical component of axial force in the arch to the abutments [14].

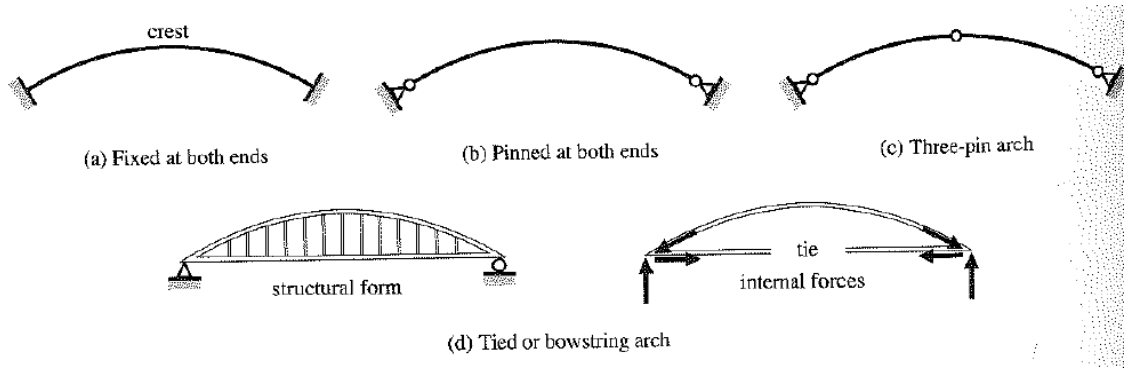

Figure 2. 19 Structural forms for arches [14].

2.2.1.3 Slenderness

The slenderness is expressed by the ratio between the total rise of the bridge (f) and the span (l). For concrete bridges with an upper deck a frequent slenderness is ¼, that produces arches with a correct geometric shape. If we decrease the rise, the arch becomes visually tenser. For metallic bridges with an upper deck we have slenderness of 1/4.8 (New River Gorge), 1/6.5 (Saikai Bridge),1/8 (Sella Arriondas Bridge).

For the bridges with intermediate or lower deck, the slenderness can vary, because the rise and the span are independent, so the design team chooses in order of resistant efficiency. Normally the slenderness is near 1/6.

It is easy to understand the importance of slenderness analyzing 4 different cases with ratio L/5, L/16, L/6,6 and L/10. All the cases have a span of 100 m and a section with variable width so the tension would be similar in the four cases. The results of this analysis for the antifunicular load, represented in fig.2.20, showed that the resultant forces are very different for each case. The forces in the case with ratio L/16 can be 16 times higher than in an arch with ratio of L/5 and this difference is identical if the structural form is an arch fixed at both ends or pinned at both ends [18].

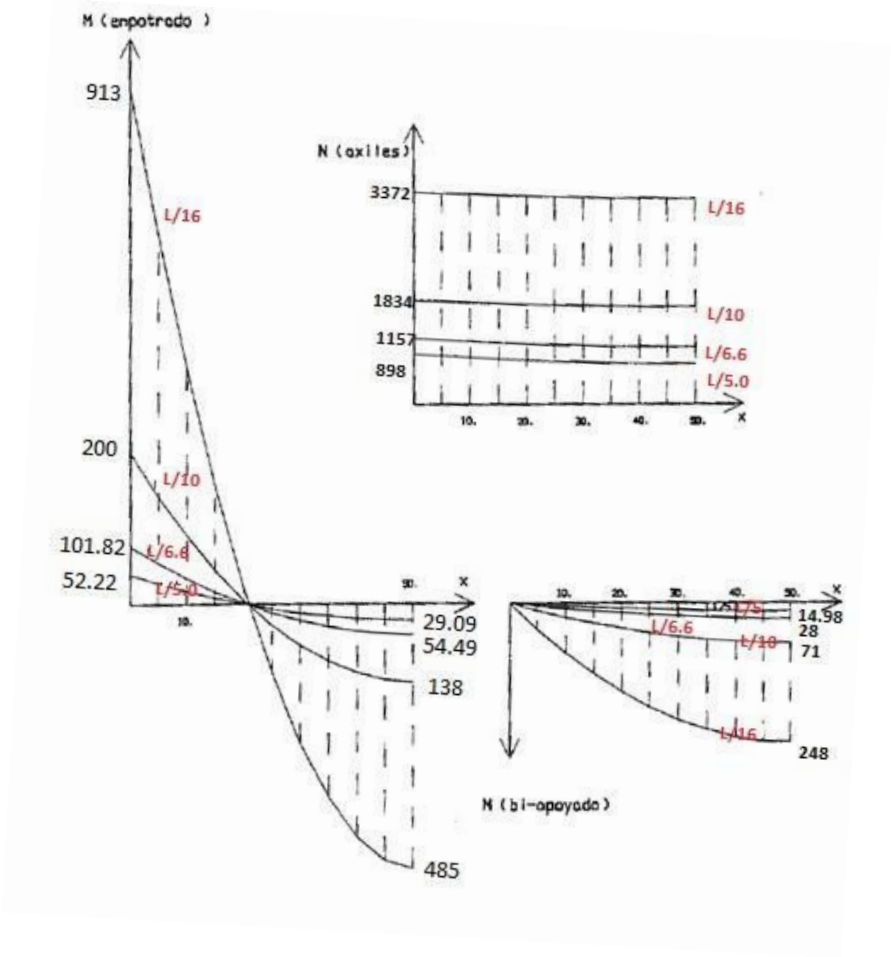

Figure 2. 20 Comparison of internal forces taking into account slenderness [18].

The Infant Henrique Bridge (fig.2.21) shows high technical and aesthetic qualities with L/f=11,2. In this bridge, the “static coefficient” (L^2/f>3000), which is directly proportional to the axial force existing at the crown of the arch, is the largest of any arch built to date (2016) [9].

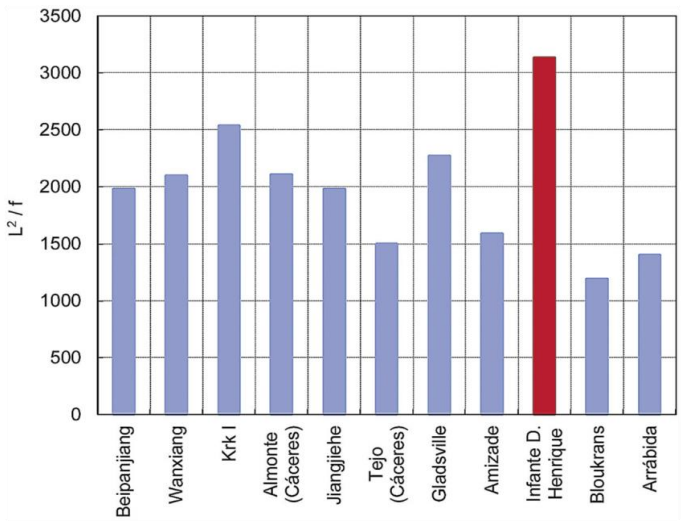

Figure 2. 21 "Static coefficient" of world arch bridges with long spans [9].

2.2.2 CONCEPTUAL DESIGN AND CONSTRUCTION ELEMENTS

2.2.2.1 Load Paths

In the bridges with an upper deck the transmission of the forces is done from the piers till the arch and then till the abutments; in the bridges with intermediate deck, forces flow through the zone of the pillars and hangers; in the arch with lower deck, the deck works in longitudinal and transversal bending to transfer the loads acting on it into the lower ends of hangers, via the cross girders and sometimes later beams. The forces are then transferred from the hangers into the arches [14].

The shape of an arch should coincide with the antifunicular curve, in other words, with the compression line that is defined by the internal forces due to the loads. In this way, we can avoid having bending in our arch. The ideal shape of an arch subjected to the uniform distributed load over a horizontal surface would be parabolic as shown in fig.2.22. For the concentrated loads at the hanger or pillar positions, the form would be polygonal. Loads that are not uniformly distributed over the arch give place to bending moments.

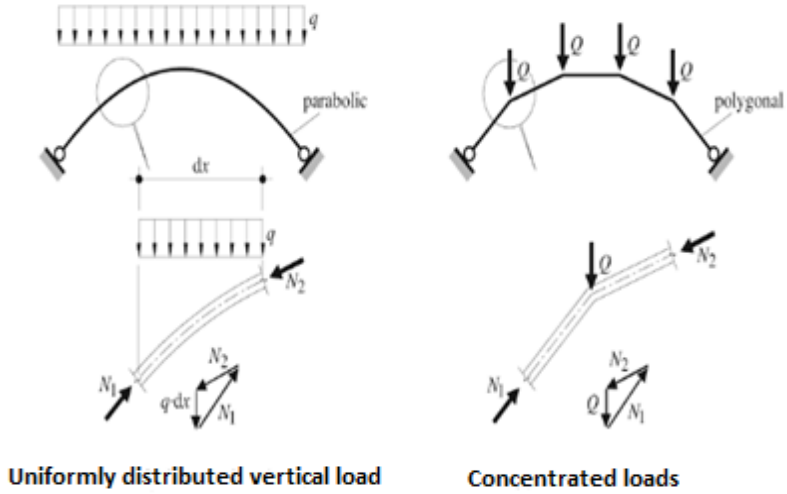

Figure 2. 22 Ideal form for an arch, depending on the loads [14].

The bending moment may be defined by the product of the normal force acting in the cross section and its eccentricity relative to the axis of the arch.

To obtain this “perfect” arch shape the most appropriate method is to the determinate the law of bending moments [14].

A parabolic arch that is pinned at both ends, of span *l* and rise *f*, is not subjected to any bending moment as a result of a load *q* that is uniformly distributed relative to the horizontal. It is exposed to a normal compressive force, which has a horizontal component H given by:

$$H = \frac{\mathrm{ql}^2}{8\mathrm{f}} \tag{1}$$

And the normal force is given by:

$$N = \frac{H}{\cos\alpha} \tag{2}$$

Where α represents the angle between the tangent to the axis of the arch and the horizontal.

Self-weight acts along its axis, not relative to the horizontal (fig.2.23), that means that the ideal shape to resist its own weight is not parabolic but rather an inverted catenary. When a bridge has other loads acting or when the phenomenon of deformation occurs, the bridge is subjected to bending moments.

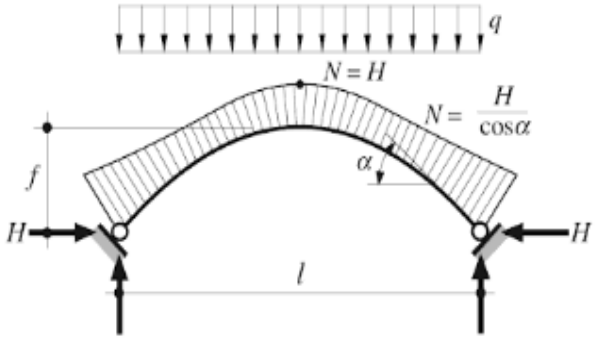

Figure 2. 23 Normal compression force in a parabolic arch that is pinned at both ends and subject to uniform vertical load [14].

2.2.2.2 Imposed Deformations

There are imposed deformations due to settlement of abutments, concrete shortening, and variation of temperature, creep and shrinkage of concrete. The effects of those deformations on axial force do not depend on the structural form that was adopted. Therefore, the same doesn't happen with the bending moments, where, when the degree of redundancy increases the variation is bigger.

The bending moments and deformations in arches that are fixed at both ends are higher than in the arches that are pinned at both ends accordingly to fig.2.24. Arch that is three-pinned is isostatic and there are no bending moments [18].

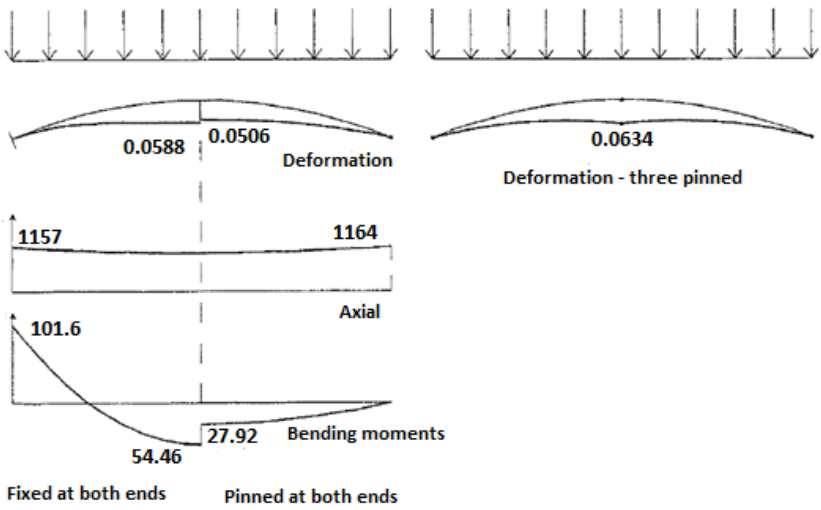

Figure 2. 24 Internal forces due imposed deformations (arch fixed at both ends, pinned at both ends and three pinned arch) [18].

2.2.2.3 Asymmetric loads

In fig.2.25, that represents an arch that is either pinned at both ends or tied, it is possible to verify the difference on the deformation and forces when the arch is subjected to a symmetrical and asymmetrical load. As expected, in the arch that is subjected to a symmetrical load there are no bending moments and for the arch subjected to asymmetrical it results in great bending moments [14].

Though, the normal force is less than for the symmetrical load.

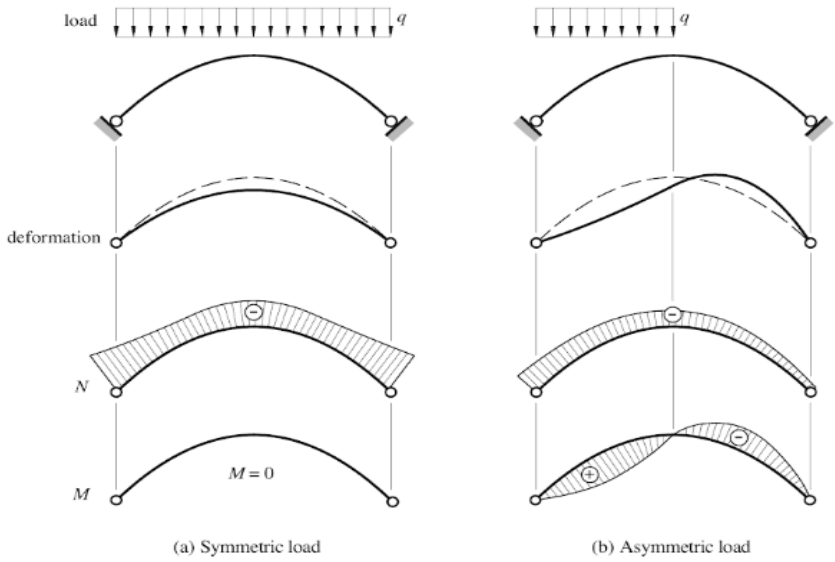

Figure 2. 25 Effect of symmetric and asymmetric uniform loads on deformation, normal force, and bending moment [14].

These results don't take in account the bending stiffness of the deck, assuming that the loads are directly applied on the arch. However, the interaction between the arch stiffness and deck stiffness may have a significant influence on the distribution of internal moments and forces in the structure. The fig.2.26 represents two extreme cases- flexible arch and stiff deck and vice-versa.

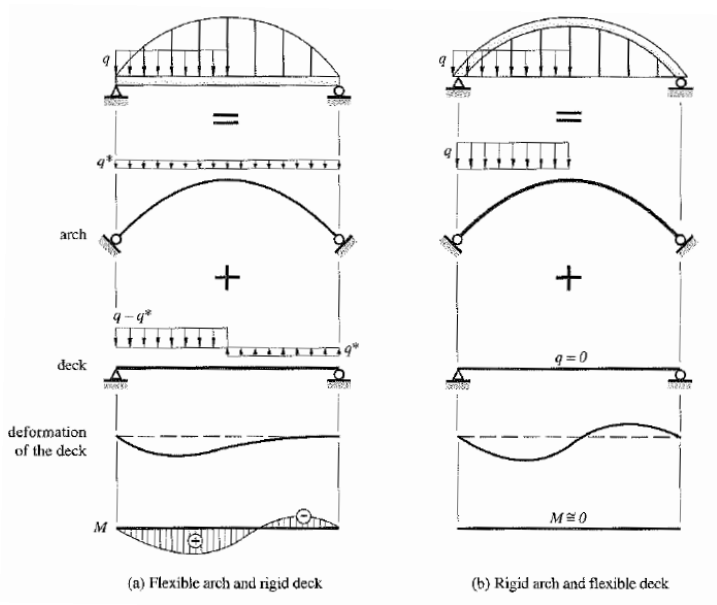

Figure 2. 26 Influence of the stiffness of the arch relative to that of the deck, for symmetric uniform load [14].

When the deck is stiff it centers and converts the small portion of the load into the antifunicular and transfers to the arch, the rest of the load is carried in bending of the deck. For a flexible deck, almost the entire load is transferred to the arch.

Flexible deck in bending follows the deformed shape of the arch without supporting the load. It is up to the designer to decide if it is deck or arch that will transfer the asymmetric part of the loading to the supports. If the deck is stiffer, the inertia of arch doesn't allow to take centring until the deck is concreted and hardened [14].

2.2.2.4 Concentrated Loads

The magnitude of the resulting forces on the arch due to concentrated loads depends very much on the structural form of the arch. The arches that are three-pinned have the resultant forces much bigger than the arches that are fixed on both ends or are pinned at the both ends. The deformation can be 5 or 6 times higher compared to other structural forms [18].

2.2.3 CONSTRUCTION

Initially, the construction method consisted in the use of centring for bridges with small spans made from stone. With the appearance of iron and later steel, to construct metal bridges a new method was used, the cantilever method. This method later was applied in the construction of concrete arches, firstly for erection of scaffoldings and later for the concrete arch itself. Use of large centering in difficult access areas, such as valleys and important watercourses, was of great difficulty besides economic issues. In the fig.2.28 is shown the construction of Maria Pia Bridge using cantilever method.

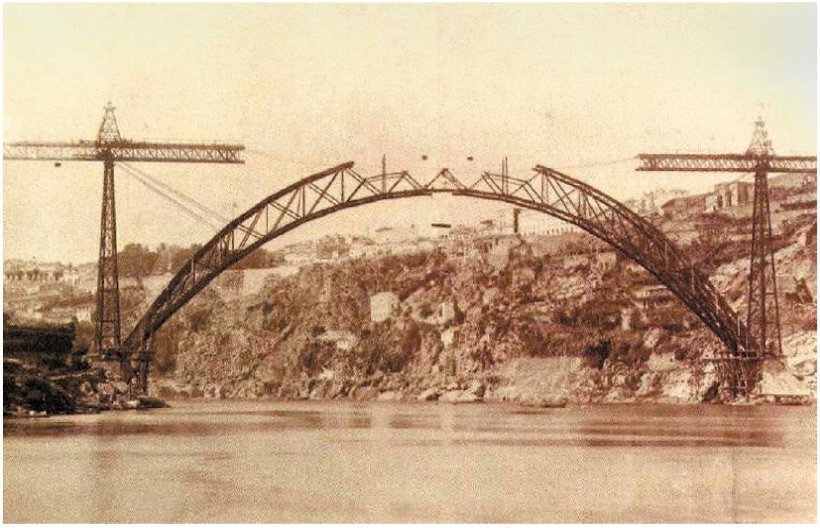

Figure 2. 27 Maria Pia Bridge- Portugal, 160 m span (designed by Théophile Seyrig and built by Gustave Eiffel) [3].

2.2.3.1 Centring

It was the first system to be used in bridge construction mostly due to its facility of construction. This method is appropriate for small and medium span arches and not for the large ones that needs large extensions of centering making the cost of it almost the same as the cost of the bridge itself.

Centring can be made of wood or metal and be supported on many points or structures with isolated supports or even with the same span as the final arch. Fig.2.29 shows different centring used for stone arches.

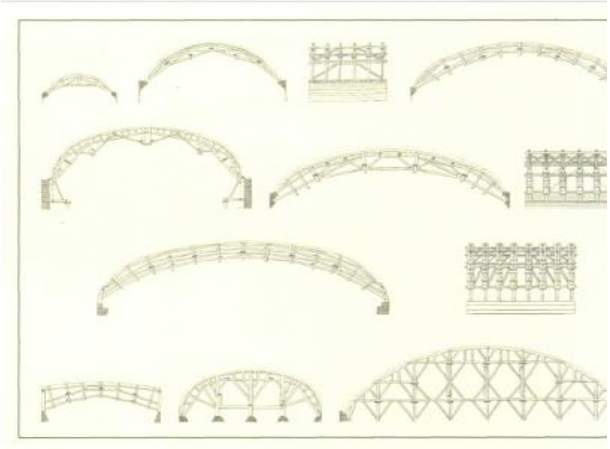

Figure 2. 28 Timber centring for stone arches from the book by M.Gauthey.

Joseph Melan in his bridge Schwimmschule, in Steyr, Austria, used a method where iron scaffolding became the reinforcement of the finish concrete arch. However, this method needs an amount of steel for scaffolding higher than the reinforcement needed for the final concrete arch. This method was used for a construction of a bridge in China, Beipanjiang with a 445 m span making it concrete arch World Record that is represented in the fig.2.30 [9].

Figure 2. 29 High-speed train Beipanjiang Bridge- China (445 m span,2016) [9].

Freyssinet built his arches using centring and Plougastel Bridge over the Elorn River with three arches and a 186 m span it is an authentic work of art. This bridge, shown in fig.2.31, was built with only one centring that was used for the three arches of the bridge. The centering was supported on two barges under the arch feet, by which they were transported from one arch to the other. The centring was supported on the abutments used for the arch concreting [19].

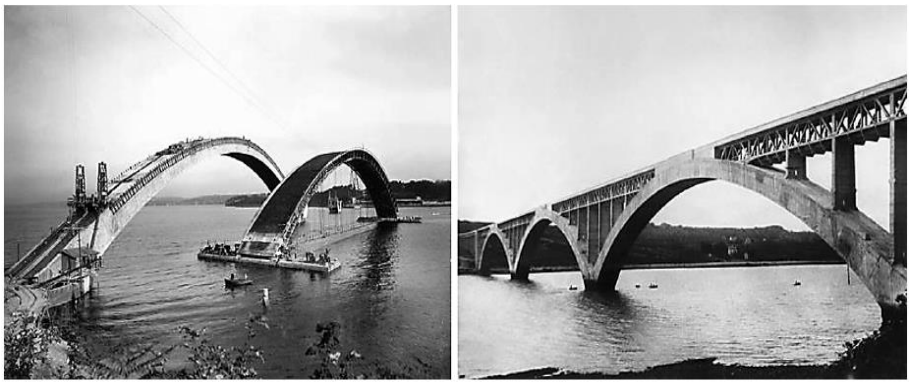

Figure 2. 30 Albert Louppe Bridge - France (3 spans of 186 m, 1930) [19].

In projects that are special due to environment or architecture reasons, the centring can present the same or even a higher degree of difficulty and are authentic works of art. In the fig.2.32-34 it is possible to find two bridges with their centring.

The first is a bridge over the River Cávado, located at Km 76 + 626 of EN 304 and which is intended to cross the reservoir of the Caniçada Dam. The bridge project, by Prof. Edgar Cardoso, was carried out in 1952-53 and the execution took place from 1952 to 1954. It is a work with maximum height, near 60 m, due to the high depth of the valley of the river Cávado in the place. The bridge has a total development of 177.8 m between the expansion joints. The deck is a variable inertia slab which rests on hollow masonry piers. The framework is supported by the piers that were previously built [20].

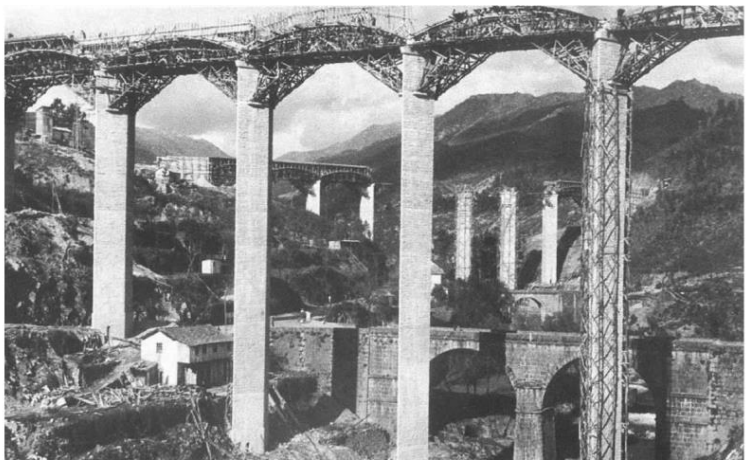

Figure 2. 31 Bridge over river Cávado (1954) [20].

The second bridge is located in Foz do Sousa, at EN 108. The project of the bridge is also of Prof. Edgar Cardoso and was held in 1950. The arch has a span of 115 m and 14.75 m rise, with rigid connections in the supports. The deck is constituted by longitudinal beams and panels

The solution of a single arch overcoming the valley was specially conditioned by the geological conditions of the site of implementation, since the river has a layer of sludge that reaches 30 m thickness. The construction of the arch was made using a wooden centring of intermediate supports, constituted by five main crankshafts in the transverse direction that in the upper part radiate, passing the number of crankshafts to 12 at the level of arches.

All joints of the pieces were made using rigid wooden blocks. The arch was cast according to a previously prepared plan, so that no appreciable tensions could be produced in its different sections, resulting from its functioning as a beam before the closing of the arch [21].

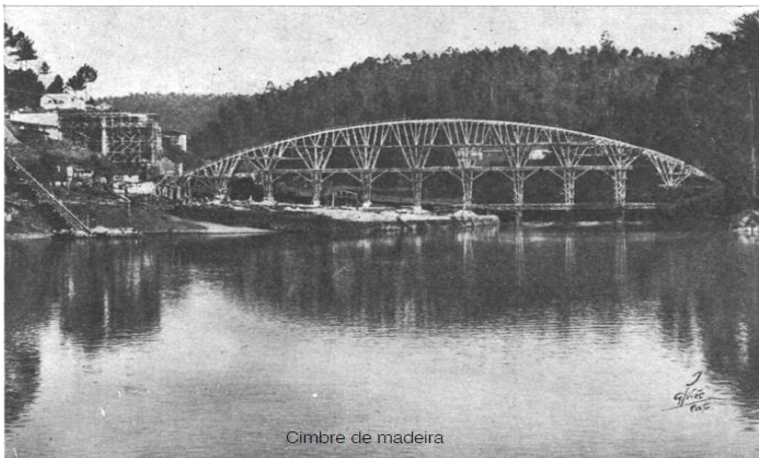

Figure 2. 32 Centring of Foz do Sousa Bridge (1950) [21].

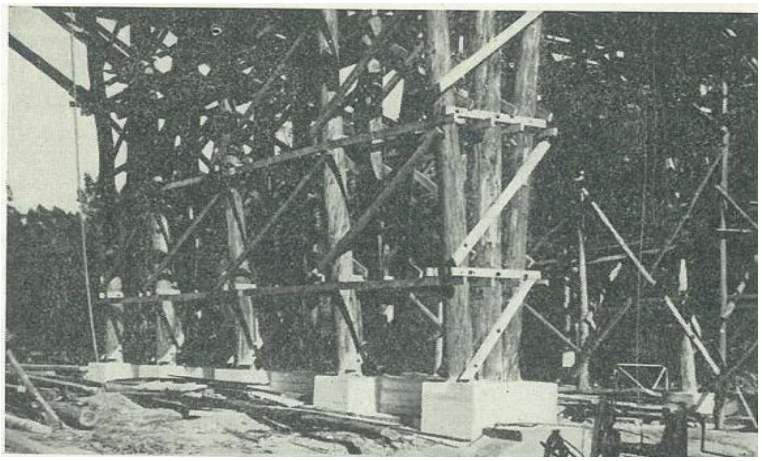

Figure 2. 33 Detail of a bridge support [21].

Freyssinet entered in history of bridge construction with another project that is represented in fig.2.35. The arches of la Guairá, Venezuela, with spans of 152 meters, built in 1952 for the motorway linking Caracas to La Guairá airport, was built using an innovation method.

The construction method consisted of advancing a wooden scaffolding from both sides stayed with trusses from the approach piers, leaving a middle span of 80 meters. Next, a central scaffolding for the remaining 80-metre span was lifted into place. Finished the process of fixation, the 80 meters were cast section by section, together with the end arch parts [22].

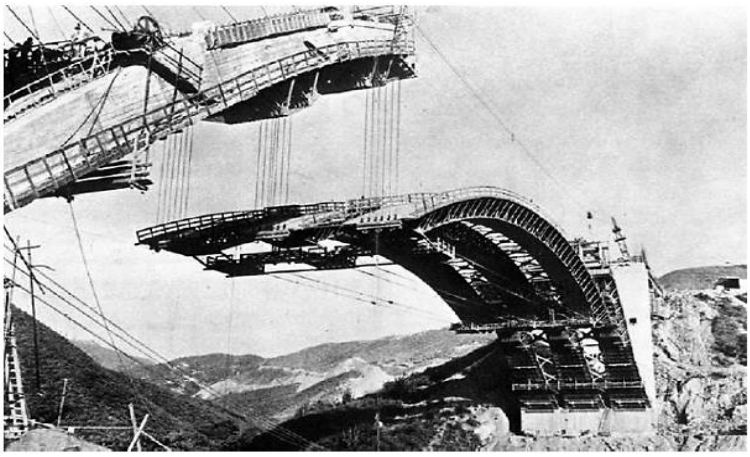

Figure 2. 34 Central scaffolding in the three Guaira Viaducts – Venezuela [22].

For the construction of Arrábida Bridge (1963), shown in fig.1.36-1.37, a steel scaffolding was used. Construction of the scaffolding begins on both sides of the bridge with cantilevers that are cable stayed to the pilasters/access viaducts and supported on a temporary bent.

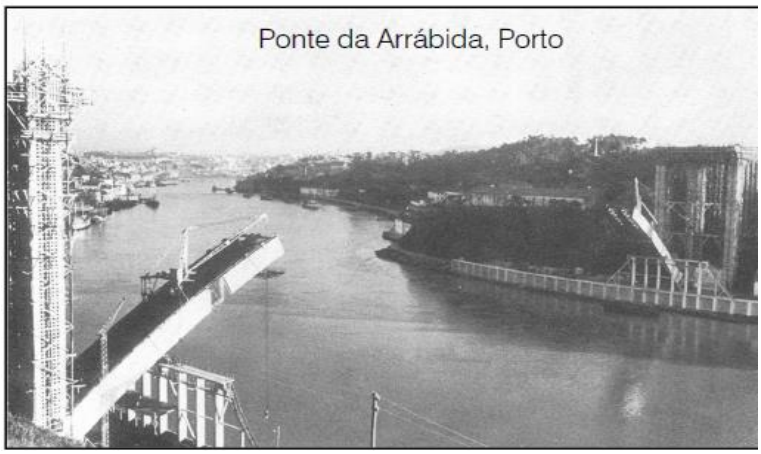

Figure 2. 35 Arrábida Bridge (Porto) [8].

The final part is the positioning of the central section with 78 m and 500 ton, raised from the river, in order to close the scaffolding.

Figure 2. 36 Closing of scaffolding with the central part [8].

The casting of the arches is done on top of the scaffolding. After the concreting of the first arch, the scaffolding lowers about 40 cm with the help of the hydraulic jacks and is pushed about 15 m to proceed with the concreting of the second arch in the same position as the first. The cost of arch scaffolding is very high that's why this technique is not widely used nowadays [8].

2.2.3.2 Successive cantilever advance method

James B.Enes introduced the cantilever advance method in bridge building. St. Louis Bridge (fig.2.38) over the Missisipi River was the first one to be built by this method and finished in 1874. This method permitted steamboat traffic to continue.

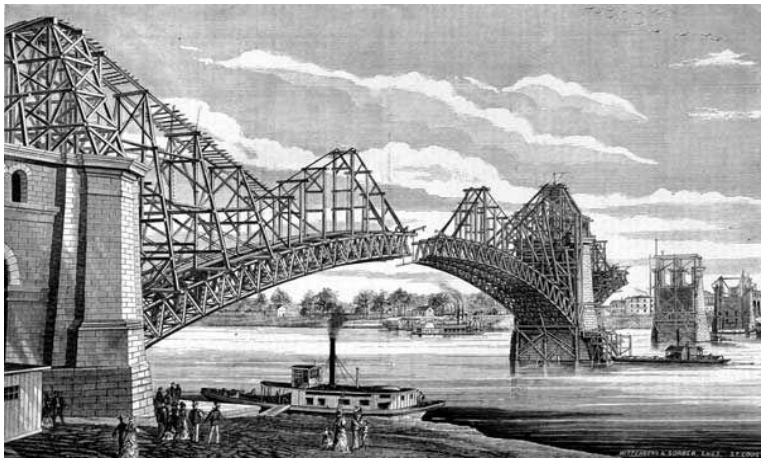

Figure 2. 37 St. Louis Bridge (The Eads Bridge) construction [3].

The construction by successive cantilever advance method consists in advancing with the arch in a cantilever using formtraveller or precast segments, tied to the deck of bridge or temporary towers, in order to control the great internal forces that are generated due to the arch being in cantilever. This provisional staying is required until the crown is closed.

This method is one of the most universal methods for the construction of bridges and the most suitable for large-span bridges other than the suspension type.

There is also an unstayed method that does not require any provisional support, where the triangulation depth allows the cantilever bending moment to be resisted without any temporary support.

This method was used on the Sydney Harbor Bridge (fig.2.39) which was built in 1932 and with a span of 503 meters [3].

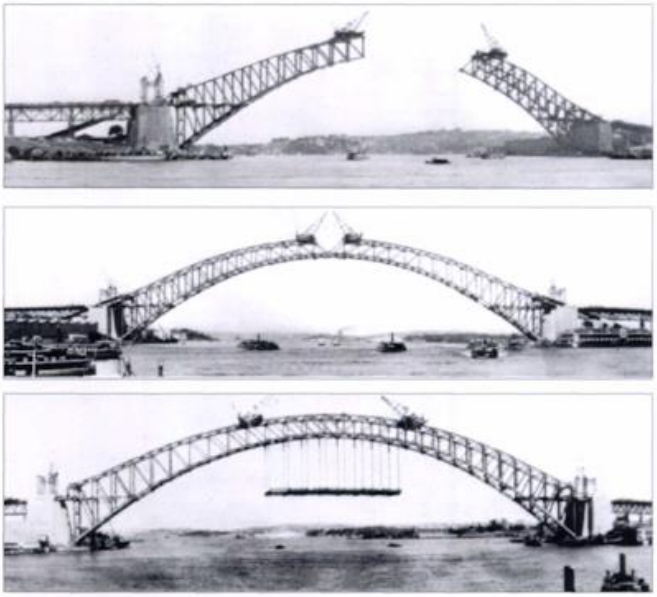

Figure 2. 38 Sydney Harbour Bridge (503 m span) [3].

Freyssinet was the first to apply successive cantilever advance method to the Guairá viaduct in Venezuela using concrete. The design of a bridge was double hinged to be able to control the differences that the arch would suffer due to the effects of the temperature in the bow and the tie rods.

In the successive cantilever advance method there are two variants of the construction of the deck. In the first variant, the deck is built after the arch is finished and in the second the two elements are built at the same time.

In the Viaduct of the river Tagus, part of the high-speed line Madrid-Extremadura, the deck of the bridge was built after the arch. The projected arch has 324 m of length between supports, rising above its foundations to a height superior to 70 m. The piers have variable height to adapt to the terrain profile, exceeding 72 meters in the area closest to the crossing of the river. All piers have a hollow shell-shaped cross-section except at their head where the section is massive to withstand the loads coming from the deck.

In this work, high strength cements were used for both the arch and the deck. The foundations are large in size to be able to distribute loads (fig.2.40). In addition, holes were drilled in foundation where cement mortar was injected in order to fill the possible fractures in the rocky soil in order to reduce future deformations and settling of the structure.

Figure 2. 39 Construction of foundations (arch supports and piers) [23].

In the foundations of arch supports that have strong inclinations, it was necessary to carry out excavation in phases and to apply soil support methodologies. The foundations of the piers, subjected to the forces of the tie rods, were given double attention due to the great internal forces during the construction phase.

The part of the deck that is situated over the piers was done using a self-supporting centring. The construction of the arch was performed using successive cantilever advance method, cantilever system trolleys were assembled at both ends of the starter pier cap that were made with the centring. In order to perform the arch, a very complex tie rod system is required that can support the 46 parts of each half-arches until the closing pier cap is built (fig.2.41).

Figure 2. 40 Construction of the deck and arch [23].

This process is carried out with the help of temporary towers. After casting the final pier cap, the temporary structures are removed, and the deck is constructed.

On the two sides of the bridge, the self-supporting centring advances with the construction of the deck in order to create symmetrical loads and decrease bending forces. The closing of the tray in the middle of the bridge is realized through a centring directly supported in the arch.

To ensure that the bridge is able to maintain the desired geometry and that there is no greater effort than anticipated the bridge is equipped with several control systems: load cells, bar extensometers, servo inclinometers, thermal probes and anemometers [24].

The construction of the deck could be carried out using incremental launching method, shown in fig.2.42. As the increase of the load due to this process can be very big and antisymmetric, in order to reduce the increase of bending moments the ballast is often placed in symmetrical zones to the load in order to reduce the asymmetry of loads, as represented in the fig.2.43.

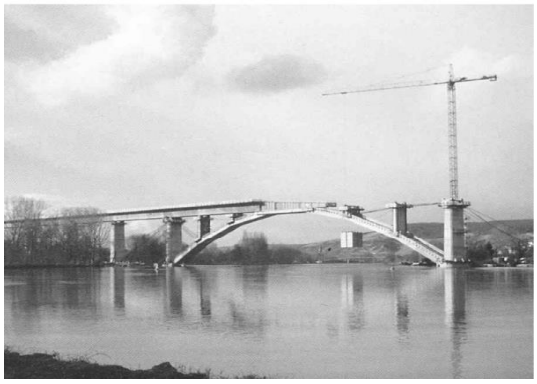

Figure 2. 41 Launching method for deck construction [8].

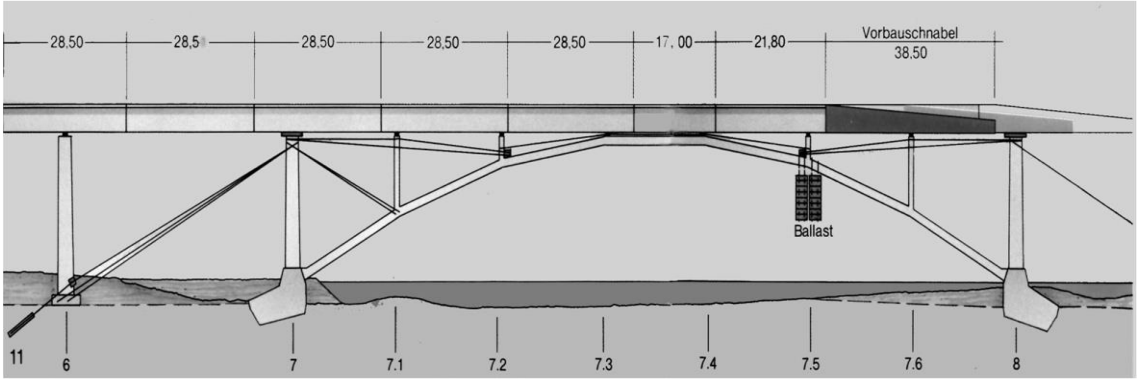

Figure 2. 42 Ballast in order to reduce asymmetry of loads [8].

It is also possible to construct the arch and deck simultaneously. This type of construction was first employed on the Hokawaza Bridge in 1978. The deck is constructed by successive advances in front of the arch (distance between two consecutive piers of the arch). When advancing with the arch diagonals are used to fasten the new section to the deck to establish connection. This method was used in Rip Bridge that comprises 2 cantilever trusses each 147 meters long and a central suspended span 46 meters long.

2.2.3.3 Lowering Method

This method was employed in Italy by Riccardo Morandi in Lussia Footbridge (fig.2.44). It is an effective method to build an arch bridge with spans of about 100 m. Each half of the arch can be built on both sides of the abutment, or each part of the arch can be built in the construction site near the bridge area and transported across the deck to the abutments.

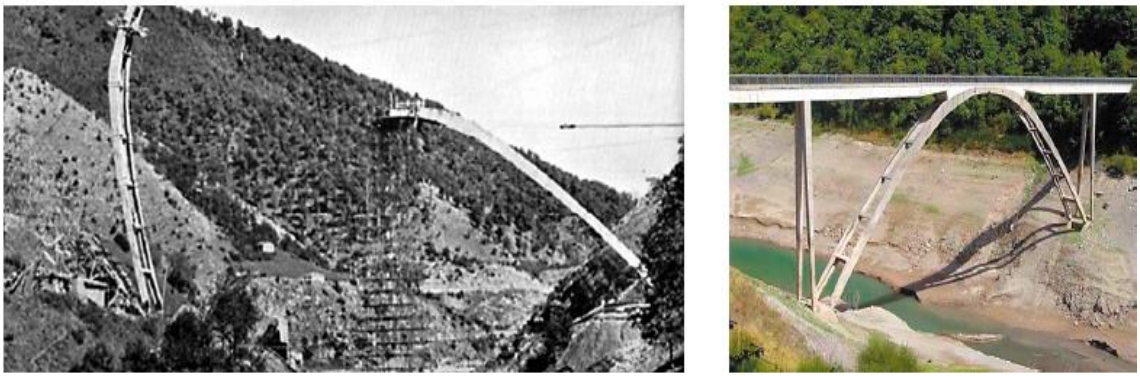

Figure 2. 43 Lussia Footbridge [25].

Bridge over the Tagus River in the Alcántara reservoir is formed by two metallic arches with a span of 220 m and 42.50 m rise. This is the arch with the longest span built with lowering method in the world up to now. The goal was to build the bridge as fast as it could be so the basic idea consisted in assembling most of the structure on land to then subsequently locate it in its final position.

Construction started with excavating foundations and construction of the piers from the footing with maximum height of 52 m (fig.2.45). Half of each deck was built behind each abutment and then moved to its final position using the launching method. The first 22 meters of top slab were not concreted in order to reduce stresses in the deck when it was overhanging.

Figure 2. 44 Construction process of the Bridge over the Tagus River in the Alcántara [26].

Each arch is divided into 16 m long parts which are assembled horizontally and moved over the deck to the front part where a metal gantry picks it up for the advancing, overturning and lowering operations until connecting previously placed bottom piece. The gantry is fitted with moving elevation and retaining mechanism formed by hydraulic jacks operating vertically arranged cables.

The next quarter arch is then carried over the deck until connecting with the previous part in an area provided with hinges. Then it is hoisted and overturned with the use of a crane until reaching a position close to the vertical.

Vertically acting hydraulic jacks, placed on deck supported steel auxiliary towers, are used instead of crane hosting in order to control movements in the last phase when the 2nd quarter of the arch is rotated.

The arch section is then completed by plate welding where the hinges are located. The arch is finally ready to be lowered down. The lowering operation starts by pushing the semi-arch towards the reservoir with telescopic jacks fitted on the deck and the holding cables, acting in the opposite direction. When the jacks reach their maximum extension, the arch starts to descend only under gravity, controlled by holding cables.

A guide system is fitted on the front of each semi-arch in order to fit them both together and at the same time align them with each other. When lowering operation has concluded the hinges are locked by fitting anchor bars and reinforcements followed by concreting the area. In the end, middle piers are constructed using crane followed by the launching of the deck [26].

All the construction process is represented in the fig.2.46.

Figure 2. 45 All the construction phases of the Bridge over the river Tagus at Alcántara [26].

3.
INTRODUCTORY NOTE EARTHQUAKE

An earthquake event is characterized by the release of large amounts of energy that is felt as vibratory ground motions and results in shaking or/and ground failure. Energy is transferred in a form of waves that can be of 2 types: body (P and S) and surface (Love and Rayleigh) waves. This vibration of the ground can be due to a natural (tectonic ground motions, volcanism, landslides, etc...) or human cause (man-made explosions) and the equipment used to register it is the accelerograph.

When the wave reaches the structure, it tends to follow the accelerations of the ground. The change in static position depends on the rigidity and mass of the structure. This transition of accelerations generates inertial forces in the structure that are responsible for the dynamic response.

Unfortunately, it is with tragic events that seismic engineering has been evolving over the years, through tests in laboratories and analytical studies. In figures (3.1 to 3.3) we can find information of earthquakes advances, and images of induced damage. The main damage in bridges occurs mainly at the ends of piers [27].

Year	Earthquake	Major Lessons	Major Advances
1964	Prince William Sound, AK	Ground failure due to liquefaction, span unseating	Site susceptibility to liquefaction, longer support lengths
1964	Niigata, Japan	Ground failure due to liquefaction, span unseating	Site susceptibility to liquefaction, longer support lengths
1971	San Fernando, CA	Column failure, span unseating	Capacity design, longer support lengths
1989	Loma Prieta, CA	Non-ductile details in older structures, span unseating, soil amplification effects	Restrainers, column jackets, extensive tool box of retrofit measures, revised site amplification factors
1994	Northridge, CA	Adverse load distribution in piers with unbalanced stiffness, unseating in skewed bridges, flared column failures, cross-frame damage in steel plate girder superstructures	Balance pier stiffnesses in multi-span continuous structures, longer support lengths, new details for flared columns, explicit design of load path in plate girder superstructures, displacement-based design
1995	Kobe, Japan	Damage to steel superstructures and bearings, non-ductile response of concrete columns	Increase in minimum connection forces, full scale testing of Japan-designed bridge columns on E-defense shake table in Kobe
2001	Nisqually, WA	Liquefaction, cross-frame damage in steel plate girder superstructures	Site remediation, estimation of lateral flows due to liquefaction, ductile cross frames for plate girder bridges
2008	Wenchuan, China	Span unseating and abutment damage due to rockfalls, curved girder unseating	Stabilize adjacent rock slopes, explicit design of load path in curved bridge superstructures; longer seat lengths
2010	Maule, Chile	Span unseating due to inadequate shear keys, rotation in skewed and non-skewed spans, liquefaction-induced column settlement and shear failures, tsunami-induced scour and column damage	Explicit design of load path in all bridge superstructures including diaphragms and connections; longer support widths for skewed bridges, remediation of liquefiable sites under bridge foundations to minimize settlement and lateral flow
2010, 2011	Christchurch, New Zealand	Liquefaction induced lateral flow damages abutment piles and when resisted can buckle single span bridge superstructures in compression, aggressive retrofitting program reduced extent of bridge damage	Ground improvement under bridge approaches to reduce extent of lateral flow (site remediation), benefits of seismic retrofit program demonstrated
2011	Great East Japan Earthquake, Japan	Bridge damage due to shaking was mainly in bridges not yet retrofitted, or only partially retrofitted. Bridge damage due to tsunami inundation was greater in non-integral bridges	Benefits of seismic retrofit program demonstrated, survival during tsunami inundation is possible if adequate connection provided between super- and sub-structure

Figure 3. 1 Major earthquakes and advances that resulted from them [27].

After the earthquakes referred in Fig 3.1, several rules started to be employed:

- New bridges designed for a minimum 0.6 m seat;
- Larger diameter used for the spiral reinforcement at a closer spacing in columns to allow them to deform without failing in flexure or shear;
- Regularity on the elements and parts of the bridge to avoid non-uniform distribution of the forces. All the bridge elements should have, approximately, the same mass, stiffness and period.

If the bridge is regular, continuous and confined, it is possible to eliminate most bridge collapses resulting from shaking of the ground.

Figure 3.2 Example of unseated span due to insufficient support length and superstructure damage due to inadequate load path [27].

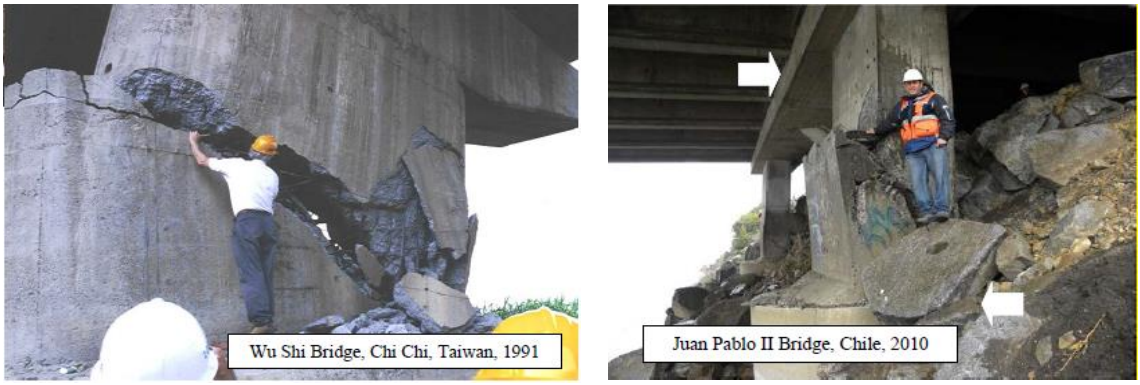

Figure 3. 3 Example of pier damage due to lack of ductile detailing and structural damage due to ground Failure [27].

In the piers, failures may be due to bending and shear. Failures due to bending are usually due to absence of confinement in the area of formation of the hinge. If the concrete is not well confined with steel, its resistance to compression is lower and concrete disintegration may occur. Also, if the longitudinal reinforcement is discontinued or the overlap length is not enough it can originate a weak section susceptible to deformation. Shear failures are more common in short piers and those where the section changes in length, combination of shear and bending originates this type of failure in the zone just below the widest part of the pier [28].

In the zone of the connection between the beam and the pier, major forces are developed, that need more scrupulous analysis and detailing of the reinforcement.

Designing a bridge for earthquake is not easy due to the difficulty of characterizing the action in the models of analysis and perform a proper representation of the nonlinear regime of the materials. Characterization of the seismic event is important and depends on many factors as intensity, distance from epicentre and ground properties.

Before 1973, the seismic design was based on forces proportional to building mass. According to *AASHTO (American Association of State Highway and Transportation Officials):*

$$EQ = \mathrm{C} * \mathrm{D} \tag{3}$$

EQ= Lateral force applied horizontally.

D= Dead Load of Structure.

C = 0.02 for structures on material rated at 4 tons or more per sq ft.

= 0.04 for structures on material rated less than 4 tons or more per sq ft.

= 0.06 for structures on piles.

After San Fernando earthquake in 1971, the design practice for seismic resistance was revaluated. Traditional approach consists in an elastic design (static and dynamic) that uses an elastic earthquake forces reduced by the appropriate Response Modification Factor (R) that tends to include the real behaviour of the material that is non-linear and varies based on typical inelastic response of structural types [27].

Nowadays, it's becoming more common to perform inelastic analysis because it is more realistic, and does not require knowing the R factor, which is difficult to quantify. Furthermore, an inelastic analysis can provide performance parameters, forces and ductility of the structure. A scheme of the seismic analysis procedure proposed in "Seismic Analysis and Design of Bridges Reference Manual" by FHWA US is shown in fig.3.4.

PART A: PERFORMANCE LEVEL DETERMINATION

Step 1: Determine required performance level in consultation with the Owner. In most cases this will simply be the 'collapse prevention' requirement.

PART B: DEMAND ANALYSIS

Step 2: Determine seismic loads at the bridge site from either national maps of design coefficients or a site-specific seismic hazard assessment exercise.

Step 3: Determine soil conditions at the site and modify seismic loads accordingly.

Step 4: Analyze the bridge for given loads using one of several possible elastic dynamic methods chosen according to the complexity of the bridge. As a minimum, obtain maximum values for forces and displacements. Perform this analysis in each of two orthogonal directions and combine the results to give values for use in design.

PART C: CAPACITY DESIGN

Step 5: Select locations in the bridge where yielding will be permitted, i.e., select the plastic hinge mechanism.

Step 6: Design yielding elements to have capacity in excess of the demand from Step 4 without degradation. Detail these locations for ductility.

Step 7: Check the load path through the bridge and protect all components (except the yielding members) against damage. This step is known as 'capacity protection'.

Figure 3. 4 The road map for the seismic design of a bridge [27].

3.1 TYPES OF ANALYSIS

3.1.1 ELASTIC ANALYSIS

As said before, this type of analysis uses a linear stress-strain relationship but incorporates a correction factor (R) to permit better consideration of the nonlinear characteristics of the response.

The *fundamental mode method* quantifies the total seismic action in inertial forces, given by the product of the vibrating mass by the maximum seismic acceleration, which is obtained from a spectrum of inelastic accelerations for the period of vibration of an equivalent system of one degree of freedom with the same condensed stiffness and mass properties of the structure under analysis. This analysis is permitted for structures which do not have irregular structural systems. All the restrictions should be checked before applying this type of approach because it assumes continuity of the structure and distributes seismic forces along all elements of the bridge and is based on the fundamental mode of vibration in either longitudinal or transverse direction.

In the *response spectrum method*, the structure is not represented as one degree of freedom system (SDOF), but rather several SDOFs representing the various modes of vibration of the structure, making

this procedure more accurate than the previous one. Structure, even being regular and having a symmetrical distribution of mass and rigidity, present several modes of vibration that can have greater or lesser influence in its global dynamic behaviour.

Therefore, the seismic response must attend to all the modes that influence it, combining them according to a consideration of the relative importance embodied, quantified by the modal mass they effectively mobilize. This combination of the responses of the various systems of one degree of freedom uses the method of modal combination to obtain the states of tension and deformation experienced by the structure.

It is important to note that no direct check of the displacement capacity is made with an elastic analysis. Forces are obtained using the R factor, as shown in Fig 3.5, then the yielding members are designed to provide the requested strength. The bridge displacement capacity is presumed to be provided by detailing.

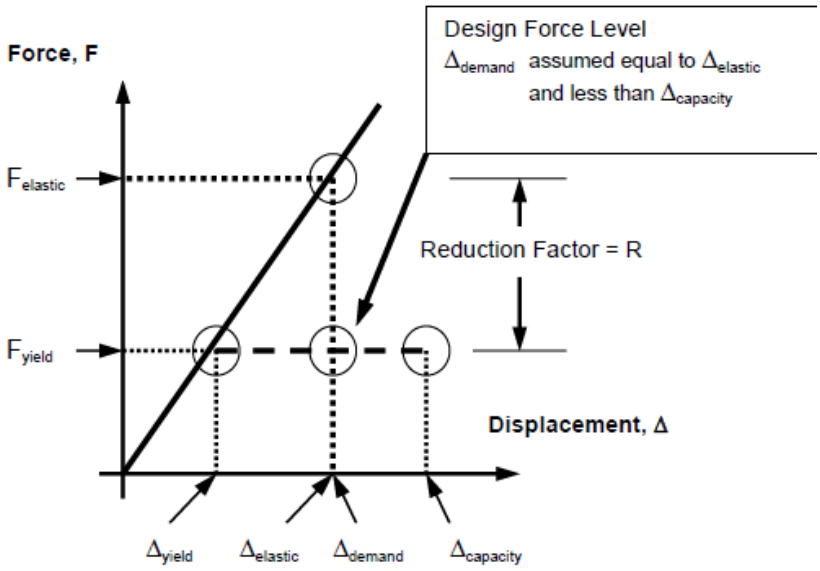

Figure 3.5 Calculation of Design Force Level [27]

3.1.2 NONLINEAR ANALYSIS

This type of analysis predicts the non-linear behaviour of a structure under seismic loads. It allows to identify potential weak areas in the structure and can demonstrate how progressive failure in building really occurs and identify the mode of final failure.

In a *Static inelastic analysis*, known as pushover analysis, a structural model directly incorporating the nonlinear load-deformation characteristics of the elements is “pushed over” by a monotonically increasing lateral load representing inertia forces in an earthquake until a predetermined value or state is reached. From this analysis results a Capacity Curve that represents the variation of the total lateral seismic shear demand, “V” of the structure, with the lateral deflection of the bridge at the deck level. The intersection between this curve and a demand curve results in the Performance Point, and the project performance objectives can be judged by evaluating where the performance point falls on the capacity curve.

Time history analysis is a nonlinear dynamic analysis that reproduces the dynamic behaviour of the structures more correctly and provide a realistic internal forces. This approach considers nonlinear damping, stiffness, load deformation behaviour of members including soil, and mass properties. The

structure is subjected to forces based on *accelerograms*, often recorded in historical earthquakes, simulating a real seismic event, or synthetically generated. A nonlinear system is approximated as a series of linear systems and the response is calculated for a series of small equal intervals of time Δt and equilibrium is established at the beginning and end of each interval. The computational and time-consuming demands of these analyses are very high, which is why they are not so common and mostly used only for bridges of high importance and in zones susceptible to earthquakes as a tool to verify a design obtained from other simpler calculation methods [29].

3.2 EARTHQUAKE GROUND MOTION

The ground shaking is represented by the *accelerogram* that contains acceleration of the ground, in the three orthogonal directions, registered in a specific location during an earthquake. Velocities and displacements are usually determined by numerical integration. The accelerations recorded at locations that are approximately at the same distance away from the epicentre may differ significantly in duration, frequency content, and amplitude because of the different local soil conditions.

There are different levels of earthquake ground motion for which the structures are designed, that vary depending on the design code used. For example, for the ATC 40 – 3.3 [30]:

The Serviceability Earthquake (SE): Ground motion with a 50 percent chance of being exceeded in a 50-year period (Return period of 100 years).

The Design Earthquake (DE): Ground motion with a 10 percent chance of being exceeded in a 50-year period (Return period of 500 years).

The Maximum Earthquake (ME): Maximum level of ground motion expected within the known geologic framework due to a specified single event (median attenuation), or the ground motion with a 5 percent chance of being exceeded in a 50-year period (Return period of 1000 years).

To evaluate the response of structure to the ground shaking, it needs to be treated as a superposition of short-duration impulses. An impulse can be defined as the product of the force times duration. Integrating all the excitation we can obtain the total response of the structure. This is usually referred to, as "Time History Analysis" [29].

3.2.1 RESPONSE SPECTRA

"The spectrum is defined as a relation between peak values of a response quantity (acceleration, velocity or displacement) and structural dynamic characteristic (frequency or natural period). It represents the peak response of all possible SDOF systems to a particular ground motion [29]."

3.2.1.1 Elastic Response Spectrum

To obtain the response spectrum of an elastic structural system, the following steps must be taken:

- Define the ground acceleration time history (typically at a 0.02 second interval).
- Select the natural period Tn and damping ratio ξ of an elastic SDOF system.
- Compute the deformation response u(t) using any numerical method.
- Determine uo, the peak value of u(t).
- Calculate the spectral ordinates by D=u0, V=2π D/Tn and A = (2π/Tn)^2*D
- Repeat steps 2 and 5 for a range of Tn and ξ values for all possible cases.
- Construct results graphically to produce three separate spectra as shown in Figure 3.6 or a combined tripartite plot [29].

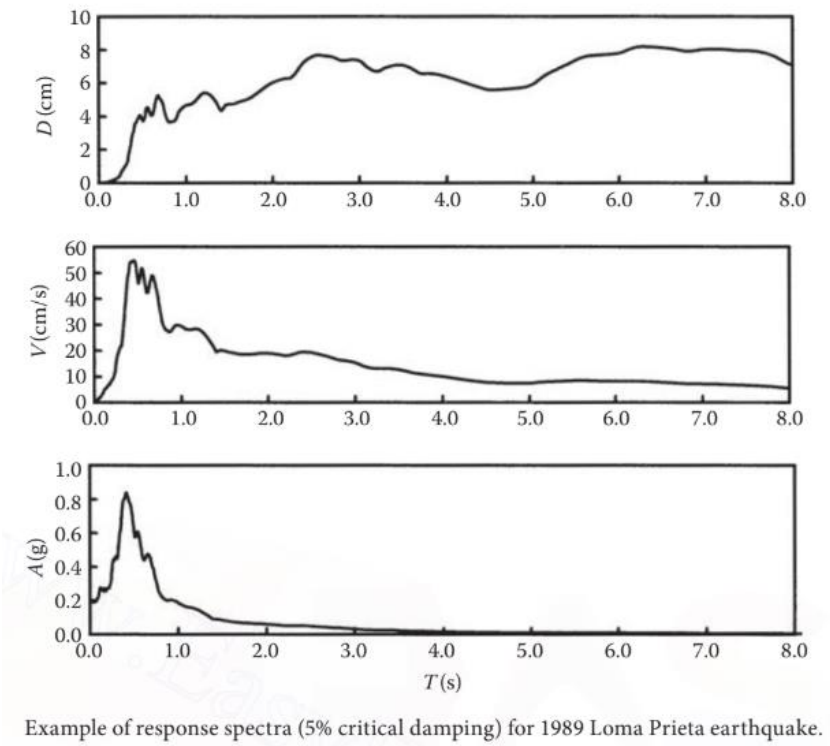

Figure 3. 6 Response spectrum of an elastic structural system [29].

3.2.1.2 Elastic Design Spectrum

The structure should resist future earthquakes which characteristic are unknown that's why using a response spectra that is based in a previous earthquake is not proper for design.

The elastic design spectrum is produced to represent the envelopes of ground shakes based on the past earthquakes registered at that zone. The development of this spectrum is based on statistical analysis of the response spectra for the group of ground motions. In the fig.3.7 it is possible to observe some of the past earthquakes registered and the proposed design curve.

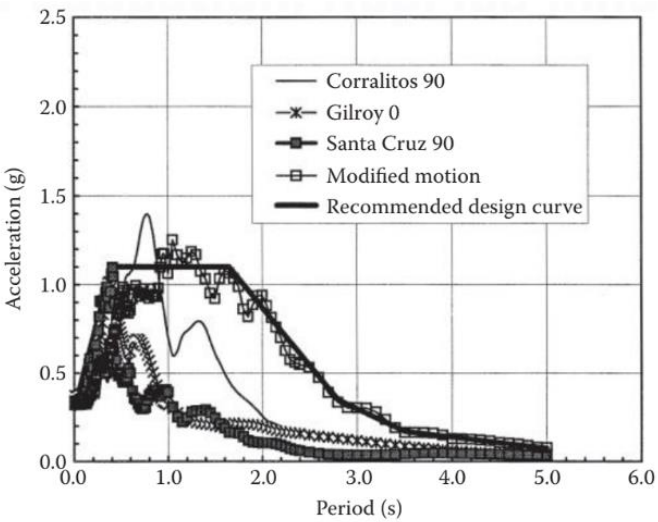

Figure 3. 7 Project-specific acceleration response spectra for the California Sonoma Creek Bridge [29].

3.2.1.3 Inelastic Response Spectrum

During earthquake a bridge can experience inelastic behaviour, dissipating seismic energy by damping and yielding. Yielding is defined as localized inelastic deformation converting into heat and other forms of energy that vary depending on structural material, configuration and load path on the structure. In the viscous damping the dissipation of energy occurs by the internal friction loss when deformed and depends mainly on structural materials.

To consider inelastic behaviour of the material without performing nonlinear inelastic analysis the elastic response spectrum needs to be transformed into inelastic spectrum by considering its ductility (μ). During an earthquake, to ensure that a structure can resist this kind of forces it is necessary to provide sufficient ductility to deform.

Ductility μ is defined as:

$$\mu = \frac{\Delta u}{\Delta y} \tag{4}$$

Δu= ultimate displacement capacity

Δy= yield displacement

The next step is to scale the elastic design spectrum by some function of the available ductility of structural system [29].

$$ARS_{inelastic} = \frac{ARS_{elastic}}{f(\mu)}$$

$$f(\mu) = \begin{cases} 1 & \text{For } T_n \leq 0.03 \text{ s} \\ 2\mu - 1 & \text{For } 0.03 \text{ s} < T_n \leq 0.5 \text{ s} \\ \mu & \text{For } T_n > 0.5 \text{ s} \end{cases}$$

Figure 3. 8 Transformation of elastic design spectrum into inelastic [29].

Where:

$ARS_{inelastic}$ = Inelastic design spectrum;

$ARS_{elastic}$ = Elastic design spectrum;

T_n = Period.

Tn ≤ 0.03 s: the elastic displacement demand Δed is less than displacement capacity Δu. The reduction factor f (μ) =1 implies that the structure should be designed and remained at elastic to avoid excessive inelastic deformation.

0.03 s < Tn ≤ 0.5 s): elastic displacement demand Δed may be greater or less than displacement capacity Δu and reduction factor is based on the equal energy concept.

Tn> 0.5 s: the reduction factor is based on the equal displacement concept.

For the static analysis Elastic/Inelastic Response Spectrums are used, and for the dynamic analysis real *accelerograms* of past earthquakes are used.

3.3 NONLINEAR STATIC ANALYSIS – PUSHOVER ANALYSIS

Design of structures evolved over time, passing from a perception in which the goal was to avoid collapse to the one that incorporates different levels of performance. The concept of “strength” is no longer understood as a guarantee of better performance, if the strength is increased without a corresponding increase in the ductility of the structure, the performance of the structure in the event of an earthquake could be worse. The structure must be designed according to its "importance" and performance required by the code or the owner of the project. Pushover analysis allows, for a given seismic action, to estimate its performance and check if it meets the desired one. However, in order to perform the pushover analysis, it is necessary to know all the elements of the structure and the behaviour curves of the materials, so this type of analysis is used to validate the previous design.

A brief description of the pushover has been made previously. In this chapter, it will be discussed how this nonlinear static analysis is performed and the various proposals that exist for its realization. The nonlinear designation is due to the fact that various elements are modelled using a non-linear mathematical model.

To apply this type of analysis the following steps must be taken that are also represented in the Fig.3.9 [31]:

- *Define the mathematical model with the nonlinear force deformation relationship for the various components/elements;*
- *Define a suitable lateral load pattern and use the same pattern to define the capacity of the structure;*
- *Define the seismic demand in the form of an elastic response spectrum;*
- *Evaluate the performance of the building.*

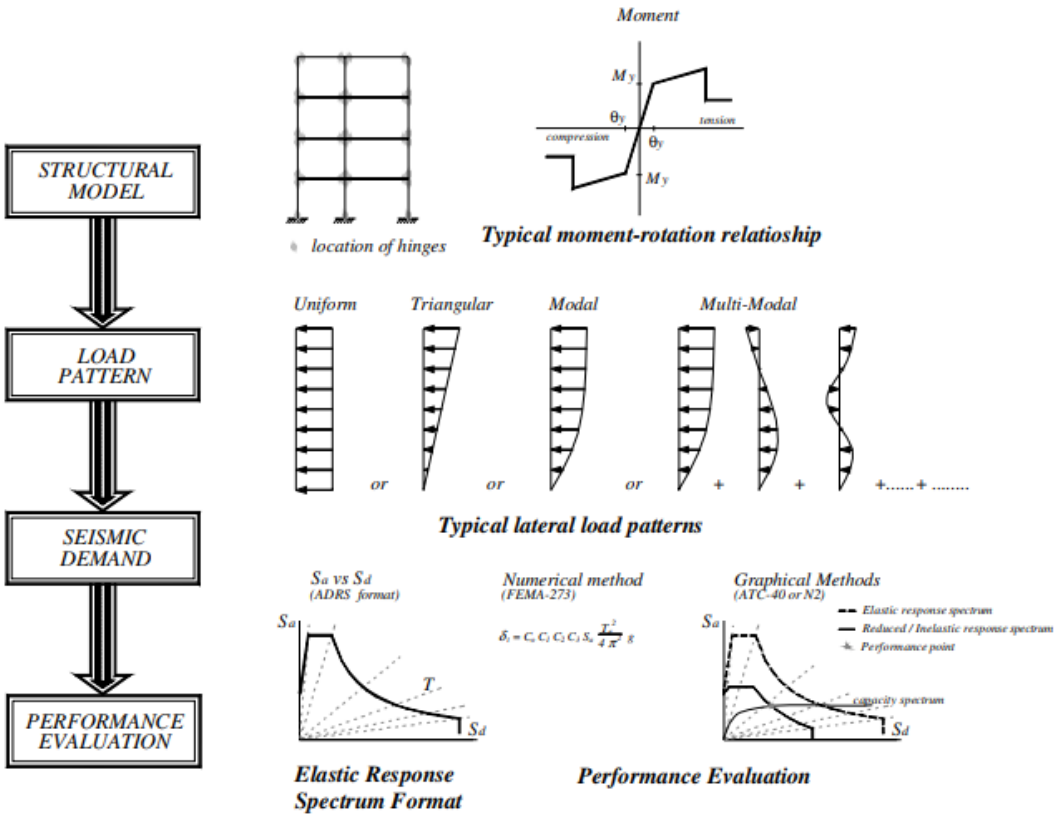

Figure 3. 9 General flowchart for Nonlinear Static Procedure [31].

Mathematical model for the elements can be based on the experimental results or in numerical analysis.

Some of the methodologies that were developed for this type of analysis are:

- The Displacement Coefficient Method (FEMA-273 updated to FEMA-440) [32];
- The Capacity Spectrum Method (ATC-40 updated to FEMA-440) [30], [32];
- The N2 Method (EC8) [33].

FEMA 273 NEHRP *Guidelines for the Seismic Rehabilitation of Buildings* and ATC 40 *Seismic Evaluation and Retrofit of Concrete Building* were the first earthquake guidelines, developed by American Civil Engineers, on the application of nonlinear analysis. Later improvements have been proposed in FEMA 440 .In Europe, in turn, the N2 method is implemented in the Eurocode. These methods differ on the clarity of theoretical base and simplicity of the application, but all are based on an explicitly or implicitly defined equivalent system of SDOF.

3.3.1 LATERAL LOAD

The choice of the load to be applied is very important for the results. These load patterns should represent the likely distribution of inertia forces in a seismic design. According to FEMA and EC8, at least two load patterns should be used:

- Uniform pattern with lateral forces proportional to mass, independent of their elevation (uniform response acceleration).
- Modal pattern with lateral forces proportional to the modal lateral force distribution according to elastic analysis in the direction under consideration.

Using an invariant load pattern is possible and representative of reality when the structural response is mainly influenced by the first mode and has only one yielding mechanism. Using this type of load may not allow to consider correctly the inertia forces redistribution in the structure. Some other types of load patterns were proposed in ATC-40 that intends to consider this factor [31]:

- For each increment beyond yielding, adjust the forces to be consistent with the changing deflected shape.
- Similar to the point above but include the effects of the higher modes of vibration in determining yielding in individual structural elements while plotting the capacity curve for the building in terms of first mode lateral forces and displacemens.

3.3.2 NONLINEAR STATIC SEISMIC ANALYSIS- METHODOLOGIE PROPOSED IN FEMA440

The procedure for the static nonlinear seismic analysis consists in verifying the capacity of the structure to withstand a certain seismic displacement, and can be divided in two parts:

- Definition of the capacity curve (pushover analysis)
- Calculation of the demand displacement through one of the following procedures:
    - Capacity spectrum Method
    - Displacement coefficient Method

3.3.2.1 Capacity Spectrum Method (Equivalent Linearization)

A step-by-step procedure for the method is described in the following lines:

1. Define the initial response spectrum, Sa vs. T, with initial damping βi (normally 5%)

2. Modify, if required, the selected spectrum, as appropriate, for soil-structure interaction (SSI). This involves both potential reduction in spectral ordinates for kinematic interaction and a modification in the system damping.

3. Convert the response spectrum to Sa vs. Sd format.

The response spectrum in forms of Sa versus period T is converted to Sa versus Sd by the following relations:

$$S_d = \frac{{T_i}^2}{4 \times \pi^2} S_{ai} \times g \tag{5}$$

Where:

S_d is spectral displacement;

T_i is period;

S_{ai} is spectral acceleration;

g is gravitational acceleration.

This transformation is represented graphically in fig 3.10.

"Every point on a response spectrum curve has associated with it a unique spectral acceleration, spectral velocity, Sv, spectral displacement, Sd and period, T. To convert a spectrum from the standard Sa vs T format to ADRS format, it is necessary to determine the value of Sd, for each point on the curve (Sai, Ti) [30]."

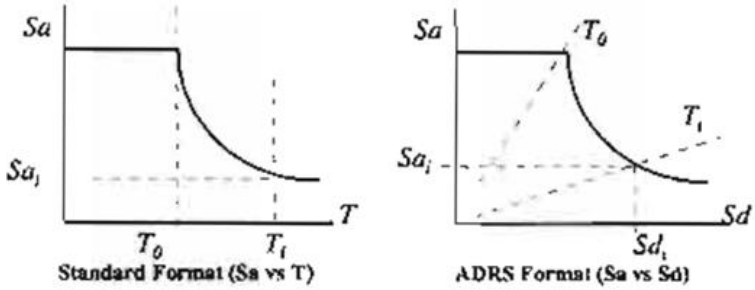

Figure 3. 10 Response Spectrum Conversion [30]

Attention is called to the fact that in these graphics, each period of the structure can be represented by radial lines parting from the origin.

4. Generate the capacity curve of the structure

The goal is to represent the capacity of the structure in the form of the capacity curve by plotting the base shear force versus the deck displacement as represented in the Fig.3.11.

The capacity of the structure depends on the strength and deformation capabilities of the structure and in order to correctly evaluate the behaviour in post-elastic regime, a nonlinear analysis is required.

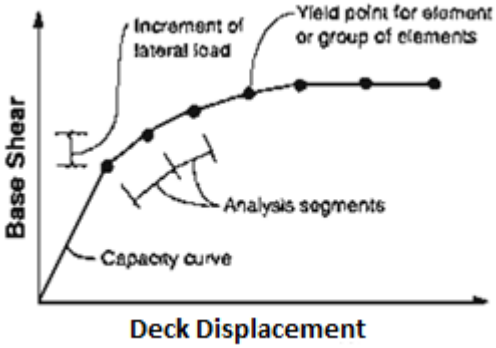

Figure 3. 11 Capacity Curve [30].

In order to obtain the capacity curve, uniform and modal lateral loads distribution are applied as mentioned before. The capacity curve shall be represented also as an idealized bilinear representation in order to calculate the yield strength and yield displacements, and the effective lateral stiffness and post-yield slope, α represented in Fig.3.12.

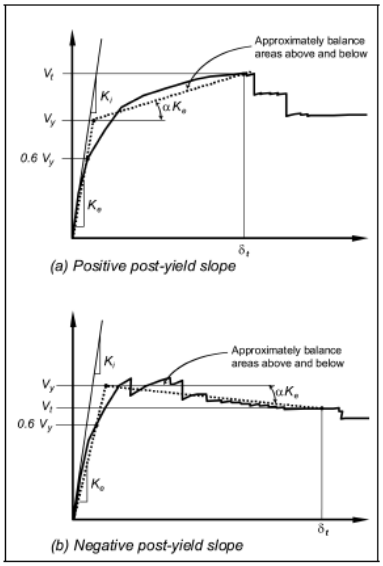

Figure 3. 12 Idealized Force-Displacement Curves [34].

5. Convert capacity curve to (Sa, Sd) format.

The capacity curve in forms of shear force vs. deck displacement can be converted to an equivalent SDOF Sa vs. Sd graph by the following relations:

$$S_a = \frac{V/W}{\alpha} \tag{6}$$

$$S_d = \frac{\Delta_{roof}}{PF \times \phi_1} \tag{7}$$

Where:

- V is the base shear force;
- W is the structural dead weight plus (if required) live load;
- α is the modal mass coefficient for the first natural mode;
- ϕ1 is the amplitude of mode 1;
- PF is the modal participation factor for the first natural mode.

$$\alpha_1 = \frac{\left[\sum_{i=1}^{N} \frac{w_i * \phi_{i1}}{g}\right]^2}{\left[\sum_{i=1}^{N} \frac{w_i}{g}\right]\left[\sum_{i=1}^{N} \frac{(w_i \phi_{i1})^2}{g}\right]} \tag{8}$$

$$PF_1 = \left[\frac{\sum_{i=1}^{N} \frac{w_i \phi_{i1}}{g}}{\sum_{i=1}^{N} \frac{w_i \phi_{i1}^2}{g}}\right] \tag{9}$$

Where:

- α_1 is modal mass coefficient for the first natural mode.
- PF_1 amplitude of mode 1 at level i.

This transformation is represented graphically in fig 3.13.

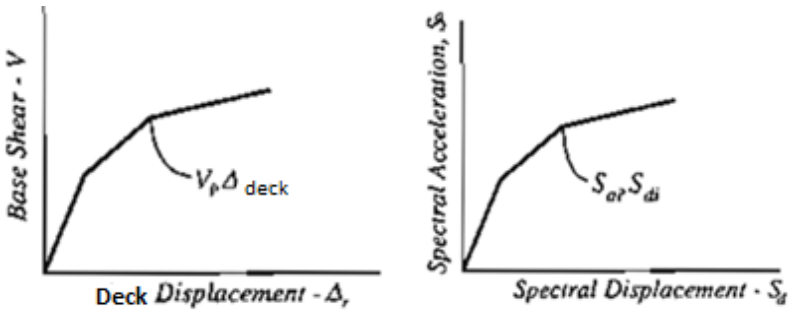

Figure 3. 13 Capacity Curve transformed into a Capacity Spectrum [30].

6. Select an initial performance point (max. acceleration a_{pi} and displacement d_{pi}). This can be done by the equal-displacement approximation or any other point based on engineering judgement (fig.3.14).
    1. The equal-displacement rule states that for long-period structures (e.g. T>1s) the inelastic spectral displacement is the same as that which would occur if the structure remained perfectly elastic. For short-period (e.g. T<0.5s) this can lead to significant differences but is a valid method to choose the initial trial performance point.

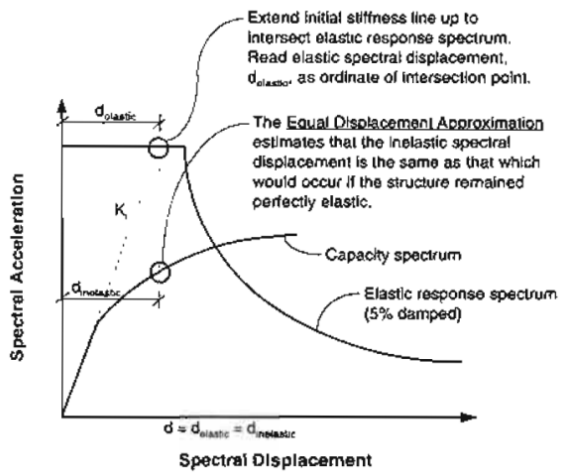

Figure 3.14 Equal Displacement Approximation [30].

7. Calculate the initial period, T_0, and the yield displacements and acceleration, d_y and a_y. These can be obtained by superimposing the capacity curve with a bilinear representation (fig.3.15) and equaling the areas between them.

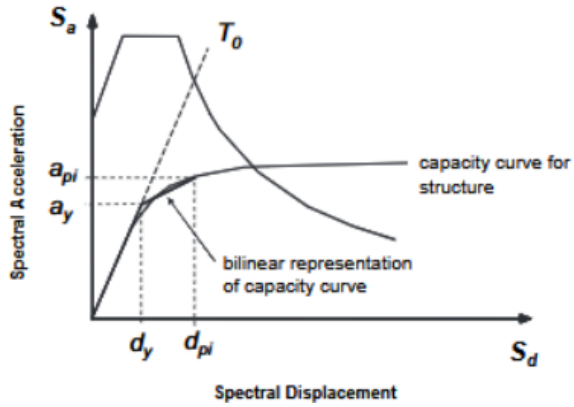

Figure 3.15 Bilinear representation of capacity spectrum [32].

8. Calculate the values of post-elastic stiffness α and ductility μ.

$$\alpha = \frac{\left(\frac{a_{pi} - a_y}{d_{pi} - d_y}\right)}{\left(\frac{a_y}{d_y}\right)} \tag{10}$$

$$\mu = \frac{d_{pi}}{d_y} \tag{11}$$

9. Using the calculated values for post-elastic stiff-ness, α, and ductility, μ, from Step 8, calculate the corresponding effective damping β_{eff} and effective period T_{eff}.

In the procedure of finding the performance point, the response spectrum has to be modified in order to consider the energy dissipation during the hysteretic cycles that lead to damage in the structure (e.g. the formation of plastic hinges).

This is done by an equivalent linear method (equivalent linearization), which consists in calculating the equivalent period (T_{eff}) and damping (β_{eff}) of the system, which are greater than the initial period and damping. With the formation of plastic hinges, the stiffness of the structure decreases, which in turn leads to increased T and damping. Both values are calculated from the maximum ductility ratio, μ. The main differences among equivalent linearization methods in the literature stem from the functions used to compute the equivalent period and equivalent damping ratio.

The FEMA 440 provides formulas for calculating T_{eff} and β_{eff} that depends on ductility and energy dissipation behaviour and can be seen in **Annex A** [32].

The FEMA440 also proposes simplified equations, in case of doubts on which model to use, that are independent on the hysteretic model or α value and are in the **Annex B**.

10. Obtain the performance point.

The FEMA440 defines 3 procedure to obtain the PP:

1. **Procedure A (direct integration) :**
   i. With the effective damping, obtain the adjusted ADRS to β_{eff}.

To obtain the adjusted ADRS to β_{eff}.:

$$S_{a\beta} = \frac{S_{a0}}{B(\beta_{eff})} \tag{12}$$

Where:

$S_{a\beta}$ is the elastic spectrum acceleration with viscous damping β_{eff},

S_{a0} is the elastic spectrum acceleration with 5% viscous damping,

$B(\beta_{eff})$ is the reduction factor given by: $\frac{4}{5.6-\ln \beta_{eff}\ (in\ \%)}$

ii. Intersect the radial effective period, T_{eff}, with the adjusted ADRS to obtain the estimated maximum displacement, d_i. The maximum acceleration, a_i, is the one corresponding to d_i on the capacity curve as shown in fig.3.16.
iii. Compare d_i with the previous (or initial) assumption. If it is within tolerances, the PP is found, otherwise repeat the process from point 6.

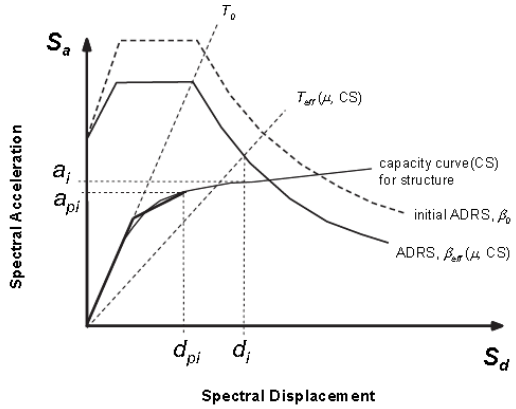

Figure 3.16 Bilinear representation of capacity spectrum [32].

- **Procedure B (Intersection with MADRS)**
  i. With the effective damping, obtain the adjusted ADRS to βeff, like in Procedure A.
  ii. Multiply the acceleration ordinates only (i.e., not the displacement ordinates) of the ADRS for β_{eff} by the modification factor, M, determined using the calculated effective period, T_{eff}.

Modified response spectrum is (MADRS), obtained by multiplying the ADRS by a factor:

$$M = {a_{max}}/{a_{eff}}. \tag{13}$$

This transformation is represented graphically in fig 3.17.

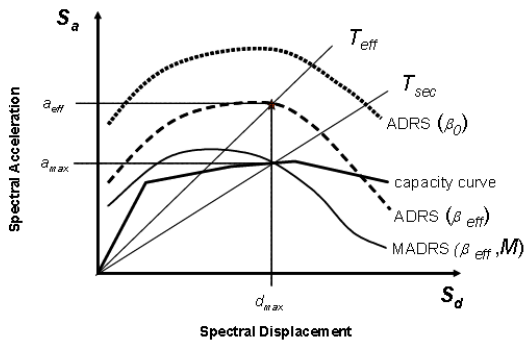

Figure 3.17 Modified acceleration-displacement response spectrum (MADRS) for use with secant period, Tsec [32].

The secant period, Tsec, is defined by the point on the capacity curve with dmax.

The factor M can also be written as:

$$M = \left(\frac{T_{eff}}{T_{sec}}\right)^2 = \left(\frac{T_{eff}}{T_0}\right)^2 \left(\frac{T_0}{T_{sec}}\right)^2 \tag{14}$$

With,

$$\left(\frac{T_0}{T_{sec}}\right)^2 = \frac{1 + \alpha(\mu - 1)}{\mu} \tag{15}$$

iii. Intersect the MADRS with the capacity curve obtain the estimated maximum displacement, d_i. The maximum acceleration, a_i, is the one corresponding to d_i on the capacity curve as shown in fig.3.18.
iv. Compare d_i with the previous (or initial) assumption. If it is within tolerances, the PP is found, otherwise repeat the process from point 6.

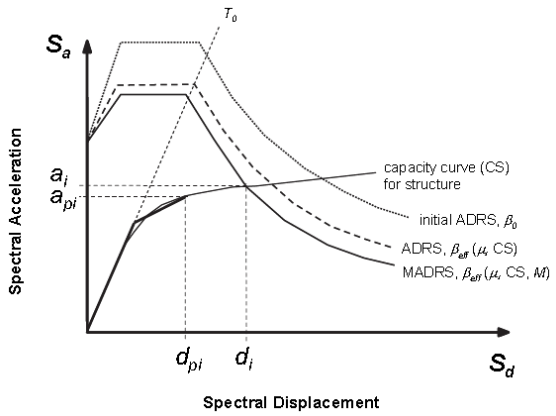

Figure 3.18 Bilinear representation of capacity spectrum [32].

2. **Procedure C** (MADRS locus of possible performance points. This procedure uses the MADRS for multiple assumed solutions (a_{pi}, d_{pi}) and the corresponding ductilities to generate a locus of possible performance points)
   i. With the effective damping, obtain the adjusted ADRS to βeff. (Described in Procedure A)
   ii. Obtain the modified ADRS, MADRS, as described previously in procedure B.
   iii. A possible performance point is obtained by the intersection of the MADRS and the radial corresponding to the secant period T_{sec}.
   iv. Increase or decrease the performance point estimated in point 6 and repeat the process to generate series of possible performance points (fig.3.19)

In this procedure the initial estimation made in point 6 should assume a ductility of μ=1.0 → d_{pi}=d_y. This would lead to the first possible performance point. In point iv) the ductility should be increased (e.g. μ=2.0 → d_{pi}=2*d_y) obtaining successive values of possible performance points until the locus of them intersects the capacity curve.

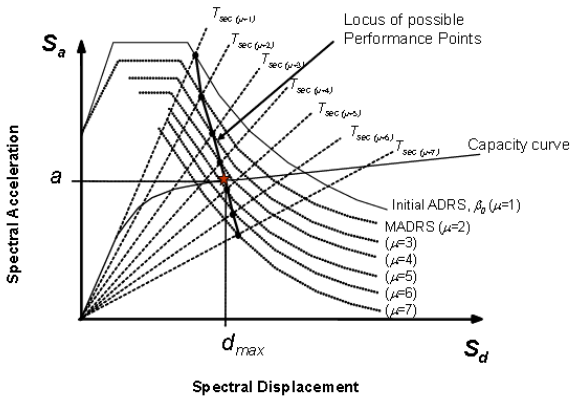

Figure 3. 19 Locus of possible performance points using MADRS [32].

3.3.2.2 Coefficient Method

The displacement coefficient method provides a direct numerical process for calculating the displacement demand.

The target displacement, which is the same as performance point, is obtained from the following equation:

$$\delta_t = C_0 C_1 C_2 C_3 S_a \frac{{T_e}^2}{4\pi^2} g, \tag{16}$$

Where:

- T_e is the effective fundamental period of the bridge in the direction under consideration: $T_e = T_i \sqrt{\frac{K_i}{K_e}}$, where:
  - T_i is the elastic fundamental period in the direction under consideration;
  - K_i is the elastic lateral stiffness in the direction under consideration;
  - K_e is the effective lateral stiffness in the direction under consideration (fig.3.20)

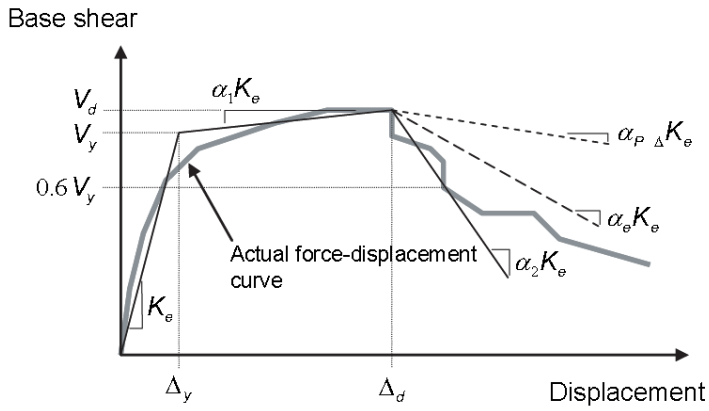

Figure 3.20 Idealized force-displacement curve for nonlinear static analysis [32].

- C_0 is a modification factor to relate spectral displacement of an equivalent SDOF system to the deck displacement of the MDOF, which can be taken as the first modal participation factor at the level of the control node or the modal participation factor at the level of the control node calculated using a shape vector corresponding to the deflected shape of the building at the target displacement.
- C_1 is a modification factor to relate the maximum inelastic displacements to the displacements calculated for linear elastic response.

$$C_1 = 1 + \frac{R-1}{\alpha {T_e}^2} \tag{17}$$

$$if\ T_e > 1s \rightarrow C_1 = 1.0$$

$$if\ T_e < 0.2s \rightarrow C_1 = 1 + \frac{R-1}{\alpha \times 0.2^2}$$

where:

- R is the strength ratio

$$R = \frac{S_a}{V_y/W} C_m \tag{18}$$

Where:

  - S_a is response spectrum acceleration, at the effective fundamental period and damping ratio of the structure in the direction under consideration;
  - V_y is the yield strength indicated in the above image;
  - W is the effective seismic weight;
  - C_m is the effective mass factor taken as the effective model mass calculated for the fundamental mode;
- α is equal to 130, 90 and 60 for site classes B, C and D

- C_2 is a modification factor to represent the effect of pinched hysteretic shape, stiffness degradation, and strength deterioration on the maximum displacement response.

$$C_2 = 1 + \frac{1}{800}\left(\frac{R-1}{T}\right)^2 \tag{19}$$

$$if\ T_e > 0.7s \rightarrow C_2 = 1.0$$

$$if\ T_e < 0.2s \rightarrow C_2 = 1 + \frac{1}{800}\left(\frac{R-1}{0.2}\right)^2$$

In nonlinear procedures or in structures with non-degrading systems, C_2 may be taken as 1.0.

(The C_3 coefficient was removed in the FEMA440, and a limit on the strength ratio R was defined.)

3.3.3 THE N2 METHOD

The designation of the method as "N2" results from the fact that a non-linear (N) analysis is involved where two (2) mathematical models are applied.

The key points of the method that is defined in the Eurocode EN 1998-1:2004 are:

- Conversion of the MDOF structure into a SDOF system using a transformation factor;
- Determination of the idealized elasto-perfectly plastic force-displacement relationship (capacity curve);
- Determination of the target displacement using the period and spectral acceleration of the idealized SDOF system.

This method is of application for structures whose behavior is not significantly affected by higher modes than the fundamental mode in each direction. This condition is deemed to be fulfilled when the fundamental period is smaller than $4T_c$ (T_c is the upper limit of the period of the constant spectral acceleration branch) and 2,0s.

The procedure is defined in point 4.3.3.4.2.1 in EN1998-1: 2004. The most relevant definitions are described in the following points.

The purpose of the analysis is to:

- Verify the ductility of the structure (ratio α_u/α_1)
  Where:

  - α_u is the value by which the horizontal seismic design action is multiplied, in order to form plastic hinges in a number of sections sufficient for the development of overall structural instability, while all other design actions remain constant. The factor α_u may be obtained from a nonlinear static (pushover) global analysis;

  - α_1 is the value by which the horizontal seismic design action is multiplied, in order to first reach the flexural resistance in any member in the structure, while all other design actions remain constant.

- Estimate the expected plastic mechanisms and damage distribution.
- Asses existing structures.
- Offer an alternative to the behavior factor q-based analysis.

In the Annex H of Eurocode EN 1998-2:2005, specific rules for the pushover analysis of bridges are given that are represented in the **Annex C**.

The procedure of the N2-method will be demonstrated in the following lines with an example using a cantilever beam.

The cantilever, shown in fig.3.21-22, has a height of 5 m with a square (0.125 * 0.125) section made of concrete (C35) and with reinforcement of 7,50 mm^2 in each side of the section. In this example the capacity curve used is obtained through the software RM Bridge and the performance point is manually calculated using the European N2 method.

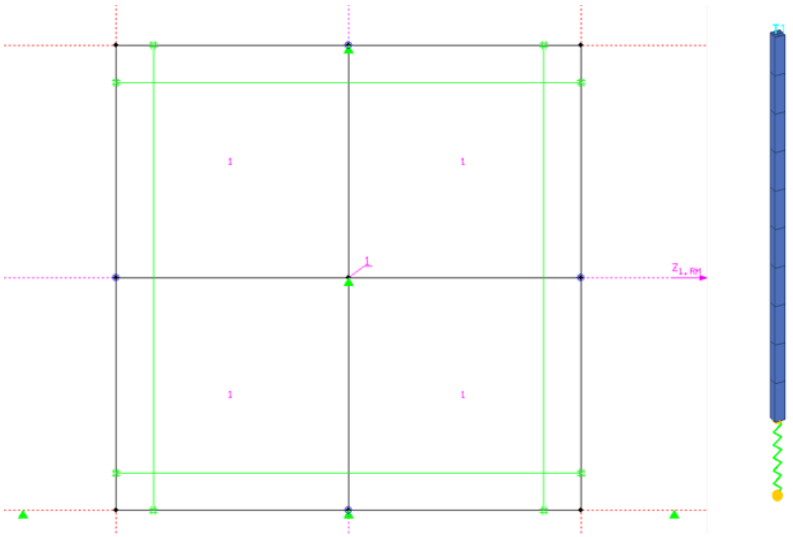

Figure 3.21 Cross-section and representation of a cantilever in software RM Bridge.

At the top of the cantilever, a weight of 0.5 kN was applied.

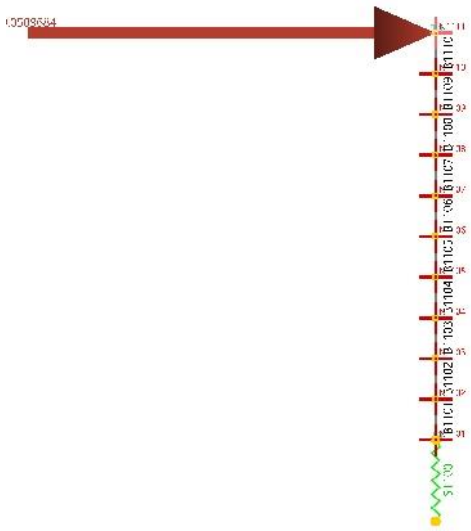

Figure 3.22 Pushover representation.

The data from Table 3.1 was used to define the response spectrum as per the EN 1998-1 (Figure 3.23).

Table 3. 1 Response spectrum data.

Ground Type	S	Tb(s)	Tc(s)	Td(s)	ζ (%)	ag/g	η
A	1	0,15	0,4	2	5	0,63	1

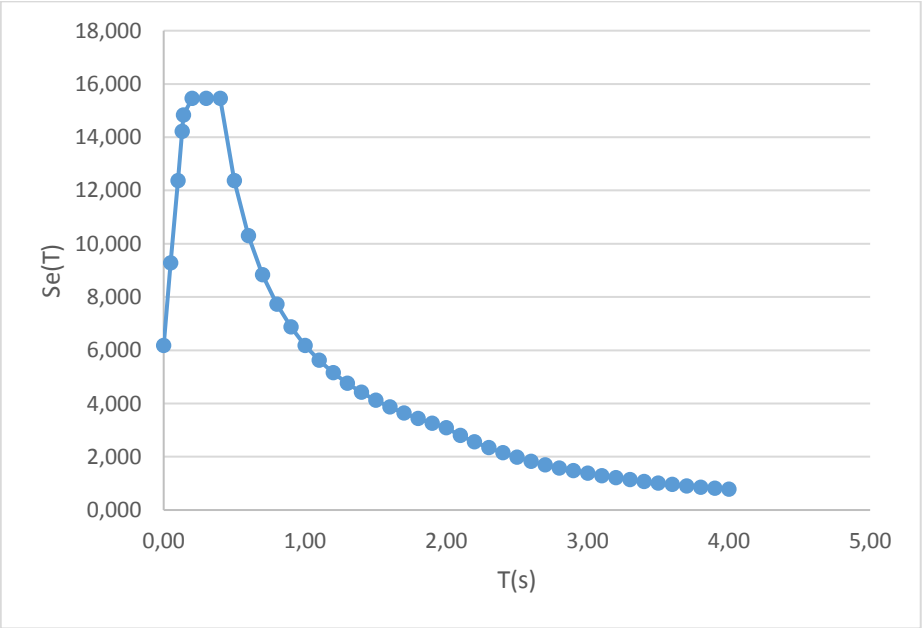

Figure 3. 23 Elastic response spectrum used for the cantilever beam example.

3.3.3.1 Definition of the Capacity Curve

The lateral load pattern shall be progressively increased (by increasing forces or displacements), and the base shear force registered reproducing capacity curve that is shown in the figure 3.24. This capacity curve was obtained using RM Bridge.

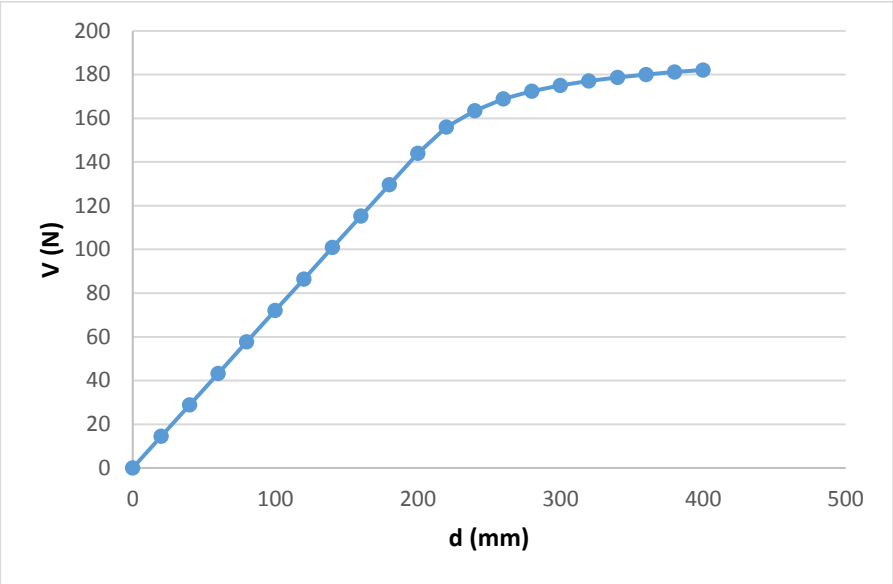

Figure 3. 24 Capacity curve obtained for the cantilever beam example.

3.3.3.2 Target Displacement Calculation

The target displacement is calculated as defined in Annex B of EN 1998-1:2004, with the following procedure:

1) The *multiple-degree-of-freedom* structure (MDOF) is transformed into an equivalent SDOF system:

- Equivalent properties of the SDOF system:
  Mass:

$$m^* = \sum m_i \phi_i = \sum F_i \tag{20}$$

  Force:

$$F^* = \frac{F_b}{\Gamma} \tag{21}$$

  Displacement:

$$d^* = \frac{d_n}{\Gamma} \tag{22}$$

Where,

- m_i is the mass of the different elements (ex:piers).
- $\phi_i$is the normalized displacement of the deck. Usually $\phi_n = 1$
- where ϕ_n is the normalized displacement of the control node.
- $F_i = m_i\phi_i$ is the normalized lateral force
- F_b is the base shear force
- d_n is the control node displacement of the MDOF
- Γ is the transformation factor:

$$\Gamma = \frac{m^*}{\sum m_i \Phi_i{}^2} = \frac{\sum F_i}{\sum\left(\frac{F_i{}^2}{m_i}\right)}$$

(23)

In this case our structure, a cantilever beam, is already a single degree of freedom system, thus, the transformation factor is 1.0.

2) Determination of the idealized elasto-perfectly plastic force-displacement relationship:

- The initial stiffness of the idealized system is determined by equaling the areas under the actual and the idealized bilinear force-displacement curve (Fig.3.25). This process is iterative, starting with the assignment of an initial value to deformation dm* and consequently F_y. Then it is possible to calculate the deformation energy (Em*) and the yield displacement (d_y^*).

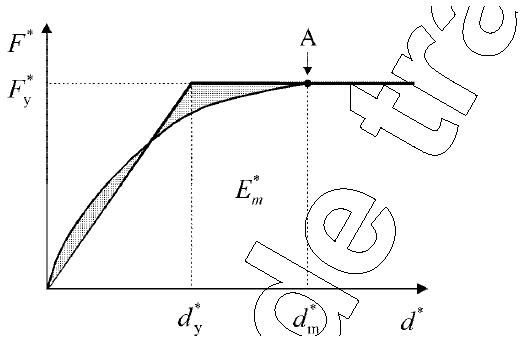

Figure 3.25 Idealized bilinear force-displacement curve [33].

In the first iteration of the worked example, dm* was adopted as 400 mm, the maximum displacement of capacity curve, and the correspondent Fy is 182 kN.

Deformation energy (Em*) is determined by calculating the area under the capacity curve, which was done using Excel, and equating the energy equation of the idealized curve (24) it is possible to calculate d_y^* (25).

$$E_m^* = \left(d_m^* - d_y\right) * F_y + \frac{d_y * F_y}{2} = 49 \text{ N.mm}$$

(24)

$$d_y^* = 2\left(d_m^* - \frac{E_m^*}{F_y^*}\right) = 2 * \left(400 - \frac{49}{182}\right) = 265\ mm \tag{25}$$

Where:

- A is the point of formation of the plastic mechanism;
- F_y* is the ultimate strength of the idealized SDOF;
- d_m* is the chosen displacement;
- d_y* is the yield displacement of the idealized SDOF;
- E_m* is the actual deformation energy until the formation of the plastic mechanism.

3) Determination of the period of the idealized equivalent SDOF system, considering the energy dissipation during the formation of the plastic mechanism.

$$T^* = 2\pi\sqrt{\frac{m^* d_y^*}{F_y^*}} = 2\pi\sqrt{\frac{51 * 265}{182 * 1000}} = 1.71\ s \tag{26}$$

(fundamental period of a SDOF system $T = 2\pi\sqrt{\frac{m}{K}}$*)*

This period is analogue to the effective period calculated in the FEMA440 method. The difference lies that the FEMA440 method uses implicit formulas relating the type of hysteretic cycles (and the associated A-H constants) and the structure ductility, whereas in the EC method the formulation relies on the deformation energy E_m.

4) Determination of the target displacement of the equivalent SDOF system.

- To obtain the displacement target it is necessary to transform the response spectrum in the format (Se, T) to format (Se, d), applying following relation:

$$d^* = S_e(T)\left(\frac{T}{2\pi}\right)^2 \tag{27}$$

(This formulation is analogue to the determination of the effective ADRS using the effective damping in the FEMA440 method.)

This transformation is represented in the **Annex D** for the cantilever beam.

Target Displacement:

4.1) The target displacement of the structure with the period (T*) and unlimited elastic behavior is obtained by intersecting the radial corresponding to T* with the $S_e(T)$ vs. d* function calculated before:

$$d^*{}_{et} = S_e(T^*)\left(\frac{T^*}{2\pi}\right)^2 \tag{28}$$

Where $S_e(T^*)$ is the elastic spectral acceleration at period T* .

For the determination of the target displacement dt* for structures in the short-period range and for structures in the medium and long-period ranges different expressions should be used:

Short period (T*<Tc):

If $F_y^*/m^* \geq S_e(T^*)$, the response is elastic and thus

$$d_t^* = d_{et}^* \tag{29}$$

If $\frac{F_y^*}{m^*} < S_e(T^*)$, the response is nonlinear and

$$d_t^* = \frac{d_{et}^*}{qu}\left(1 + (q_u - 1)\frac{T_c}{T^*}\right) \geq d_{et}^* \tag{30}$$

Where q_u is the ratio between the acceleration in the structure assuming unlimited elastic behaviour $S_e(T^*)$ and in the structure with limited strength F_y*/m*.

$$q_u = \frac{S_e(T^*)m^*}{F_y^*} \tag{31}$$

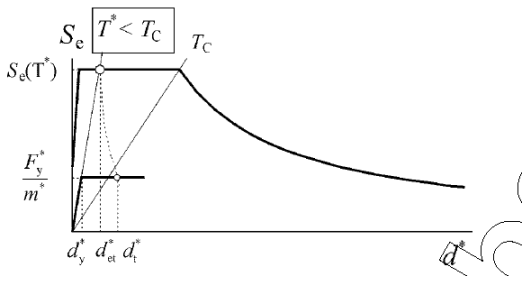

Figure 3.26 Short Period Range [33].

Medium and long period (T*≥Tc):

$$d_t{}^* = d_{et}{}^*$$

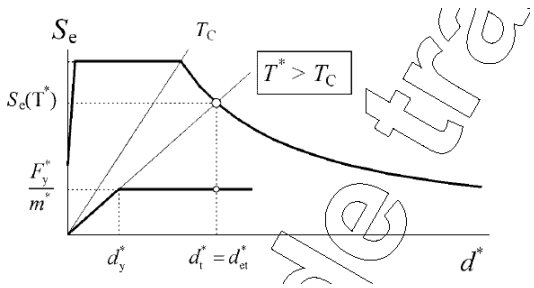

Figure 3. 27Medium and Long Period [33].

4.2) The target displacement can be obtained also by the intersection of the capacity curve of the equivalent SDOF system, converted to (Se,d*) format by dividing F* for m*, with reduced response spectrum that takes into account inelastic behavior.

It is possible to apply some formulations that exists to calculate the inelastic spectral acceleration graphic, like the ones proposed by Vidic (Vidic et. Al. 1994):

$$S_a = \frac{S_{ae}}{R_\mu} \qquad ; \; S_d = \frac{\mu}{R_\mu} S_{de}$$

Where:

- S_{ae} and S_{de} are the elastic spectral acceleration and deformation considering
- S_a and S_d are the effective spectral acceleration and deformation considering the inelastic behavior
- μ is the ductility factor given by d_{max}/d_{yield}
- R_μ is the reduction factor to account for the hysteretic energy dissipation, which can be calculated with the following equations (Miranda e Bertero 1994):
- $R_\mu = (\mu - 1)\frac{T}{T_c}$ for T < T_C
- $R_\mu = \mu$ for T ≥ T_C

In this case, T (1.71 s) of the structure is superior to TC (0.45 s) so $R_\mu = \mu = \frac{400}{265} = 1.51$. After this, it is possible to obtain the inelastic spectral acceleration, applying the Vidic formulation, that is shown in **Annex E**. Having the inelastic response spectrum, the capacity curve is transformed into the format (Se,d*) and the target displacement is obtained by the intersection between both. This target displacement corresponds as well to the intersection between the radial corresponding to the idealized period, T*, and the elastic response spectrum. The obtained target displacement was 268 mm (det*). The table 3.2 shows all the data and results obtained in analysis.

Table 3. 2 First Iteration in order to calculate displacement target.

Iteration	m*	dm*	Em*	Fy*	dy*	T*	det*	check	Rμ
1	51	400	49	182	265	1,710	268	1,49	1,51

4.3) If d_t* and d_m used in the determination of the idealized elasto perfectly plastic force-displacement relationship in point 2, are much different, points 2-4 should be repeated by using d_t* (and the corresponding F_y*) in step 2 instead of d_m*

It is possible to verify that the target displacement differs greatly from dm *, about 49%, so the second iteration was performed obtaining a target displacement closer to dm*. In the third iteration dm* was adopted as the dt* obtained in the second iteration, 263 mm, and the resulting target displacement presented a neglectable difference to this value (fig.3.28,table 3.3)

Table 3. 3 Third iteration in order to calculate displacement target.

Iteration	m*	dm*	Em*	Fy*	dy*	T*	det*	check	Rμ
3	51	263	24	169	237	1,679	263	1,00	1,11

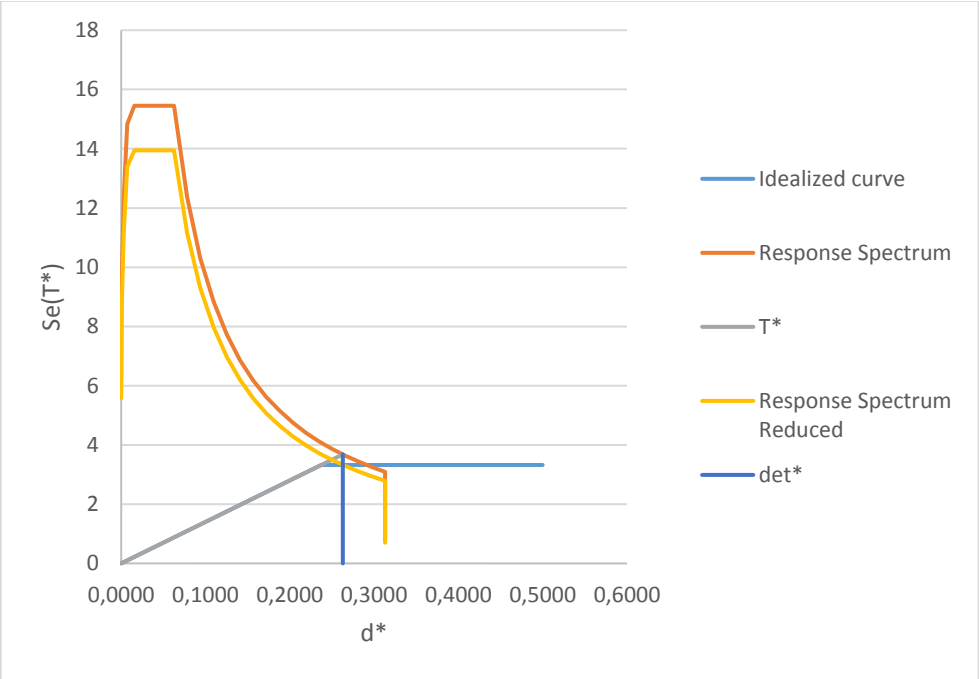

Figure 3. 28 Calculation of target displacement (EN).

5) The target displacement of the MDOF is given by:

$$d_t = \Gamma d_t^*$$

(32)

In our case, since the transformation factor is 1.0, it is the same as for the SDOF.

This analysis is performed, with the same example, in chapter 6.3, using the software used in the push-over analysis.

4.
CASE STUDY

The bridge, that is taken as case study is designated as Puente 6 de Oxec and will be situated between the kilometers 0 + 607.30 and 0 + 796.36 of the Section SB-1 of the Alternate Route of the Sur VAS in Cidade de Guatemala, Guatemala. This bridge will have a length of approximately 162 meters and will pass over the river Guadroncito. Figure 4.1 shows the location of the bridge area taken from the Google Earth application.

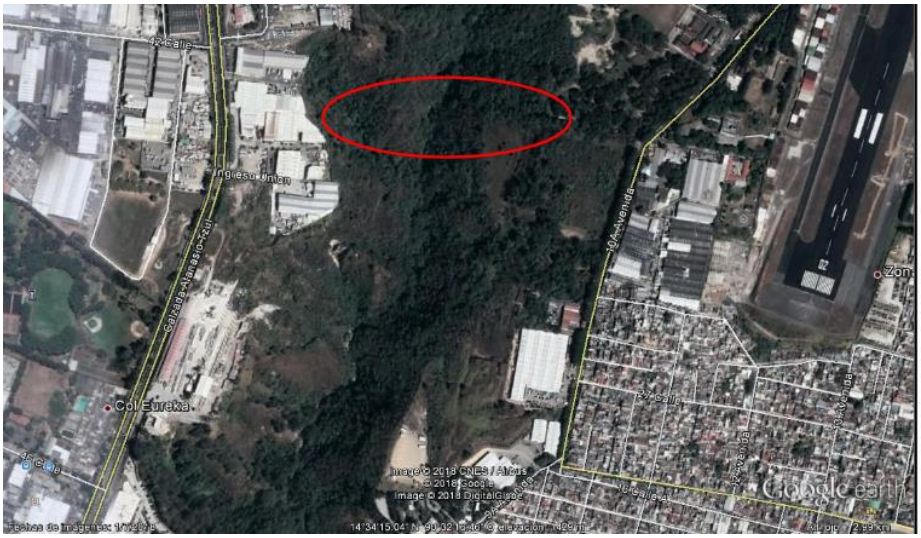

Figure 4.1 Bridge No.6 location (Google Earth), Google Earth.

As can be seen from fig.4.1 the area where the bridge will be built is currently empty, what facilitates the construction process reducing its cost.

4.1 GEOLOGICAL AND GEOTECHNICAL ENVIRONMENT

In Guatemala, three main tectonic plates interact: the one from Coco, the Caribbean and the North American, whose relative movements determine the seismic movements that are reflected on the surface. Guatemala is subdivided into four geological provinces and this project is located in the Guatemalan central mountain range. This is characterized by the presence of Paleozoic sedimentary rocks that have been weathered forming shales and phyllites, diabases and basalts.

Geologically the subsoil where most of the city of Guatemala is located, including the area where the geotechnical study was carried out, is formed by recent pyroclastic deposits of great thickness, from 200 to 400 meters. According to the document "Geological Synthesis of Guatemala" of the Center for Higher Studies of Energy and Mines (CESEM) of the USAC, the city of Guatemala is located in the physiographic province called Volcanic Belt. The pyroclastic deposits of this belt come from volcanic eruptions that have formed well-defined strata with different degrees of weathering. Some strata have also been formed by the deposition of wind ash ejected by volcanoes. The mantle of undivided volcanic rocks of this belt is at a great depth (more than 50 meters).

According to the geological map of the National Geographic Institute, the area where Bridge No. 6 will be built is of the quaternary Qtd formation, what can be seen in fig.4.2, consisting of inters stratified tephra with pumiceous diamictons and fluvio-lacustrine sediments.

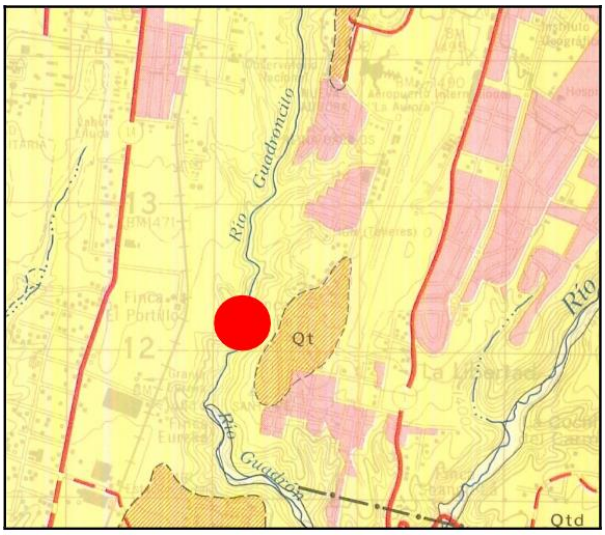

Figure 4. 2 Geological map of the zone where the Bridge No.6 will be built (Red Point), National Geographic Institute.

From the same map, it is observed that geological faults are not located in the project area. To verify the geological maps several drill holes were performed and one of them is represented in fig.4.3. The depth of exploration of the subsoil reached 15.00 meters. Coinciding with the description of the document “Geological Synthesis of Guatemala”, layers of volcanic sands were interspersed with layers of clay-like silts.

Figure 4.3 Open Drillings (Wells), PEDELTA.

4.2 SEISMICITY OF THE ZONE

The territory of the Republic of Guatemala is divided into macro zones of seismic hazard characterized by its seismicity index that varies from Io = 2 to Io = 4. The area where the bridge will be built is situated in a zone that corresponds to seismicity index Io=4 (Fig.4.4).

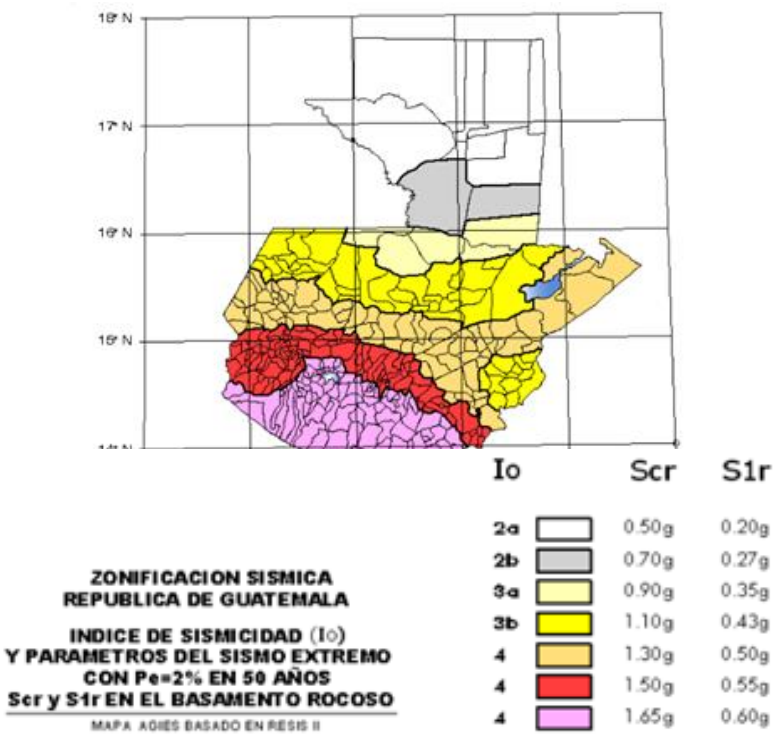

Figure 4. 4 Seismic zones in the Republic of Guatemala [35].

4.3 STRUCTURAL SOLUTION

The bridge is a steel arch of 108 m length between bow supports and 25.50 m of rise, which is completed with access spans on both sides to complete 162 m between end supports.

The deck is supported on two separate arches, with 7.50 m between axes, each of which is divided into 8 spans of 13.50 m, maintaining this same modulation in the 2 spans of each span of access to the arch. The section of the deck consists of 5 main beams, 2 located in the vertical plane of the arches, and 3 additional beams, one central and two laterals. In the fig.4.5 is represented bridge elevation view.

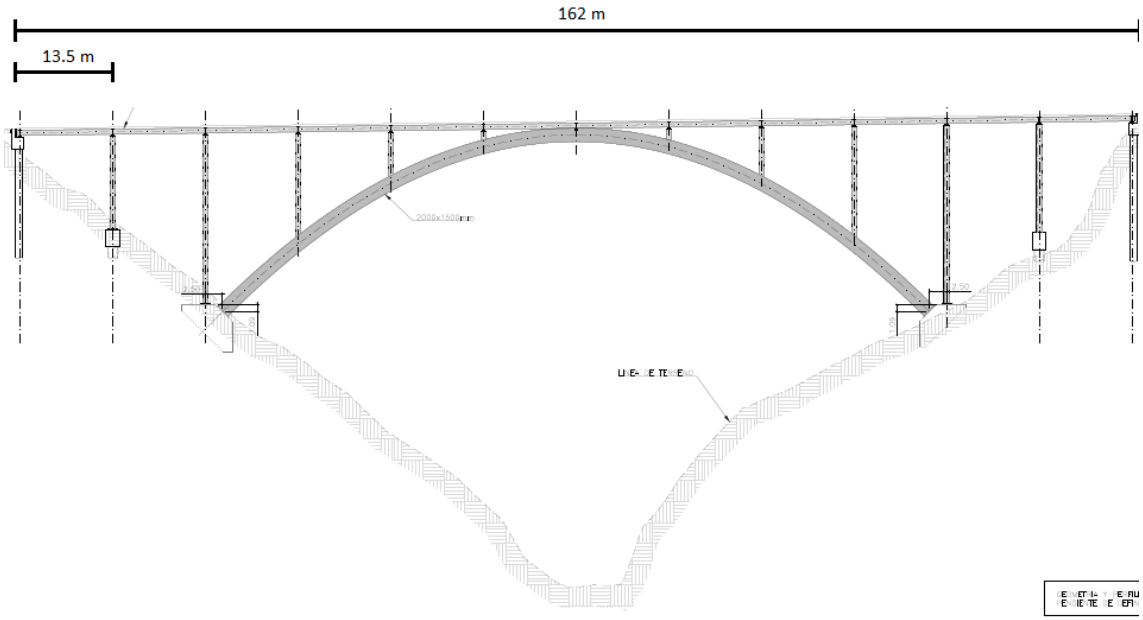

Figure 4. 5 Bridge elevation view, PEDELTA.

4.3.1 SUPERSTRUCTURE

The roadway will accommodate 4 lanes of 3.50 m plus 2 traffic barriers of 0.35 m located on the sides for a total width of 14.70 m.

The superstructure will consist of a composite deck of 1130 mm of constant depth formed by 5 longitudinal beams, of about 800mm of depth (W760x434mm), in composite action with reinforced concrete slab of 260 mm of minimum thickness.

Additionally, 4 auxiliary longitudinal girders (W360*33 mm) are disposed for the support of the lost formwork for the deck slab pouring, forming transversally small cantilevers of 500 mm (Fig.4.6).

The 5 longitudinal beams are supported on transverse beams in each pier alignment. These transverse beams are hot rolled profiles of approximately 1.10 m of depth (W1100x499) and has rigid connection in the support piles.

The piers that are in the arch are fixed in both ends. The piers outside the arch and the abutments are free in the longitudinal and fixed in the transverse direction in the connection with the deck.

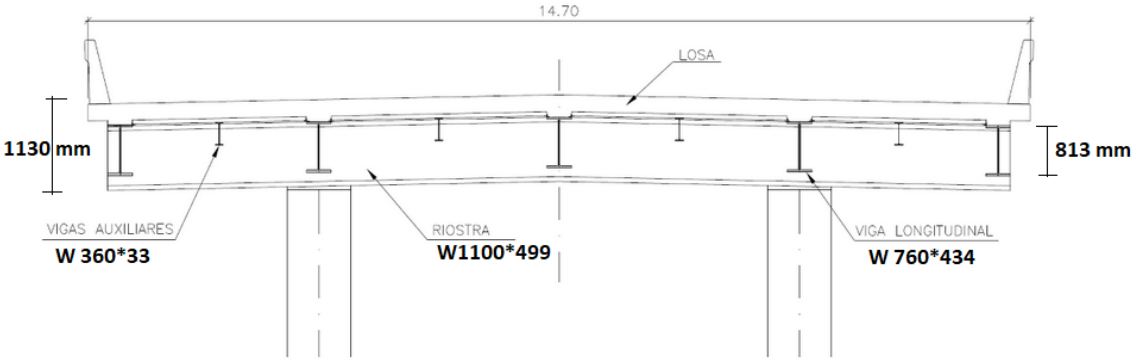

Figure 4. 6 Typical Section of the Deck, PEDELTA.

4.3.2 SUBSTRUCTURE AND FOUNDATIONS

The piers are composed by steel profiles of square section (650*650 mm) and variable thickness, fig.4.7. Their heights are also variable, adapting to the geometry of the valley and the rise of the arch. The range of heights goes from about 27 m in the final piers of the arch, to less than 2m in the piers adjacent to the key of the arches. The arches contact at the key section with the main longitudinal beams and, until the following piers (13.50 m on each key side), the contact is achieved by a stiffening plate.

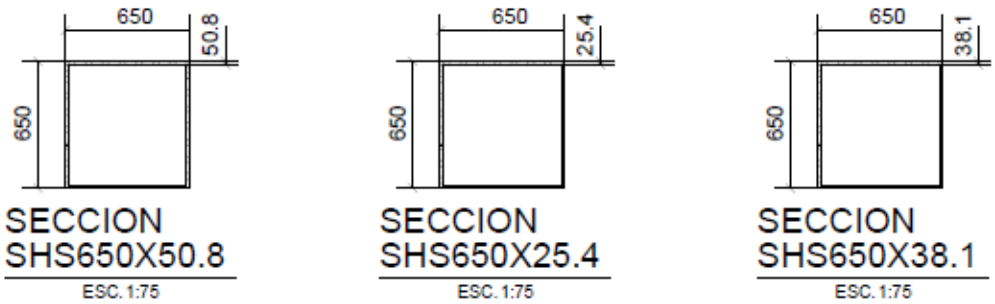

Figure 4.7 Pier Section, PEDELTA.

The arches have a parabolic shape and are designed with a stiffened bicellular constant section (Fig.4.8-9). The section is divided into two cells by a continuous central web. Stiffening is available in the vertical panels, central web and exterior walls. Although the section is relatively large, it is not considered an accessible element. Structurally, the arches are continuous and with rigid connections in the extremities.

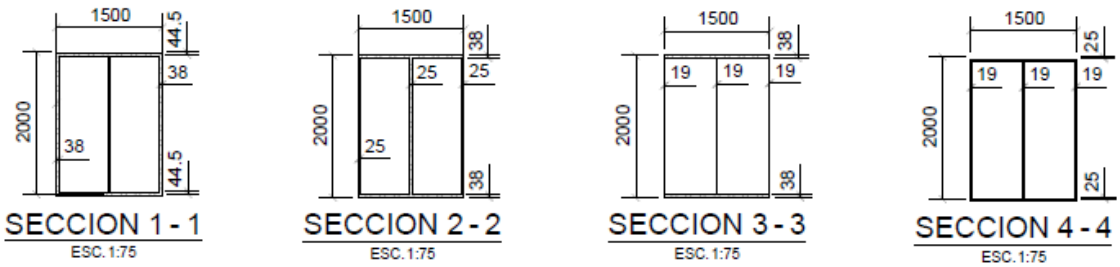

Figure 4. 8 Transverse Section of an Arch, PEDELTA.

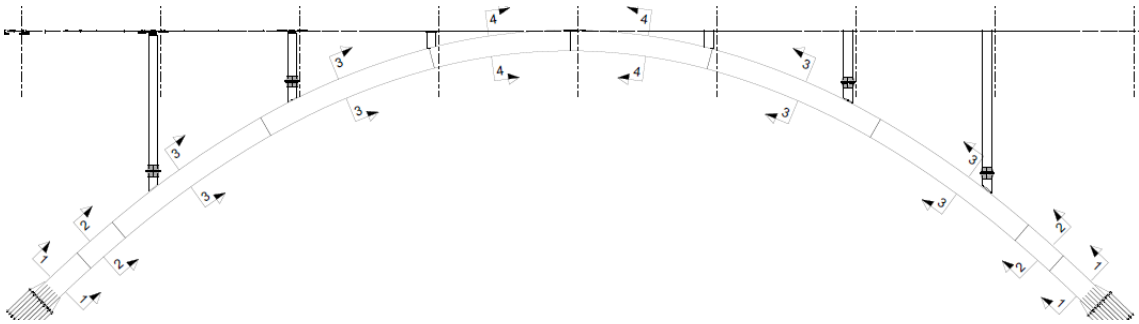

Figure 4. 9 Location of the transverse section in the arch, PEDELTA.

The foundations of piers, outside the scope of the arch, are made with concrete piles poured on site. The foundations of the arches themselves are deep and have piles of Ø1.50 m, joined in a skew head of approximate dimensions 18.50x7.60m and a depth of 4.00m, represented in the fig.4.10, which is truncated in a corner to receive the base of the arches (joint foundation).

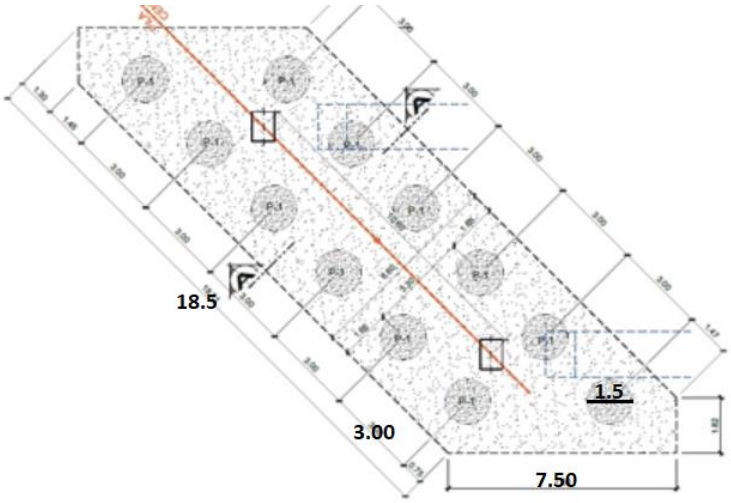

Figure 4. 10 Foundation plan-view of arch start, PEDELTA.

4.3.3 MATERIALS

Concrete:

- Deck Slab f'c = 28 MPa (4000 psi)
- Walls f'c = 28 MPa (4000 psi)
- Approach slabs f'c = 28 MPa (4000 psi)
- Piles f'c = 28 MPa (4000 psi)
- Foundation of arches and columns f'c = 28 MPa (4000 psi)

Steel and Welding:

- Reinforcement steel ASTM A706 (Grade 60), with fy ≥ 420 MPa (4200 kp / cm2).
- Structural Steel Grade 50: fy ≥ 345 MPa (3520 kp / cm2).
- Welding E70XX.

5
MODELING

For the analysis of the structure, a tridimensional model with RMBridge v8i Software from Bentley Systems was used.

The RM Bridge (Bentley Systems) is a software for the advanced calculation of structures, particularly bridges. It is a very complete tool that allows the modelling of any type of bridge and using different types of materials. The software allows to define the complete constructive process of the bridge, and to consider the rheological effects of each element. The modelling is completely parametric, so that any modification that is necessary to introduce, is updated in the whole structure, including in the loads already defined. In the fig.5.1-5.2 there is a representation of the model of the bridge.

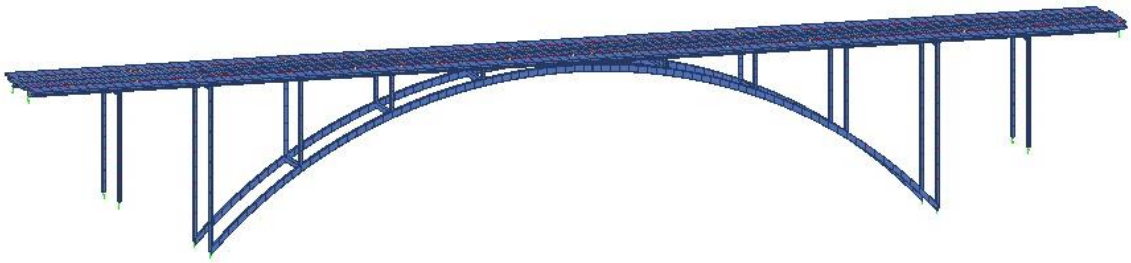

Figure 5.1 3-D View of the Model, RM BRIDGE.

Figure 5.2 Frontal View of the Model, RM BRIDGE.

As the final objective of this seismic analysis is to obtain results that refer to the substructure, the global model was adopted in this analysis, consisting only of bar elements. This type of model allows not to overload the software with unnecessary information for the effect of this analysis decreasing the calculation time and to obtain viable results.

The foundations of the piers and arch, the outer supports, are modeled by a spring with corresponding stiffnesses that have been calculated based on local auxiliary foundations model made with SAP2000 and shown in fig.5.3. A modulus of subgrade reaction of 5500 kN / m2 was used.

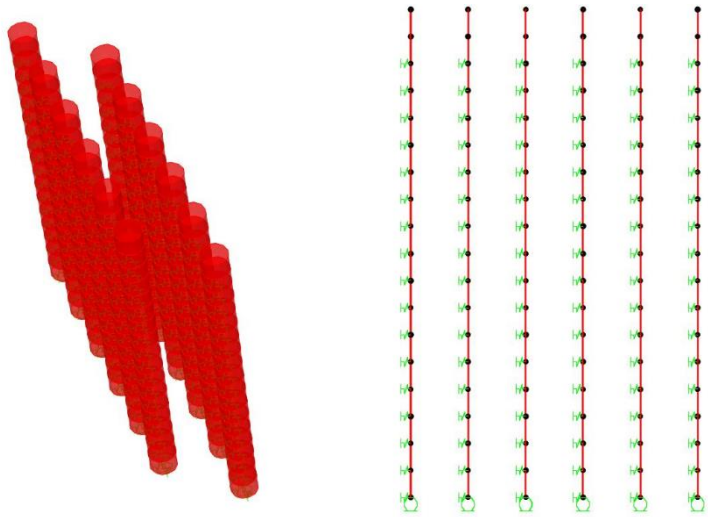

Figure 5.3 Modelled foundation with SAP2000.

As a result of this model, the following stiffnesses have been obtained:

- Klong = $4.86 \cdot 10^6$ kN/m (CY)
- Ktransv = $6.03 \cdot 10^6$ kN/m (CZ)
- Kvert = $29.3 \cdot 10^6$ kN/m (CX)
- Ɵlong = $6.07 \cdot 10^8$ kNm/rad (CMY)
- Ɵtransv = $1.34 \cdot 10^8$ kNm/rad (CMZ)
- Ɵvert = $1.45 \cdot 10^8$ kNm/rad (CMX)

The non-linear behavior between the soil and the structure will not be considered due to lack of geotechnical information and because this would imply having to define the foundations of the bridge in the general model with the corresponding non-linear behavior.

The connections between the deck and the piers that are outside the arch were modeled using simple supports, which allow displacements in the longitudinal direction and restricts them in the transversal direction.

In the case of columns connecting the deck and the arch, those are modeled so there is compatibility of displacement and rotations at the connections.

The piers were modeled using several bars and the deck is represented by 2 longitudinal beams and cross bars that simulate the transversal stiffness of the deck. In the project, the deck consists of 5 longitudinal beams, plus the auxiliary beams. However, 2 equivalent beams, representing the characteristics of the longitudinal girders, ie with an equivalent inertia (Table 5.1-5.2) were adopted.

This simplification was used in order to simplify the calculation model, because the analysis will be focused essentially in the substructure.

Table 5.1 Characteristics of the profiles in the deck.

Profile	Ix (mm4)	h (mm)	b (mm)	t (mm)	w (mm)	nº beams
W360*33	82700000	349	127	8,5	5,8	4
W760*434	6190000000	813	387	47	25,9	5

Table 5. 2 Equivalent Profile used in model.

Iresult	**31280800000**
nºbeamsModel	2
Ibeam	15640400000
h (mm)	813
b (mm)	682
t (mm)	80
w (mm)	40
I	15643591510
Ratio	1,0002

Thus, the equivalent profile has a height of 813 mm, base 682 and the thickness of the web and the flange are respectively 40 and 80 mm.

"Shear Lag" effects are not considered in this model because stress analysis of the deck will not be carried out. The modeling in RM starts with constructing the section with its real geometry and the software places the bars in the position of the center of gravity creating rigid bonds between different elements, making the modelling easier.

5.1 QUANTIFICATION OF STRUCTURE WEIGHT

The total mass of the structure to be considered in the seismic calculation includes the self-weight and the remaining permanent loads (railings, asphalt layer, traffic barriers) of the 162 meters of deck, and also 50% of the linear live load (HS20) applied along the 162 meters of road, according to the regulation – AASHTO LRFD, as the bridge is situated in Guatemala.. All these masses were introduced into the structure in the form of forces, distributed and concentrated, and in the form of masses for the modal analysis.

5.1.1 SLAB WEIGHT

The weight of the slab has been determined from its geometry with a concrete volumetric weight equal to c = 24kN / m3 (AASHTO LRFD 3.5.1).The concrete slab has an average thickness of 292 mm formed by:

- A structural thickness of 235 mm.
- An average thickness of 63.5mm / 2 = 32 mm due to the preformed sheet metal that makes the functions of lost formwork (type 22 gauge steel).
- Possible pavement variations of 25 mm (DW).

In addition, this slab will be placed above small "haunches" on the steel beams, to allow certain adjustments. The theoretical average height of the haunches is 80mm (± 5mm by pumping), considering the maximum for load effects and the minimum to fix the structural position of the slab (the haunch itself is neglected in the structural check). The additional equivalent thickness, for loading purposes, is approximately:

Haunches: 5 beams x 0.40 x 0.085 / 14.70 = 12 mm

Also, for loading purposes, the weight of the lost formwork sheet is added: 10 kg / m^2.

$$W_{slab} = \frac{(235 + 32 + 25 + 12)}{1000} m^2 * \frac{24kN}{m^3} + \frac{0.10kN}{m^2} = 7.4kN/m^2 \tag{33}$$

$$W_{slabDeck} = 108.8\ kN/m \tag{34}$$

$$PP_{slabDeck} = \frac{108.8}{2} = 54.4\ kN/m \tag{35}$$

All the loads will be applied to the two longitudinal beams (fig.5.4).

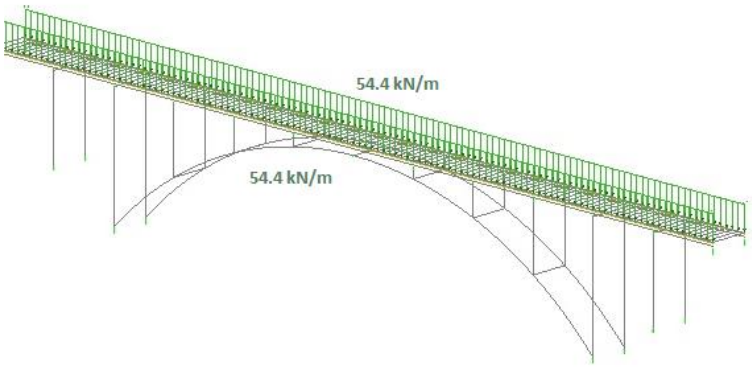

Figure 5. 4 Permanent Load of Slab, RM BRIDGE.

5.1.2 SUBSTRUCTURE WEIGHT

Permanent Load of the Substructure, shown in fig.5.5, is calculated automatically based on the cross section of the elements and density which is equal to = 77 kN / m3 (Structural Steel). The secondary element weights (stiffeners, connection plates, welding ...) have been included by increasing density to a fictitious value 10% higher.

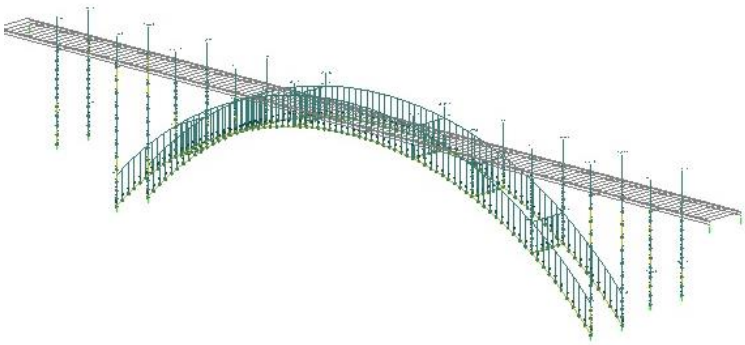

Figure 5.5 Permanent Load of the Substructure (Arch, Transverse Beam, Pier), RM BRIDGE.

5.1.3 DECK WEIGHT

Since the model doesn't include the diagonals and stiffening of the deck, the permanent load relative to the deck has been calculated separately and will be applied as an external load. For the weight of the metal part of the deck, a ratio of 209 kg / m2 + 5% due to connections, etc. was adopted based in the design developed by the company. The fig.5.6 represents the obtained load.

$$PP_{Deck} = \frac{14.7 * 219 * 9.81}{2 * 1000} = 15.83\ kN/m \tag{36}$$

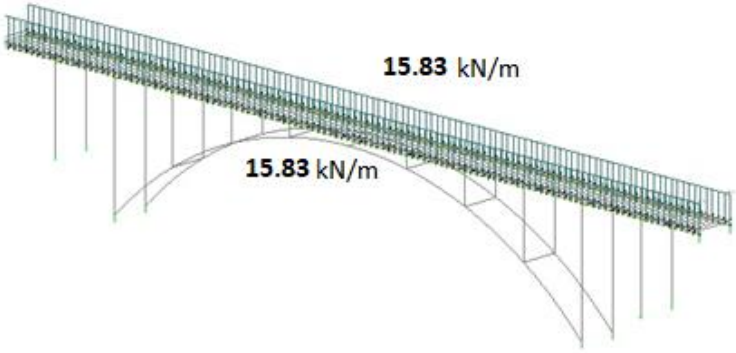

Figure 5. 6 Permanent Load of the Deck, RM BRIDGE.

5.1.4 REMAINING ELEMENTS

A weight has been taken into account due to possible future pavement (bituminous mixture) of 60 mm thickness.

$$DW_{FuturePav} = 0.06 * 23\frac{kN}{m^3} = 1.38\ kN/m^2 \tag{37}$$

The deck doesn't incorporate lateral sidewalks. The roadway is protected by New Jersey barriers on both sides whose weight is estimated at 6.00kN / m each (fig.5.7).

$$SIDL = \frac{(1.38 * 14 + 6 * 2)}{2} = 15.66\ kN/m \tag{38}$$

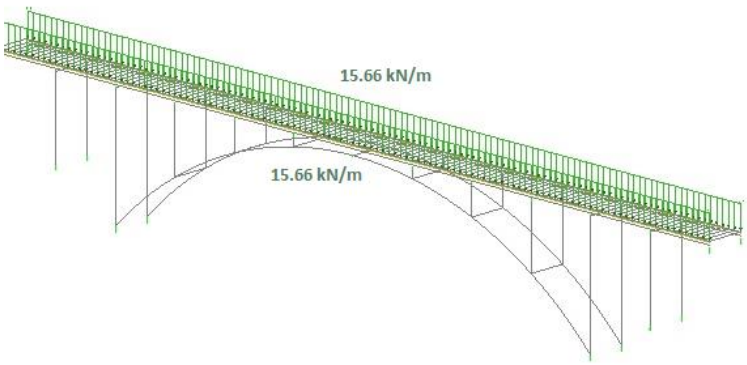

Figure 5. 7 Permanent Load (SIDL), RM BRIDGE.

5.1.5 LIVE LOAD

For the purpose of calculating the values of the live loads (vehicle load model), the AASHTO LRFD 2017 (HL-93) criterion is adopted, as the bridge is situated in Guatemala.

The number of design lines is obtained as:

$$n^{o}_{lines} = \frac{RoadWidth}{3.6} = \frac{14}{3.6} = 3.88 = 3 \text{ lines} \tag{39}$$

However, the actual lane width is less than 3.65m (3.50m), and the platform accommodates 4 real lanes, so it is designed for 4 lines of 3.50m. The multiple presence factors specified in the regulations have been adopted and summarized in Figure 5.8 according to the calculation action.

Number of Loaded Lanes	Multiple Presence Factors, *m*
1	1.20
2	1.00
3	0.85
>3	0.65

Figure 5. 8 Multiple Presence Factors,m. (AASHTO 3.6.1.1.2-1)

The vehicle load of the AASHTO-LRFD 2017 standard called HL93 consists of the combination of:

- Design Truck or Tandem and
- Design Lane Load

Design Truck:

The design truck consists of a hypothetical 3-axle vehicle with a total load of 325kN and wheelbase as shown in Figure 5.9.

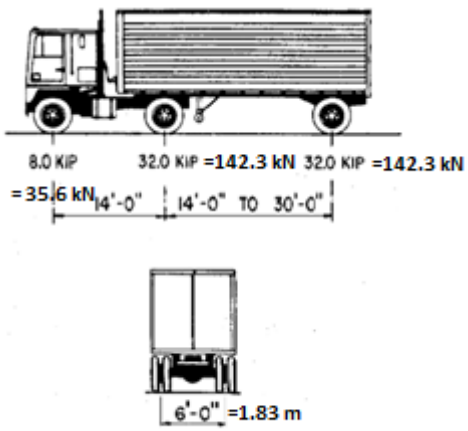

Figure 5. 9 Characteristics of the Design Truck. (AASHTO 3.6.1.2.2-1).

Additionally, the bridge must allow the passage of a special vehicles type T3-S2-R4 (Figure 5.10). This truck will not be considered in the seismic action due to the low probability of simultaneous occurrence.

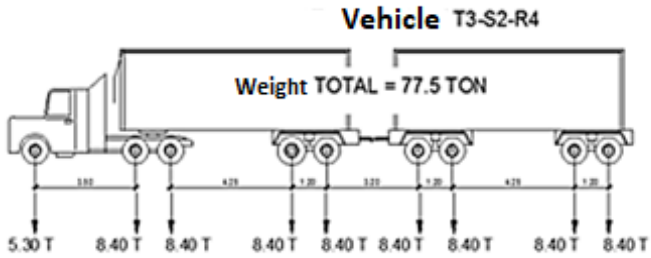

Figure 5. 10 Characteristics of the special permit vehicle (NSE Guatemala).

Design Tandem:

The tandem axis consists of two equal loads of 110kN separated 1.2m in the longitudinal direction and 1.8 m in the transverse direction.

Design Lane Load:

The rail load consists of an overload of uniform value in the longitudinal direction and equal to 0.93t / m (9.30 kN / m) applied in a lane width of 3.0m (equivalent to a surface load of 3.1 kN / m2).

The application of the loads in each lane will take the most unfavorable effect of the following two combinations:

- The effect of the design tandem axle combined with the lane load.
- The effect of the design truck combined with the lane load.

The impact factor (IM), expressed as a percentage of the live load, is determined according to Figure 5.11, applying to the loads produced by the design truck or the tandem axis. Resulting loads are represented in fig.5.12-13.

Component	IM
Deck Joints—All Limit States	75%
All Other Components:	
• Fatigue and Fracture Limit State	15%
• All Other Limit States	33%

Figure 5. 11 Dynamic Load Allowance (AASHTO)

$$D_{TrackLoad} = \frac{325*1.33*0.65*4}{2} = 562 \text{ kN} \tag{40}$$

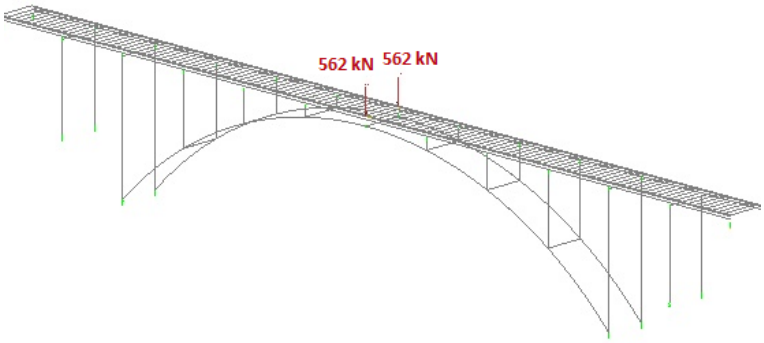

Figure 5. 12 Live Load- Design Truck, RM BRIDGE.

$$D_{LaneLoad} = \frac{9.3*0.65*4}{2} = 12 \text{ kN/m} \tag{41}$$

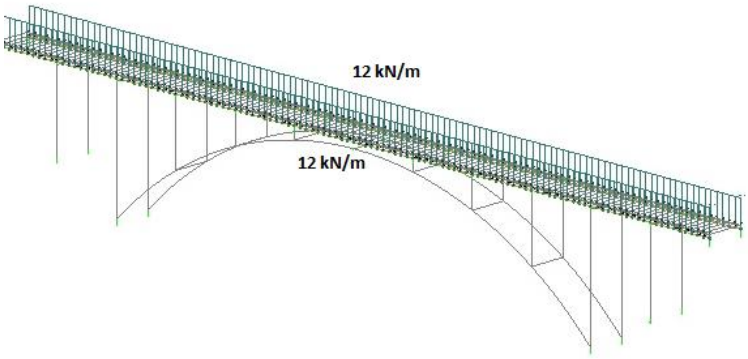

Figure 5. 13 Live Load-Lane Load, RM BRIDGE.

5.2 VERIFICATION OF THE MODEL

Once the model was finished, some checks have been performed.

Does the model reasonably replicate actual loads?

Figures 5.14 to 5.16 show the deflection of the structure according to the applied load, the dead weight of the deck. In Fig. 5.14 a constant distributed load was applied which resulted in a more pronounced deformation in the middle of the arch. This deformation was expected, since the two extreme piers of each side are supported by foundations and therefore have a high stiffness. In turn, the piers that lean on the arch have a lower stiffness in the support and with the application of the loads the deck deflects.

Figure 5.15 shows an antisymmetric load, equal to uniform load but just applied in a half of the bridge, and the corresponding deflected structure. The same effect of the extreme piers as in figure 5.14 is observed. The load applied on the deck causes the deck to "sit" and the arch to deform. The deformation of the arch where it is loaded causes the arch to bend on the opposite side of the loading, as expected. Deformation in the Figure 5.16 is also as planned, the arch deforms where it is loaded and bends in the central part.

The amplitude of the deformation differs in both cases, in the antisymmetric case it is almost twice higher.

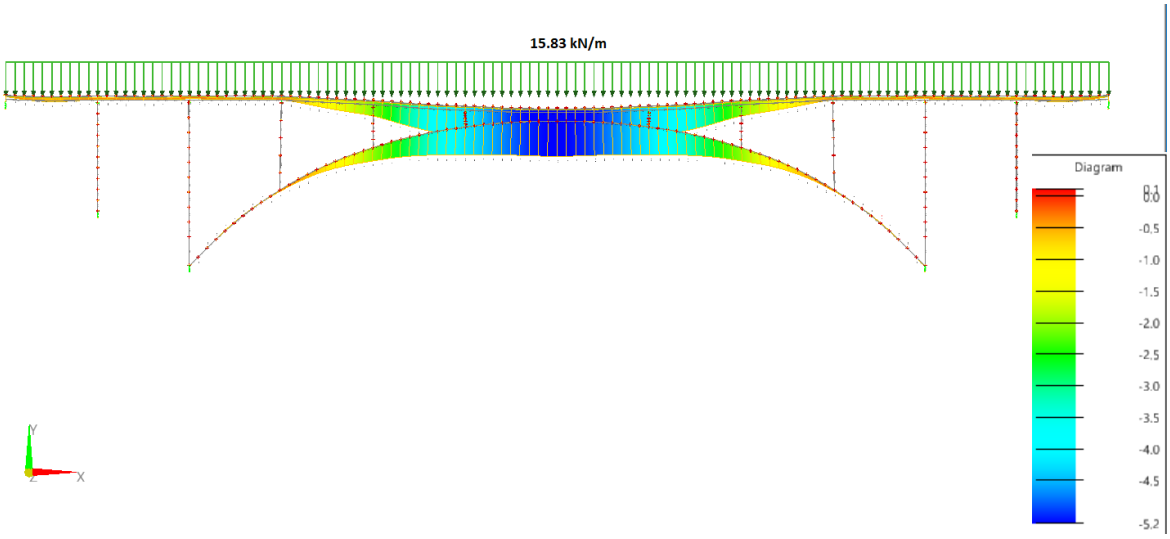

Figure 5. 14 Deflected structure due to uniform permanent load (15.83 kN/m).

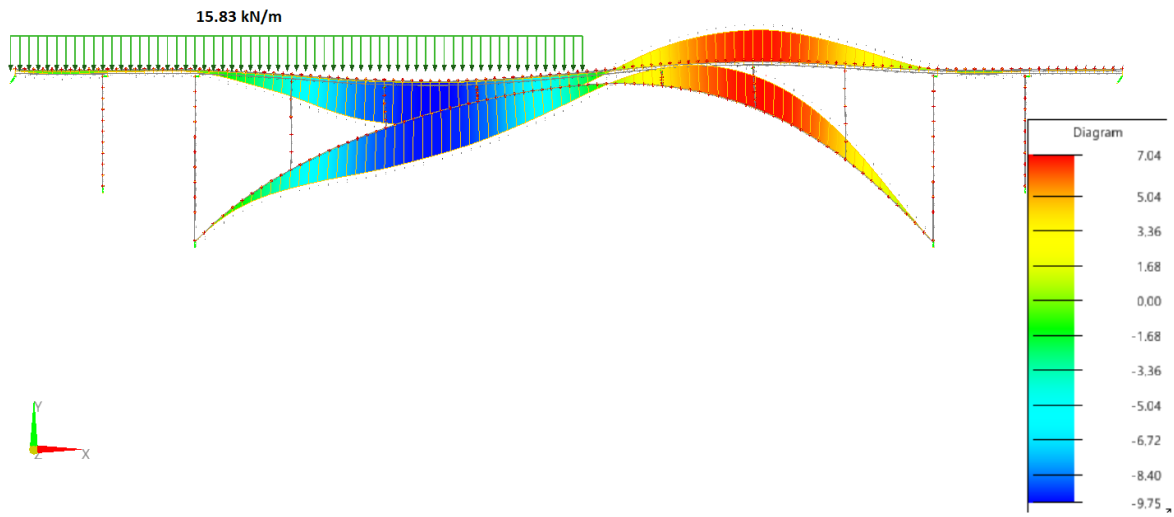

Figure 5. 15 Deflected structure due to antisymmetric load (15.83 kN/m).

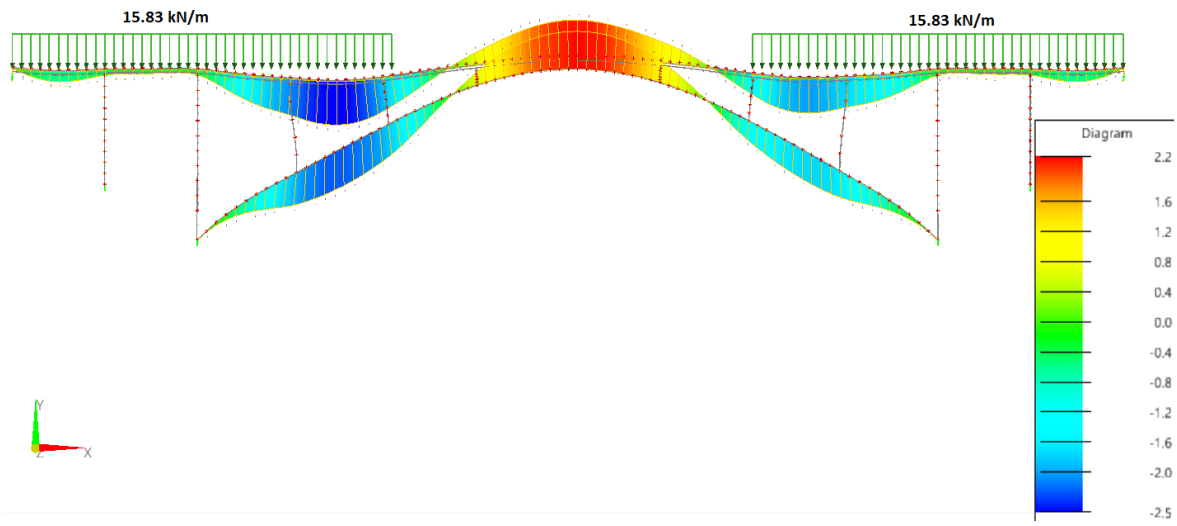

Figure 5. 16 Deflected structure due load at the ends of structure (15.83 kN/m).

Does the model reasonably replicate the load paths?

Accordingly, to Figures 5.17 and 5.18, it is possible to confirm that the load distribution is symmetrical (deck load) as expected taking into account that the structure is symmetrical and is submitted to a symmetric loading.

The sum of all vertical and horizontal loads is very close to zero, which means that the structure is in static equilibrium.

$$\sum Fv = 89.01 * 2 + 89.02 * 2 + 237.77 + 237.79 + 237.78 + 237.75 + 955.63 + 955.29 + 955.58 + 955.25 = 5128.9 - 15.83 * 162 * 2 = -0.02 \quad (42)$$

$$\sum Fh = 966.10 + 965.68 - 965.71 - 966.08 = -0.01 \quad (43)$$

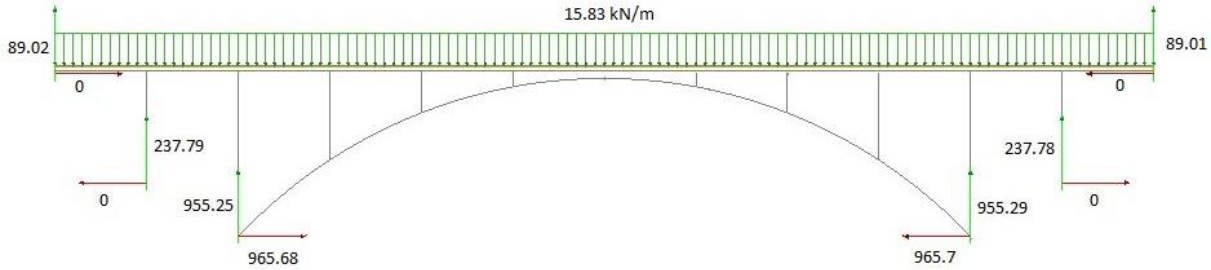

Figure 5. 17 Support reactions due to permanent load, 15.83kN/m. (Arch nº1).

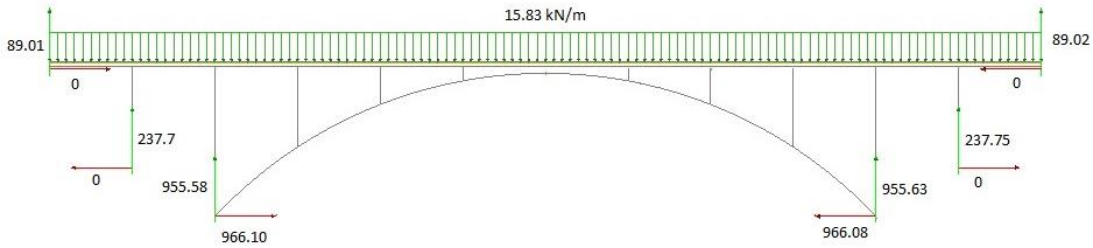

Figure 5. 18 Support reactions due to permanent load, 15.83kN/m. (Arch nº2).

Does the model fairly reproduce structural behavior?

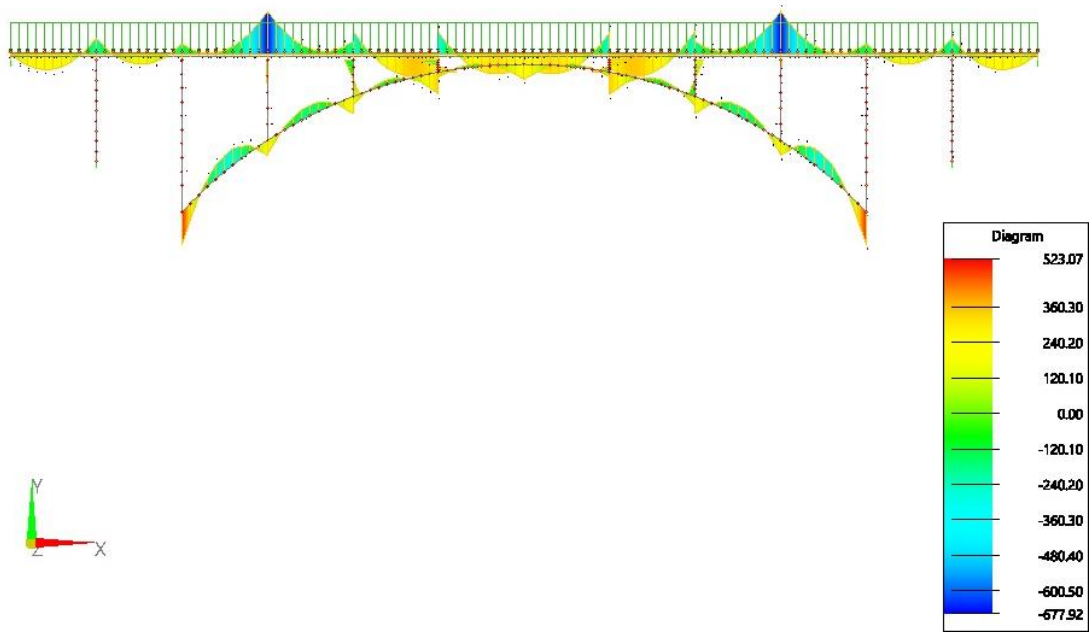

Figure 5. 19 Moments Mz due to permanent loads (deck load=15.83 kN/m).

Figure 5.19 represents the in-plane bending moments due to permanent loads corresponding to the dead weight of the deck. The analysis of this figure enables the following conclusions:

- The arch has low bending moments as it is mainly subjected to axial loads. At the supports of the arch there is a big positive moment because it is where the great amount of internal forces coming from the arch are concentrated and have to be balanced. It represents the behavior of a "inverted" continuous beam.
- The middle of the deck is subjected to positive bending moments which are consistent with the respective deformation (Fig.5.14).
- The third pier from the end has the greatest negative moment. Checking the deformation of the structure it is possible to verify that the deformation of the deck starts from that pier and great tension occurs over it and hence the respective negative moment.
- The piers that are simply supported have no bending moment, though the ones that are connected to the arch are subjected to a small moment. The shorter piers have low flexibility, so any small displacement causes internal forces.

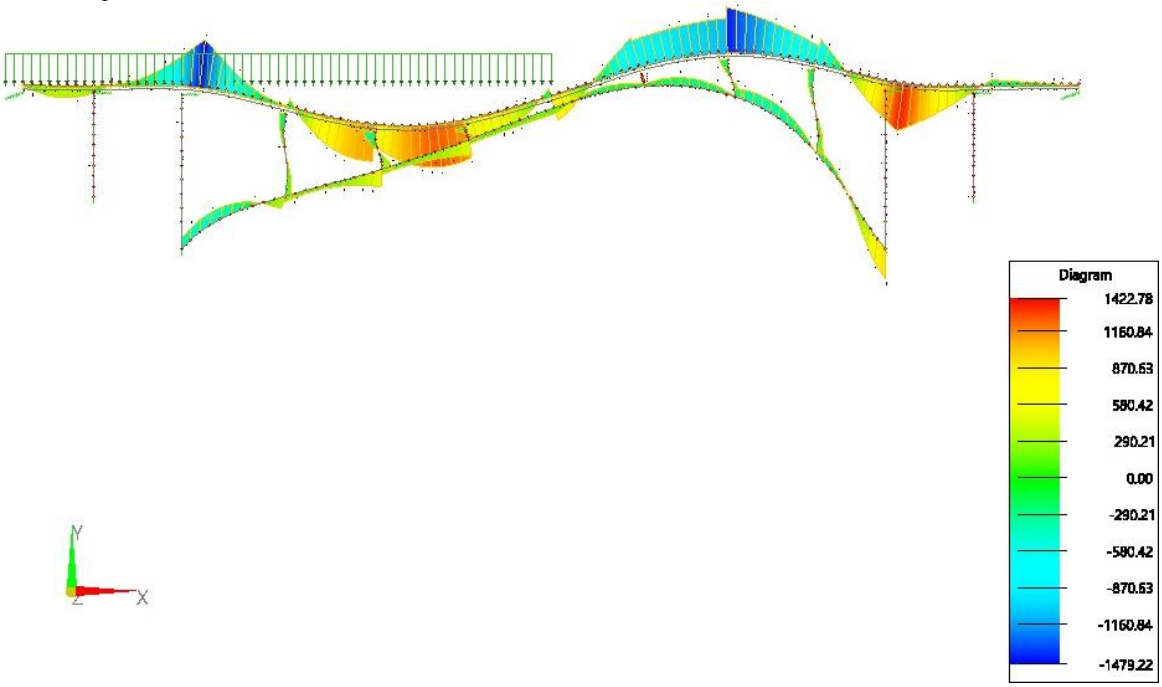

Figure 5.20 Moments Mz due to antisymmetric load (15.83 kN/m)

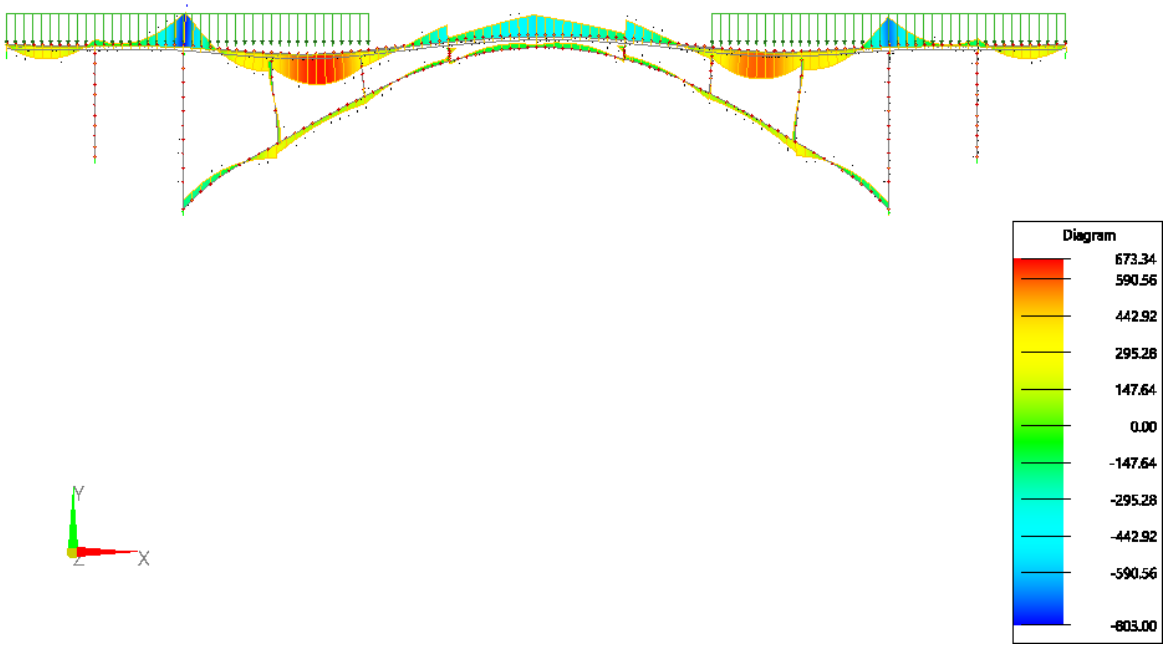

Figure 5. 21 Moments Mz due to loads at the ends of the structure (15.83 kN/m)

The resulting bending moments, due to antisymmetric load (fig.5.20), that represents a part of the load corresponding to the dead weight of the deck, and applied load at the ends (fig.5.21), are also in agreement with the expected ones:

- Low moments in the arch and piers.
- Negative moments in the zones of the deck where there is tension in the upper fiber and positive where the "sitting" of the deck occurs.

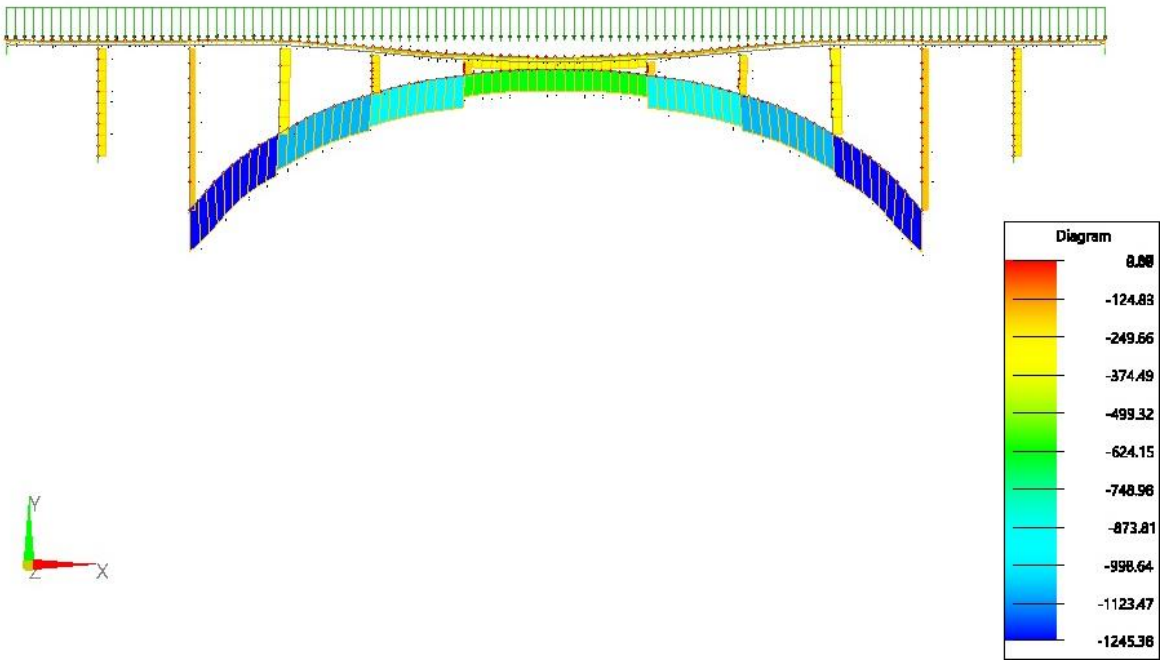

Figure 5. 22 Forces Nx due to permanent load (15.83 kN/m)

In Fig.5.22 it is possible to verify the axial load distribution, due to the dead weight of the deck, and, as mentioned earlier, these forces concentrate mainly in the arch. Each time the arch meets a pier the axial stress in the arch increases due to the transfer of load that occurs between the pier and arch.

Does the model reasonably reproduce the mechanical behavior?

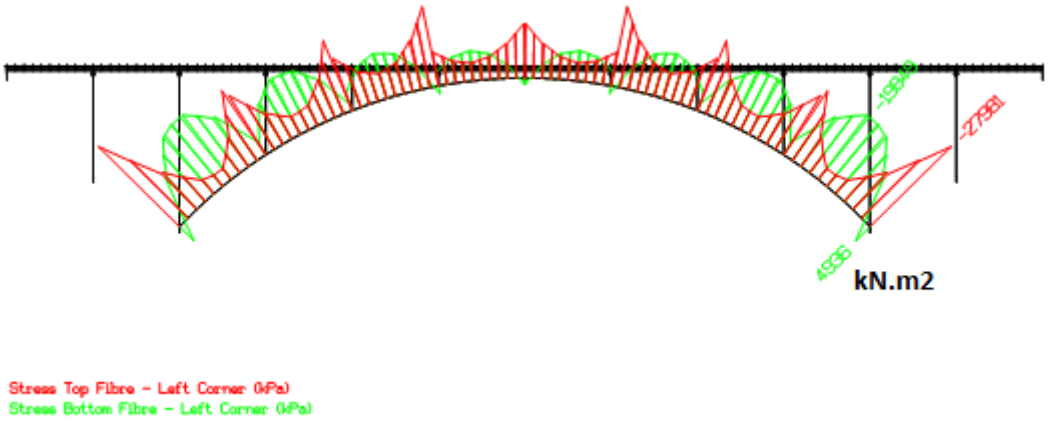

Figure 5. 23 Stresses in the arch.

In Figure 5.23 it is represented the diagram of stresses in the arch measured in the lower and upper fiber of the arch. Both stresses recorded are above the arch, which means that the arch is compressed in its totality for the case when dead weight of the deck is applied; Tensile stresses were only registered in the lower fiber in the zone of supports. This stresses are due to the large amount of concentrated internal forces in this zone.

5.3 Obtaining Natural Modes and Frequencies

Having defined the mass of the structure, a Modal analysis was performed in the software RM Bridge. This analysis is done in order to obtain the fundamental information about the dynamic characteristics of the bridge structure. In the table 4.3 it is possible to find the periods and effective mass ratios of the first 10 modes. Mode 1 is the fundamental mode in the transverse direction with an effective mass ratio of 79.2 % and period of 1.25 s, and Mode 4 is fundamental in the longitudinal direction with 43.45% of effective mass ratio. Modes 2, 3, 7, 8, 9 represent local mechanism when side piers of the bridge deflect.

Table 5. 3 Eigenvalue analysis results.

			Effective mass ratio (%)			
Mode	Frequency (Hz)	Period, T(s)	Longitudinal	Vertical	Transverse	Deflection mode
1	0,801	1,24843945	0	0	**79,2**	Out-of-plane
2	1.205	0,00082988	2,26	0	0	Local Mechanism
3	1.205	0,00082988	0	0	0	Local Mecha.
4	1.311	0,00076278	**43,45**	0	0	In-plane anti-symmetric
5	2.311	0,00043271	0	9,65	0	Out-of-plane
6	2.381	0,00041999	0	0	0	In-plane
7	2.795	0,00035778	0	0	0	Local Mecha.
8	2.795	0,00035778	0,55	0	0	Local Mecha.
9	2.998	0,00033356	0	0	0	Local Mecha.
10	2.999	0,00033344	0	0	0	Local Mecha.

The fig.5.24 shows the deflection of the structure when subjected to the first mode and the fig.5.25 for the fourth mode, that is in-plane and anti-symmetrical.

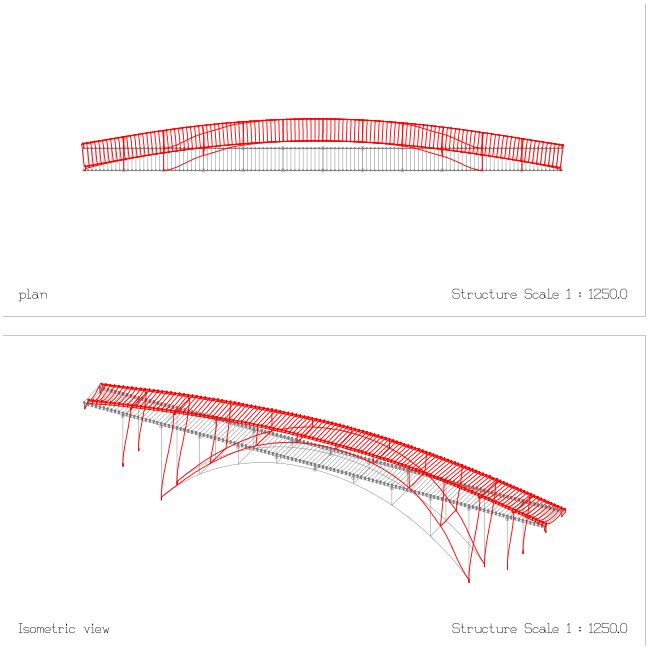

Figure 5. 24 Mode 1, f=0.801.

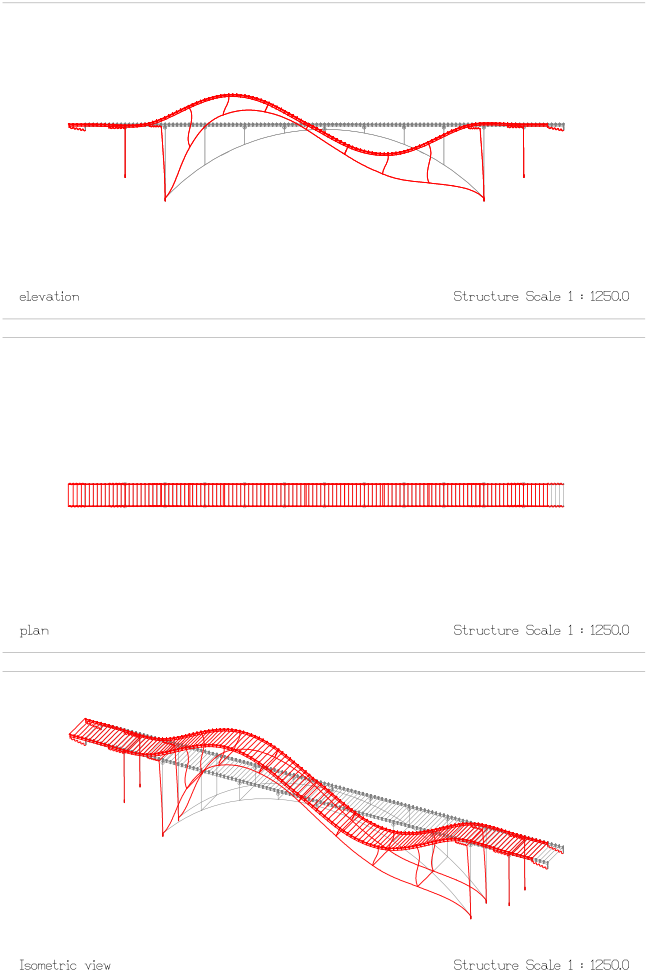

Figure 5. 25 Mode 4, f=1.311.

5.3 RESPONSE SPECTRA

A spectrum is an envelope of the maximum values recorded so it reproduces the worst-case scenario in terms of maximum seismic accelerations experienced for a given structure considering a given return period.

For the seismic calculation the Guatemalan spectrum was defined. Due to the fact that the calculation software uses internal variables characterizing the response spectrum in the pushover analysis, such as the transition period (T_C in the EC) or the structural damping (ξ), and that the structural damping isn't explicitly defined in the Guatemalan response spectrum, in order to take advantage of the implemented internal variables, the Guatemalan response spectrum was defined as an equivalent response spectrum using the EN1998-1(3.2.2.1) formulation.

5.3.1 RESPONSE SPECTRUM OBTAINED FROM STRUCTURAL SAFETY RULES OF GUATEMALA (NSE 2 DE AGIES)

As previously mentioned, the area where the bridge will be built is situated in a zone that corresponds to seismicity index Io=4,according to the Guatemala standard [35].The structure classifies as Category III (Important), with a level of seismic protection D and must be designed to a "severe" design earthquake with a probability of occurrence of 5% in 50 years with K_d=0.80 [35].

For the municipality of Guatemala, the short-period spectral ordinate Scr is 1.50 g and, with a period of one second of the extreme earthquake S1r, of 0.55g (Fig.5.26).

Figure 5. 26 Seismic zoning of Guatemala [27].

The soil profile or classification is C with a coefficient for short vibration periods Fa equal to 1.2 and for long periods Fv equal to 1.4 (Fig.5.27-5.28).

"Comentario sobre sitios clase C: Para el caso del Valle de Guatemala los posibles suelos C comprenden los depósitos piroclásticos conformados de ignimbritas, cenizas y arenas. Se presentan en casi toda la superficie del valle a algunos metros de profundidad. Los requisitos para perfil C se logran frecuentemente para proyectos con varios sótanos que penetran debajo de los depósitos superficiales menos densos.

Comment on Class C sites: For the case of the Valley of Guatemala possible C soils comprise pyroclastic deposits formed from ignimbrites, ashes and sands. They occur in almost the entire surface of the valley some meters deep. The requirements for profile C are achieved often for projects with several basements that penetrate below the less dense surface deposits [35]*."*

Clase de sitio	Índice de sismicidad				
	2.1	2.2	3.1	3.2	4.1 4.2 4.3
AB	1.0	1.0	1.0	1.0	1.0
C [1]	1.3	1.2	1.2	1.2	1.2
D	1.4	1.2	1.1	1.0	1.0
E	1.7	1.3	1.1	1.0	0.9
F	Se requiere evaluación específica - ver Sección 4.4				

[1] En los casos en que la investigación de suelos abreviada no especifique si un suelo firme clasifica como C o como D, el factor Fa se tomará del suelo C.

Figure 5. 27 Site coefficient Fa [35].

Clase de sitio	Índice de sismicidad				
	2.1	2.2	3.1	3.2	4.1 4.2 4.3
AB	1.0	1.0	1.0	1.0	1.0
C	1.5	1.5	1.5	1.5	1.4
D [1]	2.2	2.0	1.9	1.8	1.7
E	3.3	2.8	2.6	2.4	2.2
F	Se requiere evaluación específica - ver Sección 4.4				

[1] En los casos en que la investigación de suelos abreviada no especifique si un suelo firme clasifica como C o como D, el factor F_v se tomará del suelo D.

Figure 5. 28 Site coefficient Fv [35].

The value of Scr and S1r should be adjusted to the conditions on the surface, according to the profile of the soil that covers the basement on the site.

$$S_{cs} = S_{cr} * F_a \tag{44}$$

$$S_{1s} = S_{1r} * F_v \tag{45}$$

With these factors, we obtain Scs of 1.80 and a S1s = 0.77.

Thus, for a kd (this quantity has the same meaning as the importance factor) scale period of 0.80, the spectral design ordinates are obtained: S_{cd} 1.54 and S_{1d} 0.611.

$$S_{cd} = K_d * S_{cs}/\eta \tag{46}$$

$$S_{1d} = K_d * S_{1s}/\eta \tag{47}$$

The spectral ordinate Scr and S1r are both for a damping of 5% of the critical. Bolted steel structures have damping ratios of about 4% (EN1998-2 4.1.3), so it is necessary to correct the spectral design ordinates, dividing it with the damping correction factor for a viscous damping of 4%. For this, the formulation given in AASHTO-4th (7.1) was used:

$$\eta = \left(\frac{\xi}{0.05}\right)^{0.3} = \left(\frac{0.04}{0.05}\right)^{0.3} = 0.935 \tag{48}$$

The period Ts (s) that separates the short periods from the long ones is 0.428 s.

$$T_s = \frac{S_{1d}}{S_{cd}} \tag{49}$$

The spectral ordinates Sa (T) for any period of vibration T, are defined as:

$$S_a(T) = S_{cd} \text{ , if T} \leq T_s \tag{50}$$

$$S_a(T) = \frac{S_{1d}}{T} \text{ , if T} > T_s \tag{51}$$

Finally, it is possible to obtain the final spectrum accordingly to the regulations of Guatemala. This spectrum is represented in fig.5.29.

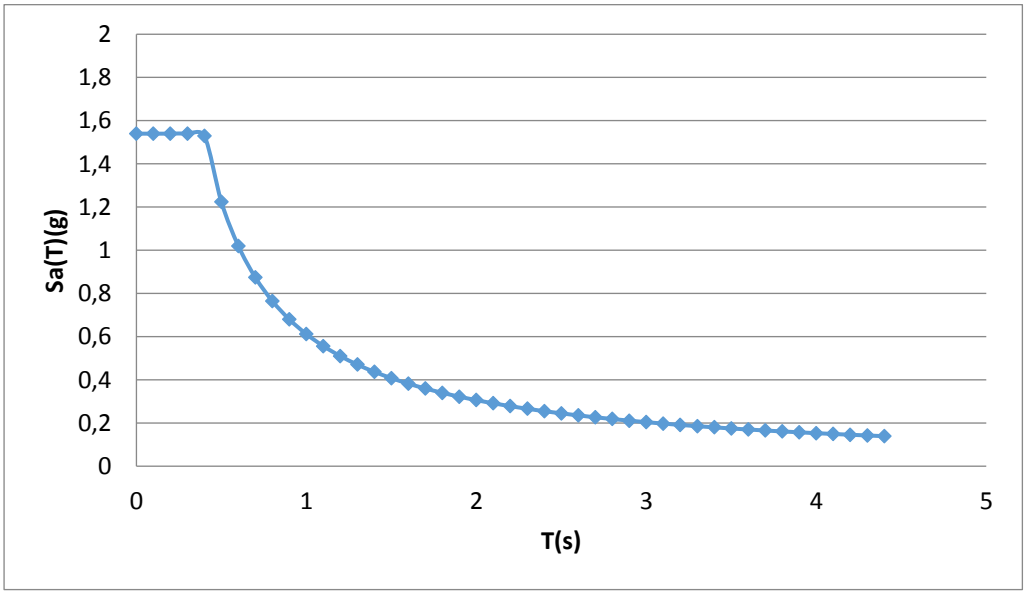

Figure 5. 29 Response Spectrum made accordingly with Guatemalan Regulations (NSE 2 DE AGIES).

5.3.2 EN1998-1: 2004 SPECTRUM

With the Guatemalan response spectrum constructed, it is possible to obtain the equivalent response spectrum as per the Eurocode EN1998-1: 2004. In order to characterize the spectrum, a soil Type A will be used, given that it corresponds to a transition period, Tc, similar to the one obtained in the Guatemalan Response spectrum, Ts. Fig.5.30 shows the response spectrum accordingly to EN.

Considering the equations of both regulations it is possible to obtain the design ground acceleration, ag, of the EN response spectrum, and scale the remaining parts that correspond to the interval 0 to Tb and from Td, which are not considered in the Guatemalan spectrum.

Table 5. 4 Information used for the transformation of Guatemalan spectrum into spectrum accordingly to EN.

Ground Type	S	Tb(s)	Tc(s)	Td(s)	ξ (%)	η	Scd(g)
A	1	0,15	0,4	2	4	1,05	1,54

$$a_g * S * \eta * 2.5 = S_{cd} \ (=) a_g = 0.58 \tag{52}$$

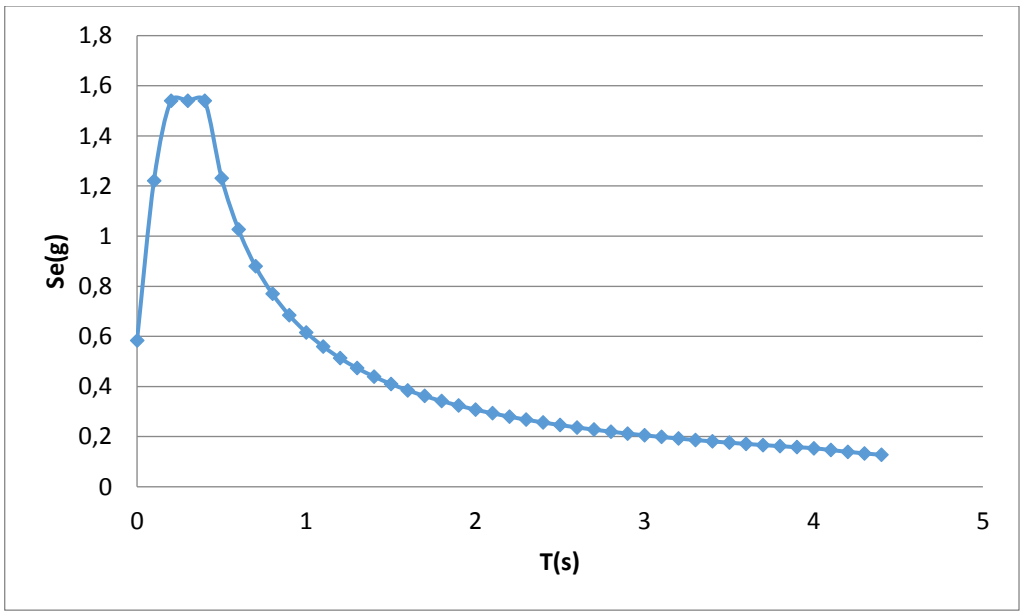

Figure 5. 30 Response Spectrum EN for the case study.

Comparing the graphics of fig.5.29 and fig.5.30 in one graphic, represented in fig.5.31, it is possible to see that the difference is small.

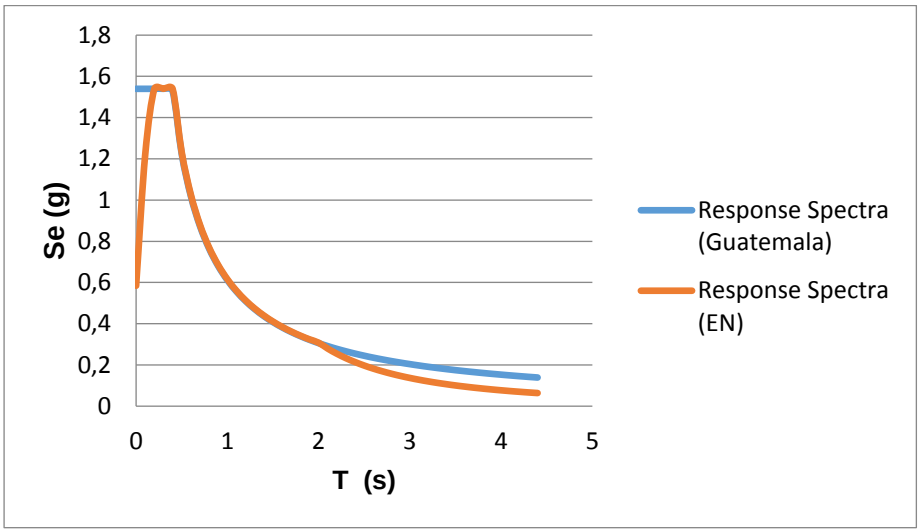

Figure 5. 31 Response Spectrum (Guatemala vs EN).

The superposition of the response spectrums represented in fig.5.31 shows that the EN spectrum starts to diverge after the period T_D, corresponding to 2s. This difference is due to the fact that in the spectrum of Guatemala and AASHTO this transition does not exist. The European spectrum considers that after a period of 3-6 s the spectral displacement tends to a constant value which implies that the acceleration spectrum becomes inversely proportional to T^2. Thus this parameter (T_D) will be modified and adopted as 4.0s resulting in the spectrum shown in fig.5.32.

Table 5. 5 Information used for the transformation nº2 to spectrum accordingly to EN (Tc=0.4 s).

Ground Type	S	Tb(s)	Tc(s)	Td(s)	ξ (%)	η	Scd(g)
A	1	0,15	0,4	4	4	1,05	1,54

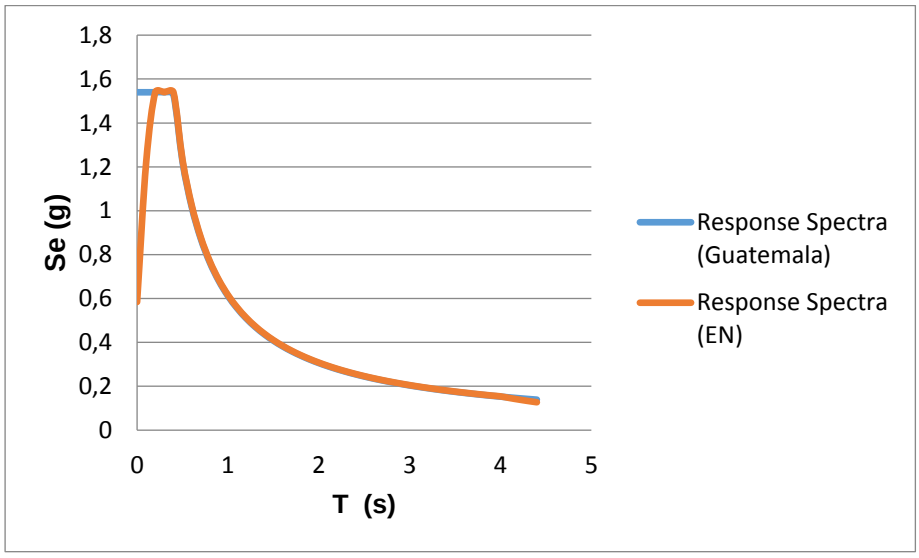

Figure 5. 32 Response Spectrum taking into account change in Tc. (Representing Guatemalan vs EN)

5.3.3 BEHAVIOUR COEFFICIENT

The response modification factors indicated in AASHTO LRFD 3.10.7.1 are not adequate to this type of structure. For this reason, in the preliminary design of the bridge, a criterion of "limited ductility" has been used, which is not too far from the elastic response. In particular, the following response modification factors have been considered during design:

- Longitudinal earthquake R = 1.50
- Transverse earthquake R = 1.50

This approach, conceptually aligned with what is exposed in other internationally accepted standards for this type of bridges, allows reasonable structural sections. For the design of connecting elements, foundations, etc. an "essentially elastic" behavior has been assumed, equivalent to a response reduction factor of 1.0.

6. NONLINEAR ANALYSIS PUSHOVER

The importance and advantages of this type of analysis has been discussed previously. However, this analysis also presents some limitations in its application:

- This analysis starts from the assumption that the structure response corresponds to a system of one degree of freedom, governed by the first mode. Structures that are governed by vibration modes with higher frequencies can result in imprecise results.
- Irregular structures may produce imprecise results due to inaccurate distribution of the forces of inertia.
- In bridges with very high piers and consequently flexible, the higher frequency modes may assume greater importance.

Therefore, pushover analysis will be done only in the transversal direction because in the longitudinal direction the modal mass that is mobilized is very low which would lead to unreliable results. Vertical excitation is not taken into account because vertical earthquake input has very little effect on the seismic behavior of steel arch bridges accordingly to Okumura et al [36]], and because the bridge is not located close to an active fault, which is the requirement for consideration of the vertical excitation in AASHTO.

6.1 CLASSIFICATION OF CROSS-SECTIONS

In order to proceed with a non-linear analysis, it is necessary to classify the sections and verify that they can develop their plastic capacity, ie if they are of class 1 or 2 (according to EC formulation). Therefore, three representative sections corresponding to the arch birth, the base of the outer pier and the first column of the arch, were classified according to EN 1993-1-1:2005 table 5.2.

In tables 6.1 and 6.2 it is possible to verify that c/t, where *c* is the plate inner length and *t* is the corresponding thickness, is inferior to C1 limit imposed for the three sections. Consequently, all of the three sections were classified as class 1 and can form a plastic hinge.

In the **Annex F** the table 5.2 from EN 1993-1-1:2005 is represented and the manual classification for the outer pier. The internal forces (N, M) corresponds to the last step of the pushover analysis, in the case of a load pattern with modal distribution. The calculated strains were obtained from a section model using Fagus.

Table 6. 1 Classification of three representative sections according to EN 1993-1-1:2005 table 5.2.

	DATA					
	N (kN)	M (kNm)	εc (def. compr. Max)	εt (def. tracc. Max)	h (mm)	Compressed height (mm)
Arch	-16543	33618	1,4	0,9	1500	913
Outer Pier	-2974	5183	6,1	3,8	650	401
Column 1	-2869	-4536	1,3	1	650	367

Table 6. 2 Classification of three representative sections according to EN 1993-1-1:2005 table 5.2.

	Classification EN					
	α	ε	c (mm)	t (mm)	c/t	limit C1
Arch	0,61	0,83	693	44,5	16	47
Outer Pier	0,62	0,83	599	25,4	24	47
Column 1	0,57	0,83	574	38	15	51

6.2 NON-LINEAR BEHAVIOR OF MATERIAL

The monotonic nonlinear behavior of the materials should be known in the form of a tensile-strain relationships, the laws of material behavior which contain the variation of the rigidity of the constituent materials as a function of the tensions and deformations to which they are subjected. In this bridge there is only one structural material which is steel. Figure 6.1 shows the considered non-linear behavior of the steel.

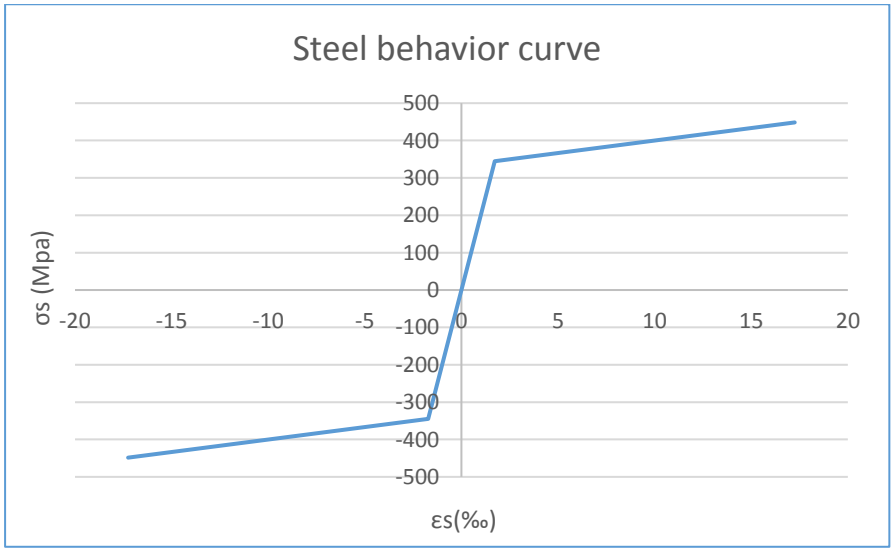

Figure 6. 1 Material curve for steel.

To create the graph, the following data, extracted from AASHTO LRFD, was used:

- Fy=345 MPa
- Fu/Fy=1.3
- εy=E/Fy=345/200000=1.725‰
- εu/εy =10

Steel elements are susceptible to local buckling effects. *"Buckling is characterized by a sudden sideways deflection of a structural member" (Wikipedia)*. Local buckling may limit the section capacity by preventing the attainment of the yield strength. To circumvent this problem that cannot be considered in the software, the curve of the material was modified, limiting the ultimate strain based on the work developed by Zheng that studied the local buckling behavior of box-sections and proposed empirical formulas of ultimate strain [36].

For unstiffened box sections:

$$\frac{\varepsilon_u}{\varepsilon_y} = \frac{0.8\left(1-\frac{N}{N_y}\right)^{1.09}}{\left(R_f-0.2\right)^{3.26}} + 3.58\left(1-\frac{N}{N_y}\right)^{0.839} \leq 20.0\,, \begin{matrix} 0.2 \leq R_f \leq 0.7 \\ 0.0 \leq N/N_y \leq 0.5 \end{matrix} \tag{53}$$

For stiffened box sections:

$$\frac{\varepsilon_u}{\varepsilon_y} = \frac{0.8\left(1-\frac{N}{N_y}\right)^{0.94}}{\left(R_f\lambda_s^{0.18}-0.168\right)^{1.25}} + 2.78\left(1-\frac{N}{N_y}\right)^{0.68} \leq 20.0\,, \begin{matrix} 0.3 \leq R_f \leq 0.5 \\ 0.0 \leq N/N_y \leq 0.5 \end{matrix} \tag{54}$$

Where:

N = Axial force

N_y=Fy*A

R_f= flange width-thickness ratio parameter of box section.

λ_s= stiffener´s slenderness ratio parameter

B = width of the flange plate

t = thickness of the flange plate.

n = nº of subpanels divided by the longitudinal stiffeners

a = stiffener`s length

r_s= radius of gyration of a T-shape cross-section consisting of one longitudinal stiffener and the adjacent subpanel of width B/n.

Q = local buckling strength of the subpanel plate.

$$R_f = \frac{B}{t}\sqrt{\frac{12(1-\upsilon^2)}{4n^2\pi^2}}\sqrt{\frac{\sigma_y}{E}} \tag{55}$$

$$\lambda_s = \frac{1}{\sqrt{Q}}\frac{a}{r_s}\frac{1}{\pi}\sqrt{\frac{\sigma_y}{E}} \tag{56}$$

$$Q = \frac{1}{2R_f}\left[\beta - \sqrt{\beta^2 - 4R_f}\right] \leq 1.0 \tag{57}$$

$$\beta = 1.33R_f + 0.868 \tag{58}$$

Approximate axial stresses of the piers and arch were obtained from the model and the equations applied, that are represented in **Annex G**. Changes in material curves occurred in elements that have greater slenderness and are subjected to axial compression, which is understandable. In the case of the piers it is the extreme ones (fig.6.3) and those that are near the key of the arch with a thickness of 25, 4 mm. In the case of the arch (fig.6.2) it is the ones with section 4-4 that are key of the arch, with a thickness of 19 mm.

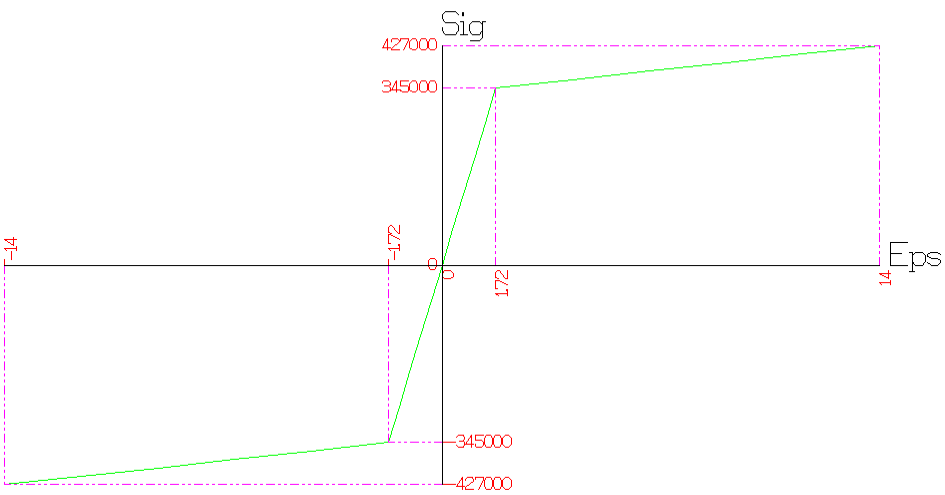

Figure 6. 2 Material curve (Arch-Section 4-4).

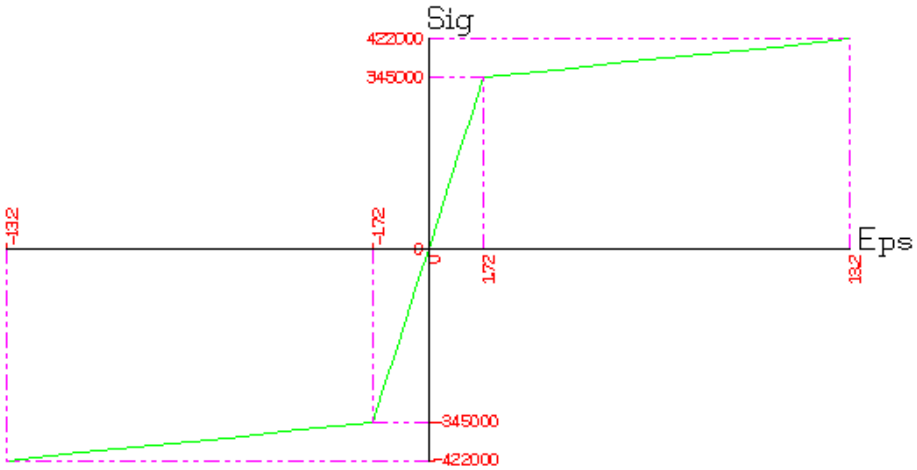

Figure 6. 3 Material curve (SHS650*25.4).

The deck was considered to perform elastically, given that, in order to properly consider its non-linear behavior a detailed definition of all longitudinal and transverse elements would be required.

Usually, in arch bridges hinges form firstly in the substructure due to transverse seismic action [37].

6.2.1 MODELING OF NON-LINEAR BEHAVIOR

There are several models to represent the plastic behavior of the element which differ in the way they distribute plasticity in the section and along the length. Figure 6.4 represents different approaches.

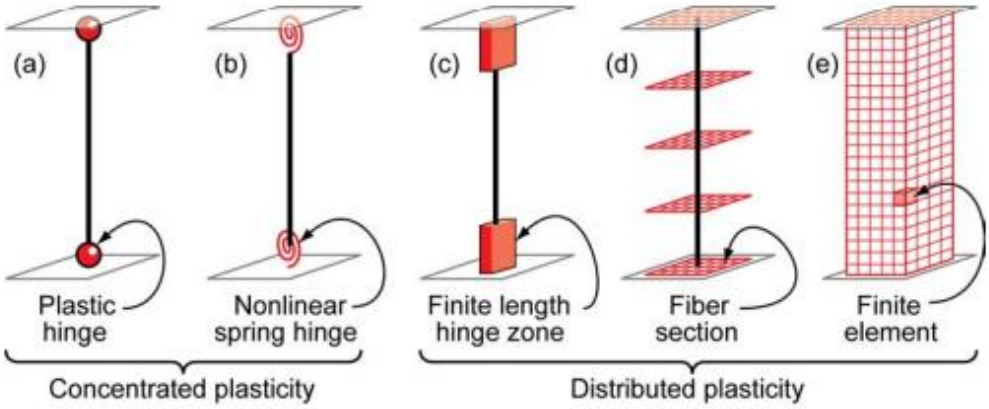

Figure 6. 4 Idealized models of beam-column elements [38].

From all the approaches, the most common and used are the fiber sections and the finite length hinge zone approaches.

The Finite length hinge model designates hinge zones at the member ends. Hinge length may be fixed or variable and there are many formulations and equations to calculate it.

In the fiber model, that is adequate for reinforced concrete structures, the sections are divided into several points of integration and the behavior curve of the material is assigned to each integration point. In other words, some fibers represent the behavior of the reinforcement while others can represent the behavior of the concrete. The section response is obtained using numerical integration over the cross-section [39].

In Rm Bridge software, a relatively new method is used, designated as “fiber-free” modal. In this method, the integration of non-linear stresses is carried out analytically without making use of the so-called fiber approach. For a better understanding of the method, it is recommended to read the Ph.D. Dissertation of Francesco Marmo “A fiber-free approach to the inelastic analysis of reinforced concrete structures” [40].

6.2.2 GEOMETRIC NONLINEAR EFFECTS

“Geometric nonlinear effects are caused by gravity loads acting on the deformed configuration of the structure, leading to an increase of internal forces in members and connections. These geometric nonlinear effects are typically distinguished between P-δ effects, associated with deformations along the members, measured relative to the member chord, and P-Δ effects [37].*”*

P-Δ effects are more important than P-δ due to effects that they produce on the structure and must be considered in the analysis.

In the RM software, the stiffness matrix of the system is updated while calculating the response to each load case corresponding to an increment of lateral load, considering the loads that are applied to the structure.

6.3 Calculation Example with a Cantilever Beam

Two small tests were carried out to verify the accuracy of the software and its correct operation. In the first example we have a 5 m cantilever, with section IPE 200 (steel S355) and a mass of 0.5 kN applied at the end, fig.6.5. With the help of the RM Bridge software the capacity curve is calculated and checked if it does not exceed the maximum theoretical force, based on the virtual deformation (fig.6.6).

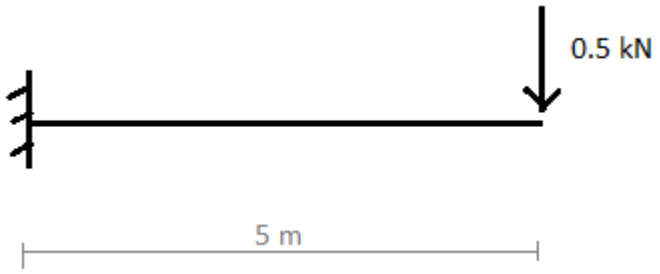

Figure 6. 5 Cantilever case study.

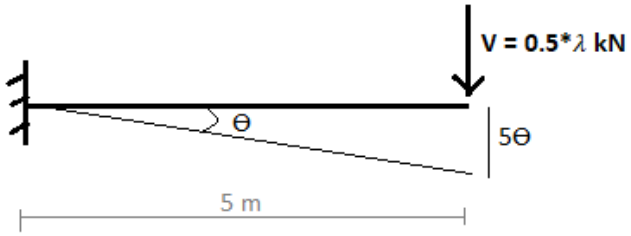

Figure 6.6 Virtual deformation of the structure.

Plastic momentum of an IPE 200 profile can be calculated with the help of the tables, an elasto-perfectly plastic model was used for the steel.

$$M_{pl} = w_{pl} * f_y = 220.6 * 10^{-6} * 355 * 10^3 = 78.3\ kNm \tag{59}$$

Performing the limit plastic analysis, by applying the virtual work theorem (TTV):

$$\lambda * 0.5 * 5 * \theta = M_{pl} * \theta\ (=)\ \lambda = 31.32 \tag{60}$$

$$V = 0.5 *\ \lambda = 0.5 * 31.32 = 15.66\ kN \tag{61}$$

The shear stress at the base is equal to V. This means that the maximum theoretical force that the structure can reach at the base is equal to 15.66 kN. The capacity curve, represented in fig.6.7, is obtained calculating the cantilever using the software RM Bridge.

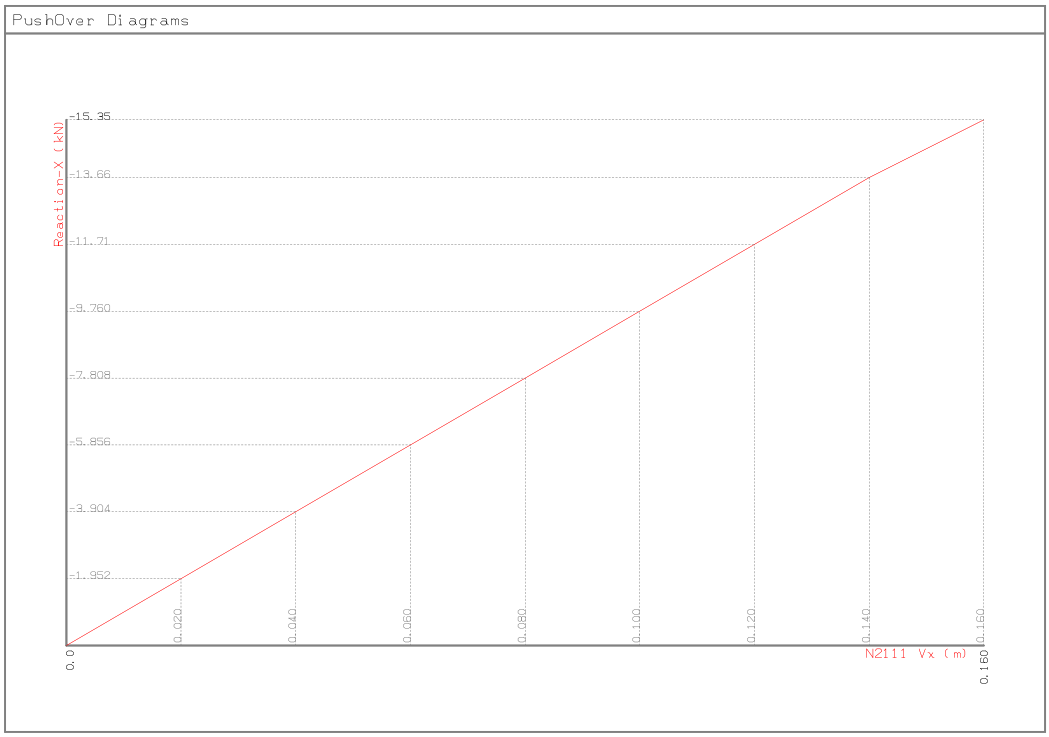

Figure 6. 7 Capacity curve obtained in RM Bridge for a steel cantilever (IPE-200).

It is possible to verify that the capacity curve obtained with a maximum shear base value of 15.35 does not exceed the theoretical maximum value.

The second example has already been presented in chapter 3.3.3, and consisted in a cantilever with height of 5 m and square section made of concrete with reinforcement of 7,5 mm^2 in each side of section, in which the performance point was calculated manually. This analysis resulted in the capacity curve shown in Figure 6.8 and in the performance point, calculated through the software RM Bridge, shown in Fig.6.9.

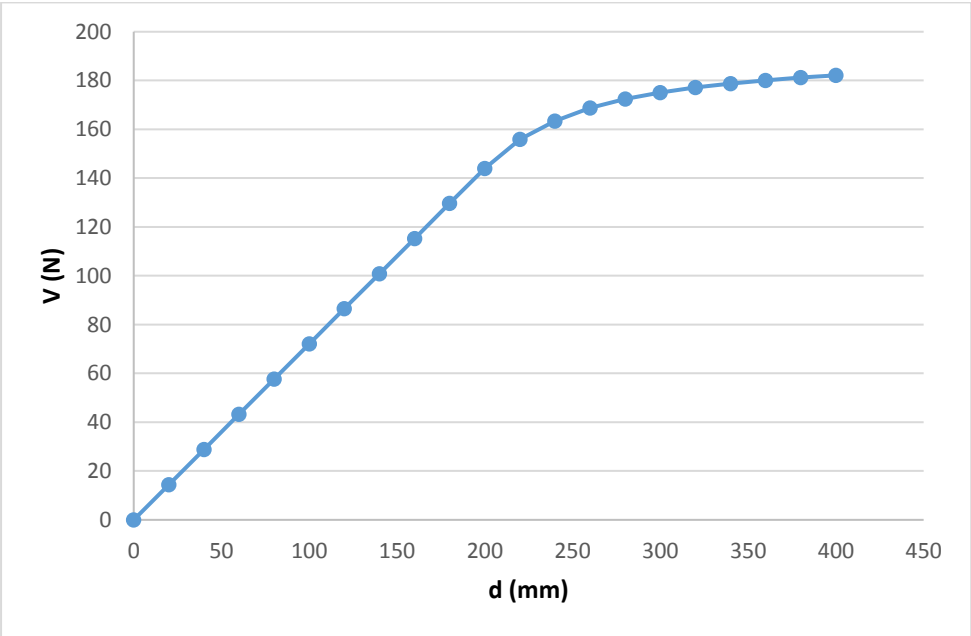

Figure 6. 8 Capacity Curve obtained in RM Bridge for the concrete cantilever example.

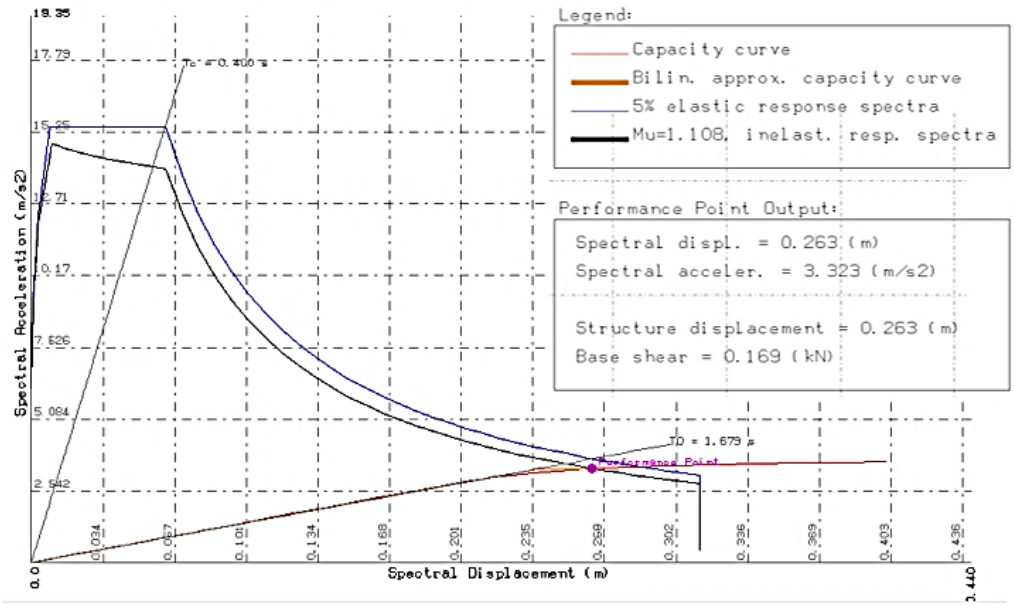

Figure 6. 9 Performance point obtained in RM Bridge for the concrete cantilever example.

It is possible to verify that the target displacement obtained through the software (0.263 m) has a equal value to the one calculated manually (0.263 m) in the chapter 3.3.3. All the data obtained from the analysis is represented in table 6.3.

Table 6.3 Data obtained from Pushover (RM Bridge) for the concrete cantilever example.

Tc = medium-long period limit	0,400
Gamma = transformation factor	1,000
m = SDOF mass	0,051
T = tangent elastic period	1,679
Kt = tangent stiffness	13,998
mu = ductility	1,108
Rmu = reduction factor	1,108
dy = yield displacement	0,23738
det = elastic spectrum displacement	0,26291
SDOF displacement	0,26291
MDOF displacement	0,26291

6.4 PUSHOVER ANALYSIS OF THE CASE STUDY

In order to proceed with the analysis, it is necessary to mention some simplifications adopted in the modelling. Some of the simplifications have been mentioned and discussed earlier. However, a brief reference is made again in this chapter:

- The analysis will be developed in the transverse direction, since in the longitudinal direction the first mode mobilizes a very small mass, what would lead to invalid results.
- The non-linear behavior of the deck is not considered because this element was not rigorously modeled. However, this factor should not influence the results since for the transversal analysis it is not usually preponderant for the formation of the first plastic hinges.
- In the project, the deck was designed to be fixed transversally at the abutments. Since in this analysis, focus will be put in the capacity curve beyond the seismic performance point, the abutment was defined as being able to carry only the reaction corresponding to the reaction obtained from the elastic response spectrum analysis, which corresponds to approximately 2500kN. Not doing so would lead to a linearly increasing reaction at the abutment that would prevent from detecting any non-linear behavior of the structure, due to the fact that the rigid abutment would have a much greater stiffness than the remaining transversally resisting elements.
- Geometric imperfections are not considered.

For the pushover analysis, the company PEDELTA proposed the use of the RM Bridge software, which until now has never been used for this type of analysis in the scope of the dissertation developed at the Faculty of Engineering of the University of Porto.

Some limitations of the software, in the pushover analysis, were detected and later confirmed in a conference with the developers of the software.

- The analysis software does not allow to obtain information on the location of plastic hinges, nor the sequence in which they form. It is also not possible to obtain information of which element of the structure fails when the capacity curve is interrupted.
- In order to circumvent this problem, the following procedure was carried out, in order to get a qualitative estimation on the location of the plastic hinges:
    - Analysis of normal stresses in all elements. Although composed equivalent stresses are not being analyzed, the normal stresses, at the qualitative level, may serve as an indication in which elements the elastic limit is first reached, since these are much higher than the shear stresses. Later, the equivalent Von Mises stresses will be calculated, to verify this approach.
    - Analysis of the variation of the stiffness of the structure through the slope of the capacity curve.
    - Analysis of the moment-curvature diagrams for the most relevant elements, for the last loading step.

Conventionally, steel arch bridges are designed using the seismic coefficient method, so the arch components behave in an elastic manner. According to some studies the seismic response is small under longitudinal direction but significantly large in the transverse direction due to plasticization formed in some segments such as arch rib ends and side piers where axial force levels are very high [37].

6.4.1 CAPACITY CURVE

Combination adopted for the analysis is Extreme Event 1 that includes the earthquake, according to the AASHTO LRFD, 2014-3-14 (fig.6.10). The load factor for the permanent load is 1.0 and for the live load is equal to 0.5.

Load Combination Limit State	*DC DD DW EH EV ES EL PS CR SH*	*LL IM CE BR PL LS*	*WA*	*WS*	*WL*	*FR*	*TU*	*TG*	*SE*	Use One of These at a Time				
										EQ	*BL*	*IC*	*CT*	*CV*
Strength I (unless noted)	γ_p	1.75	1.00	—	—	1.00	0.50/1.20	γ_{TG}	γ_{SE}	—	—	—	—	—
Strength II	γ_p	1.35	1.00	—	—	1.00	0.50/1.20	γ_{TG}	γ_{SE}	—	—	—	—	—
Strength III	γ_p	—	1.00	1.40	—	1.00	0.50/1.20	γ_{TG}	γ_{SE}	—	—	—	—	—
Strength IV	γ_p	—	1.00	—	—	1.00	0.50/1.20	—	—	—	—	—	—	—
Strength V	γ_p	1.35	1.00	0.40	1.0	1.00	0.50/1.20	γ_{TG}	γ_{SE}	—	—	—	—	—
Extreme Event I	γ_p	γEQ	1.00	—	—	1.00	—	—	—	1.00	—	—	—	—
Extreme Event II	γ_p	0.50	1.00	—	—	1.00	—	—	—	—	1.00	1.00	1.00	1.00
Service I	1.00	1.00	1.00	0.30	1.0	1.00	1.00/1.20	γ_{TG}	γ_{SE}	—	—	—	—	—
Service II	1.00	1.30	1.00	—	—	1.00	1.00/1.20	—	—	—	—	—	—	—
Service III	1.00	0.80	1.00	—	—	1.00	1.00/1.20	γ_{TG}	γ_{SE}	—	—	—	—	—
Service IV	1.00	—	1.00	0.70	—	1.00	1.00/1.20	—	1.0	—	—	—	—	—
Fatigue I—*LL, IM & CE* only	—	1.50	—	—	—	—	—	—	—	—	—	—	—	—
Fatigue II—*LL, IM & CE* only	—	0.75	—	—	—	—	—	—	—	—	—	—	—	—

Figure 6. 10 Load Combinations and Load Factors (AASHTO LRFD, 2014-3-14).

In this approach two types of distribution are considered for the representation of the earthquake loading:

- Modal shape distribution of the first mode (Figure 6.11-6.12).
- Inertia force distribution (Figure 6.13).

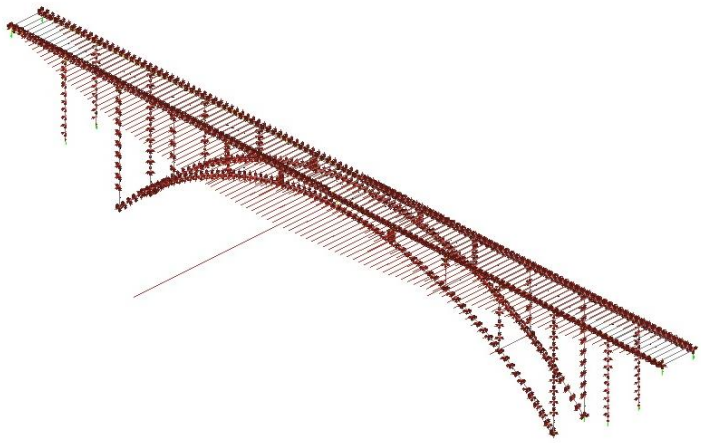

Figure 6.11 Modal shape load distribution for the case study.

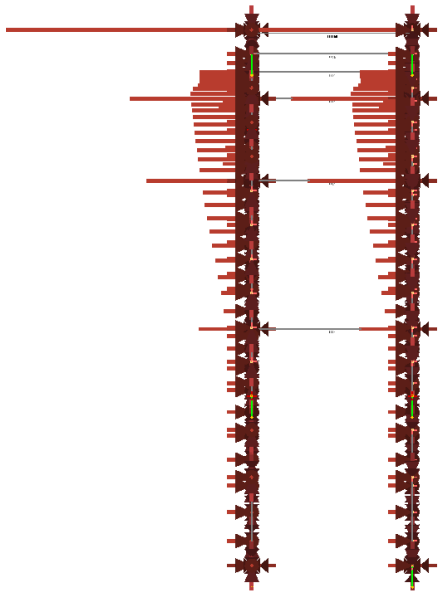

Figure 6. 12 Lateral modal shape load distribution for the case study.

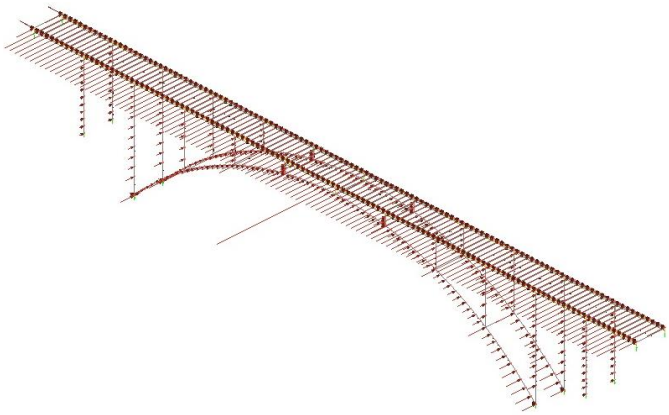

Figure 6. 13 Uniform load distribution for the case study.

With these two types of load it is possible to obtain the respective capacity curve for both load patterns that are represented in Fig 6.14 and Fig 6.15.

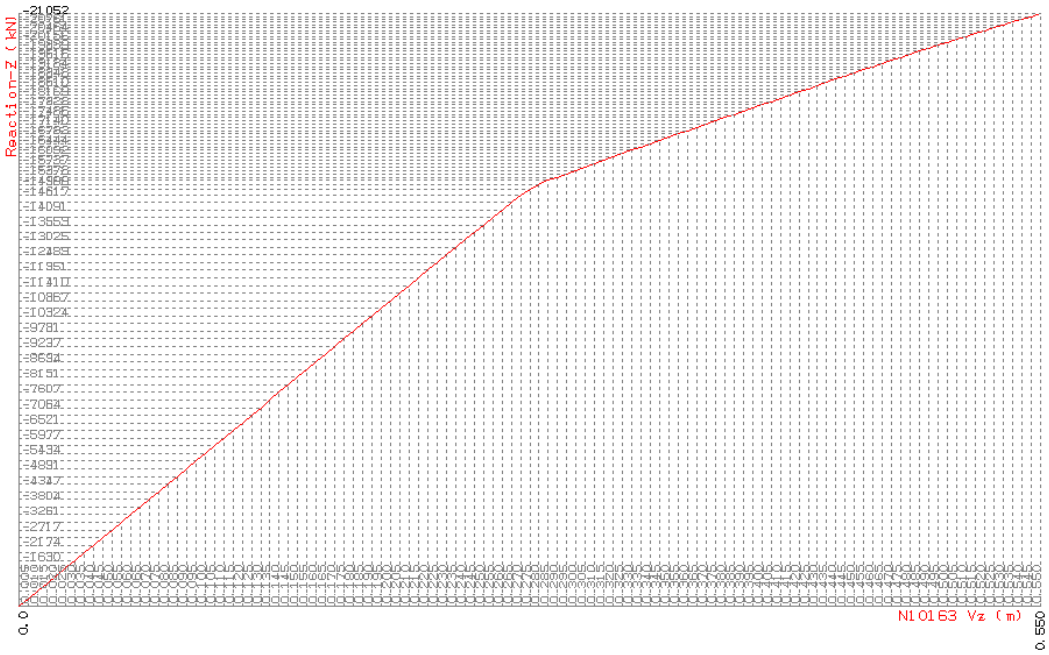

Figure 6. 14 Capacity curve obtained for the modal shape distribution.

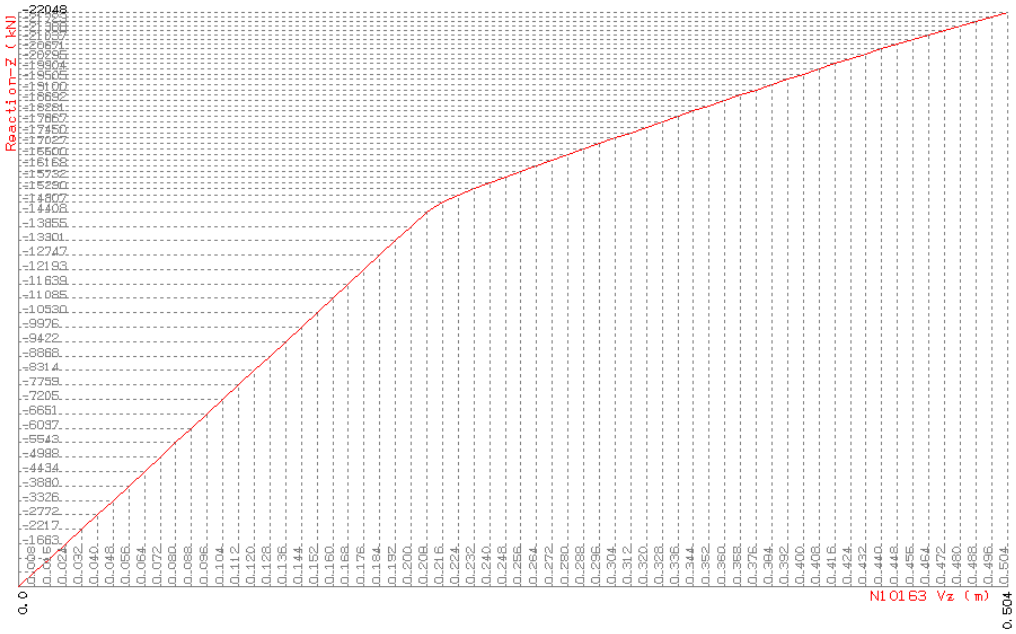

Figure 6. 15 Capacity curve obtained for the uniform shape distribution.

It is possible to verify from the figure 6.16 that the two capacity curves are quite similar. Maximum displacement of equivalent SDOF system subjected to modal and uniform loading is 0.55 m and 0.504 m respectively. As for the maximum base shear force it is 21052 kN in modal loading and 22048 kN in uniform.

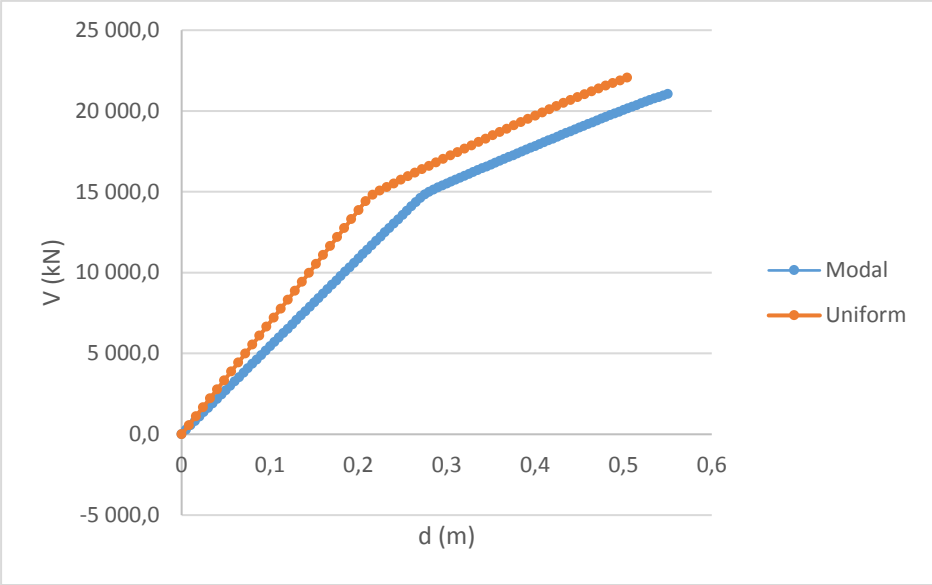

Figure 6.16 Comparation between two capacity curves for the uniform and modal shape distribution.

In the figure 6.17 the variation of stiffness that occurred in the capacity curve in both analyses is represented. It is possible to verify that the slope of the capacity curve for uniform distribution is more accentuated because, although the stiffness does not depend on the intensity of the load it depends on its distribution, and in the uniform case we have more load applied near a fix point, which are the abutments.

In the uniform distribution we apply a load equal to 100% of the mass, while in the modal distribution about 80%, which is mobilized in the first mode.

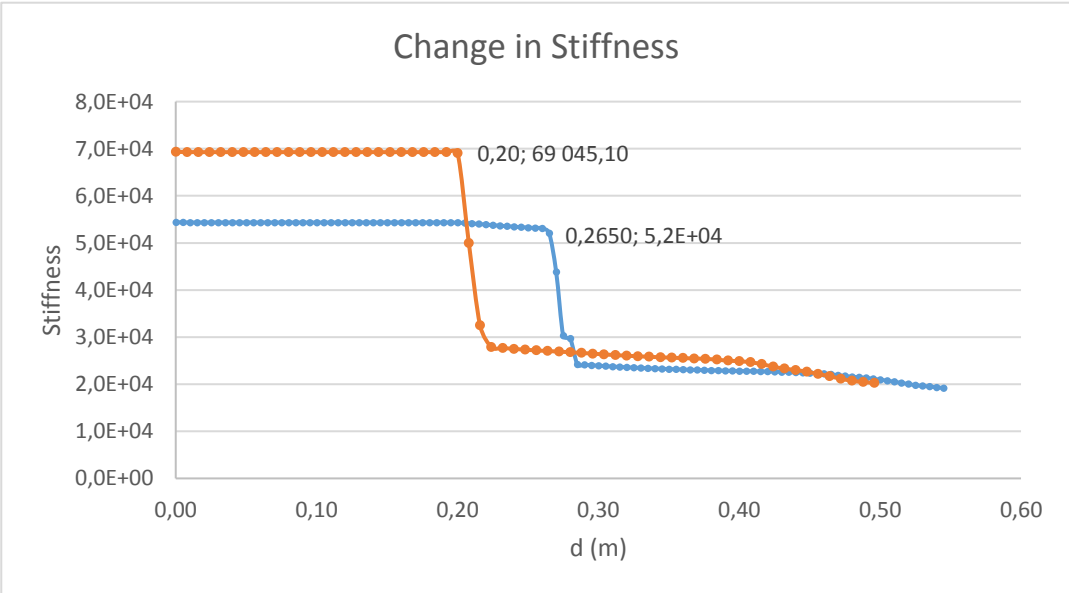

Figure 6. 17 Change in Stiffness (Blue-Modal, Orange-Uniform)

A sudden change in stiffness occurs for a displacement of approximately 0.2 m in the case of a uniform loading and for loading step 25. In case of modal loading it is for 0.265 m and step number 53. This sudden change can be associated with the fact that the abutments have almost reached the defined limit reaction in the transverse direction and can no longer absorb further load, thus reducing its contributuon

to the total stiffness of the structure. Looking at the modal load it is possible to detect that some dissipation of energy happens before the limit reaction at abutments is reached, for a displacement around the 0.215 m.

The figure 6.18 represents the diagram of the normal stresses in all steel elements of the bridge, with indication of the location of the respective elements. The values of normal stresses do not represent the exact behaviour because they do not take into account the tangential stresses, that are also important for the analysis, but can provide some hint on when the elastic limit is reached.

As mentioned before, the equivalent Von_Mises stresses were calculated using an excel sheet based on the normal and shear stresses in order to confirm that the normal tensions are the most significant ones and can be found in the **Annex H** for some of the elements at the last iteration. Then it is adequate to use the figures from RM Bridge that represent normal stresses, which allow to represent graphically, in a very simple way, the stresses in each element and each loading step, in order to have an idea of the behavior of the structure

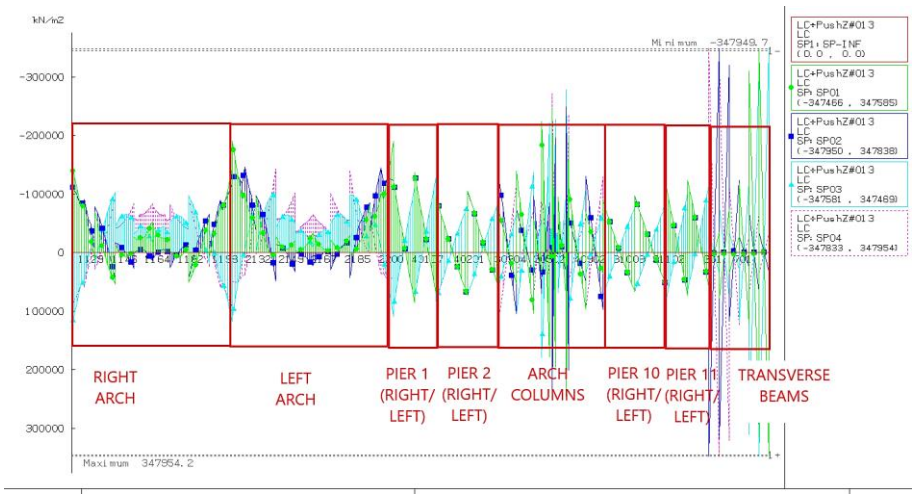

Figure 6. 18 Identification of elements in the normal stresses diagram.

The normal stresses for the modal distribution and step 53 are represented in the fig 6.19. Figure 6.20 represents the same scenario for the uniform distribution and iteration 25. It is possible to predict that the first element to form plastic hinge was the transverse beam that connects the two arches (elements at the far right of the graphic).

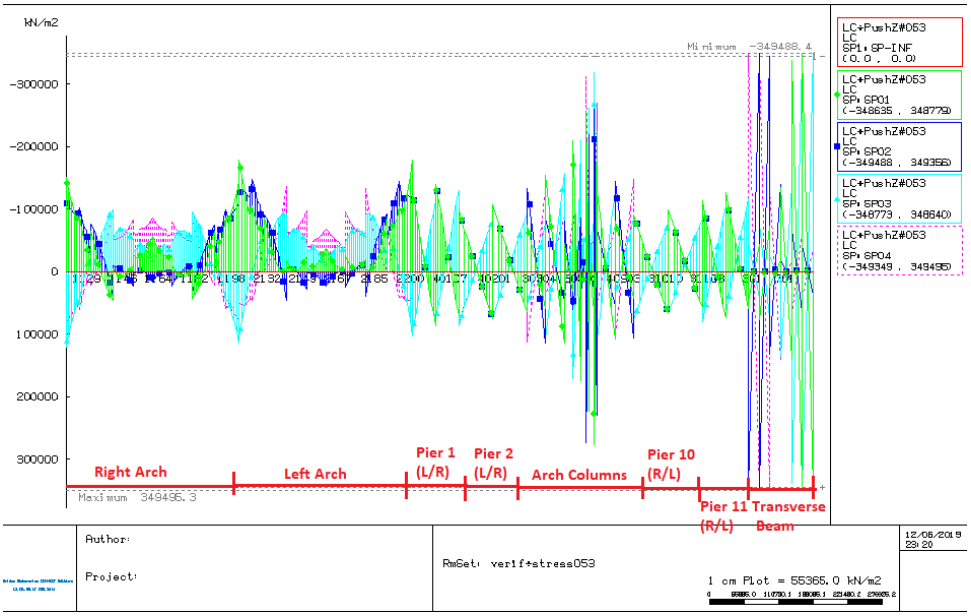

Figure 6. 19 Normal stresses for the modal load distribution in step 53.

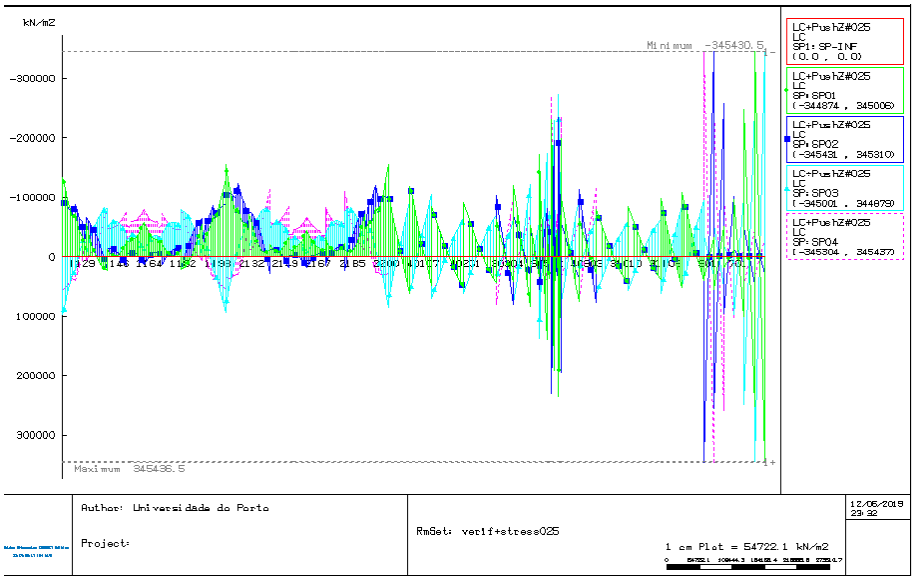

Figure 6. 20 Normal stresses for the uniform load pattern and step 25.

It is possible to verify the evolution of the forces in the abutments, in the fig.6.21, and verify that in the step 53 those are very close to the elastic limit reaching it in step 55.

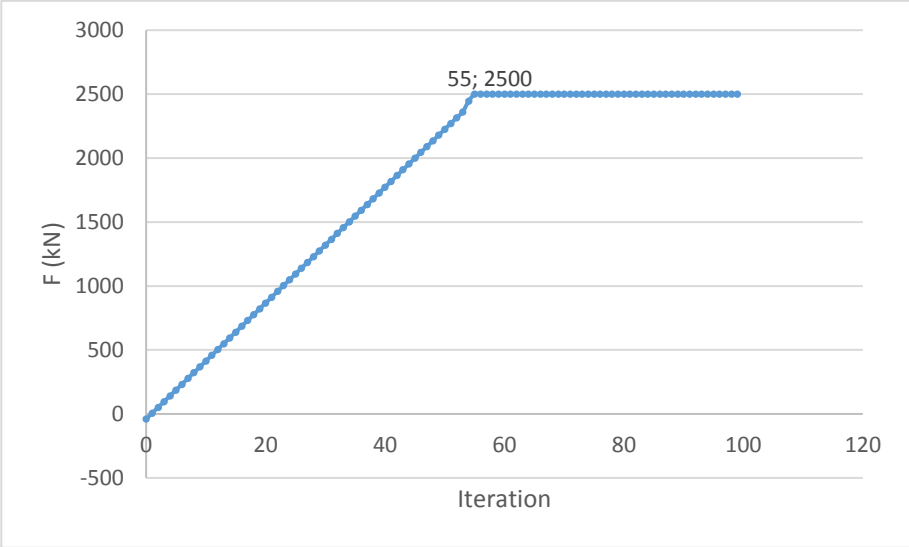

Figure 6. 21 Force in the abutments (modal distribution).

Using modal distribution, it was possible to perform 110 steps, that is 110 load increments in the capacity curve. The normal stresses of the last iteration are represented in fig 6.22 and fig 6.23 with high normal stresses in the transverse beams, arch columns and piers.

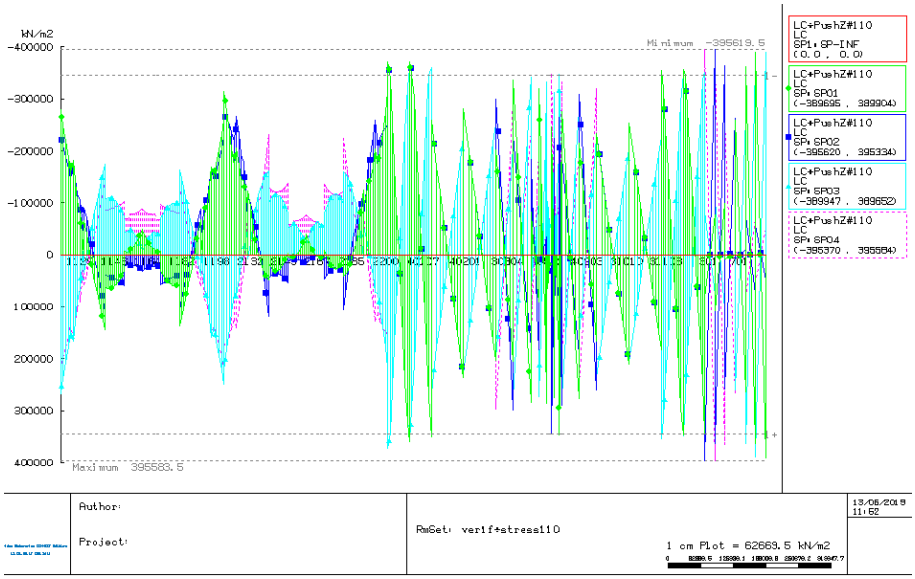

Figure 6. 22 Normal stresses (modal distribution, last increment).

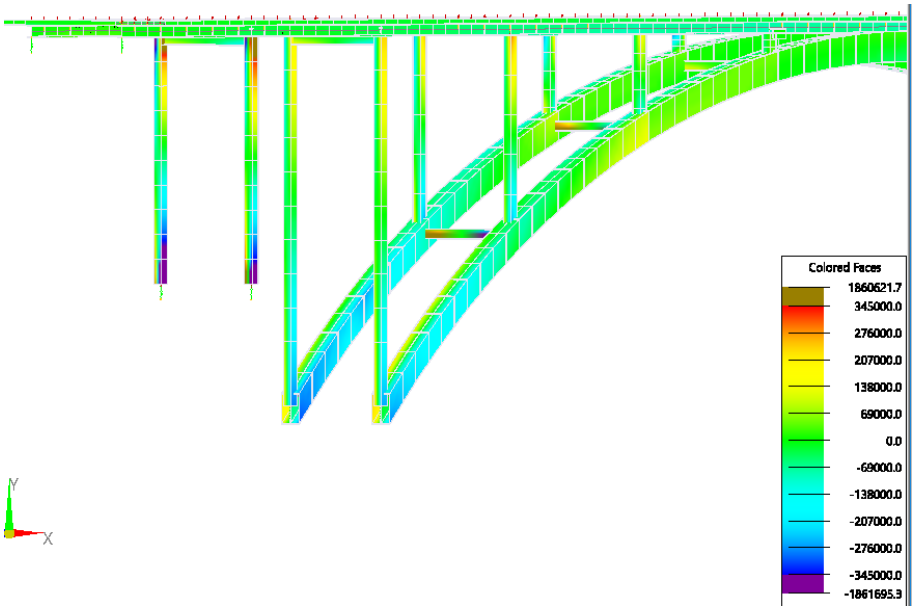

Figure 6. 23 Representation of normal stresses (modal distribution, last increment).

For the uniform analysis, 63 load increments were obtained. Figure 6.24-25 show normal stresses during the last increment and it can be seen that the highest stresses occur in the same elements as mentioned earlier for the modal distribution.

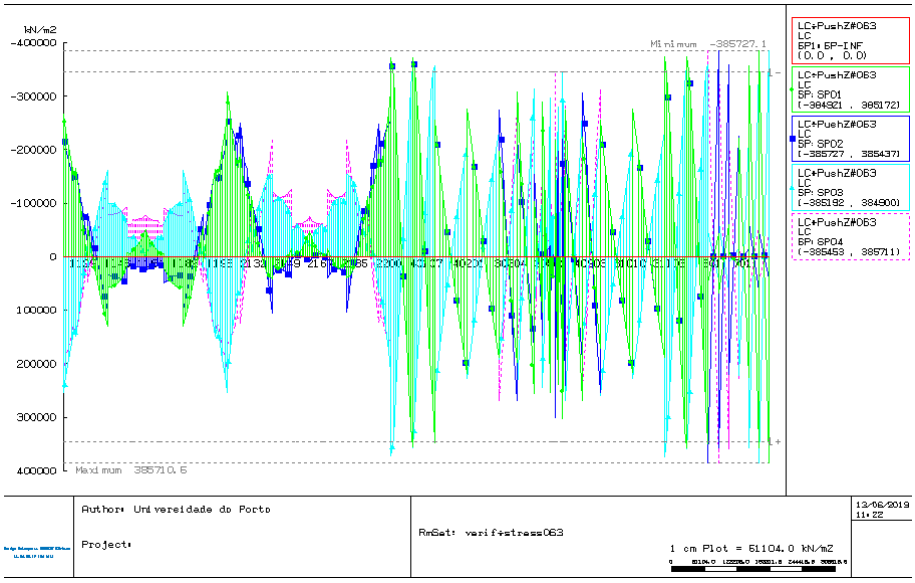

Figure 6. 24 Normal stresses (uniform distribution, last increment).

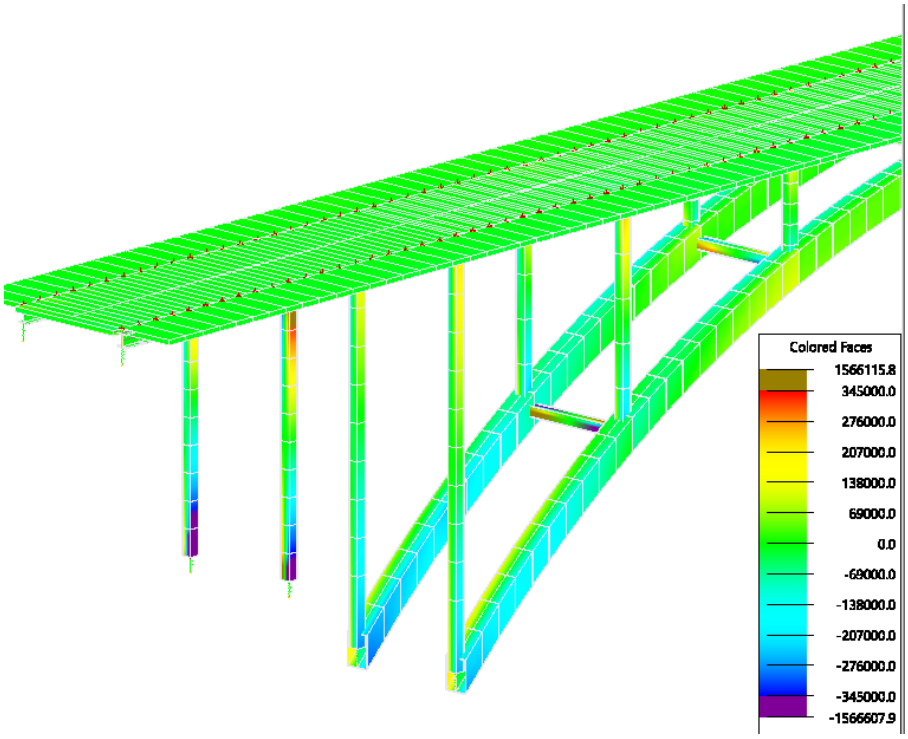

Figure 6. 25 Representation of normal stresses (uniform distribution, last increment).

In order to understand which element led to the rupture of the capacity curve, a complementary analysis, using the moment-curvature diagram of the most relevant elements, was carried out, due to the fact that the software RM Bridge does not provide this type of information. Forces were extracted from the analysis for the last iteration for the modal distribution and the respective sections of the elements were represented in the software FAGUS (Cubus) that allows to perform a sectional analysis considering the non-linearity of the material.

Through this analysis moment-curvature curves were obtained to locate at which point the respective element was at the last iteration. The diagrams were obtained for the axial force in the corresponding load step of the analysis.

Some of the elements are subject to biaxial bending that result in a curvature in two directions. The rotation angle has been calculated so as to rotate the section so as to obtain an equivalent simple flexure and the corresponding curvature.

More detailed calculation can be found in the **Annex I**, for the transverse beam, and the moment-curvature curves of some elements will be presented here.

In fig.6.26 the moment-curvature curve of an arch is presented, the line that intersects the curve represents the curvature of the element in the last iteration. It is clear that for that iteration this type of element is situated in the elastic range as it was predicted through the graphs of the normal stresses.

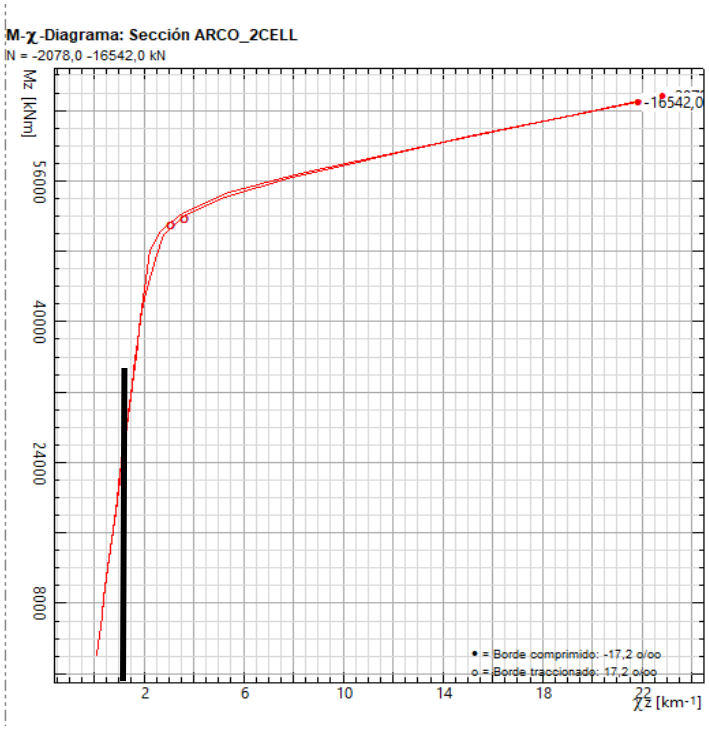

Figure 6. 26 Moment-curvature relation for arch (right and left, last iteration).

A curvature located on the plastic domain of the section was reached in the outer piers that are near the abutments, for the left and right one, and for the transverse beam which is located closer to the arch foundations and can be seen in fig.6.27-28.

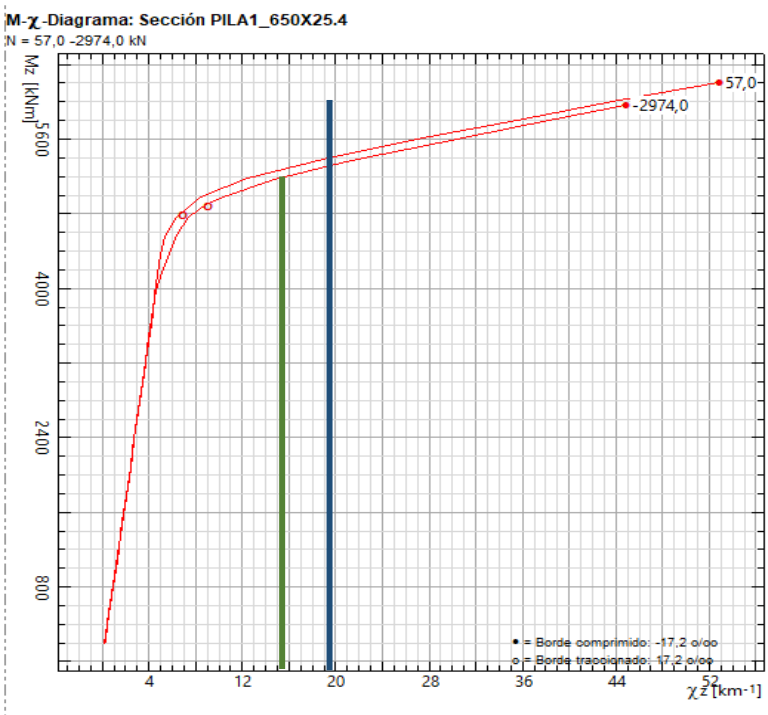

Figure 6. 27 Moment-curvature curve for the outer pier (right side pier-blue and left side-green)

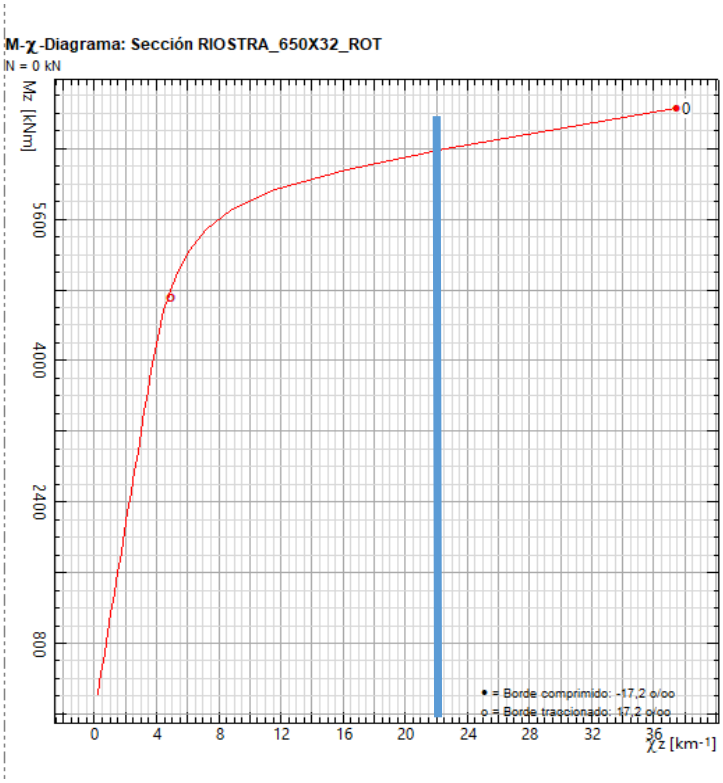

Figure 6. 28 Moment-curvature for the transverse beam situated near foundation.

It is possible to conclude that the element that, probably, lead to the termination of the capacity curve was the transverse beam situated near the foundation of the arches.

6.4.2 PERFORMANCE POINT

6.4.2.1 Modal Displacement

The target displacement of the MDOF system is similar in 3 methods (EC-N2, FEMA 440 Equivalent Linearization and FEMA 440 Displacement modification) represented in Fig 6.29-6.31: 0.252, 0.246 and 0.252 with maximum base shear force of 13679 kN, 13344 kN and 13677 kN respectively. The displacement demand of the equivalent SDOF system is equal to 0.199 m and 0.194 m with maximum displacement of 0.55 m, ie respecting the 150% of the displacement demand imposed in the Eurocode.

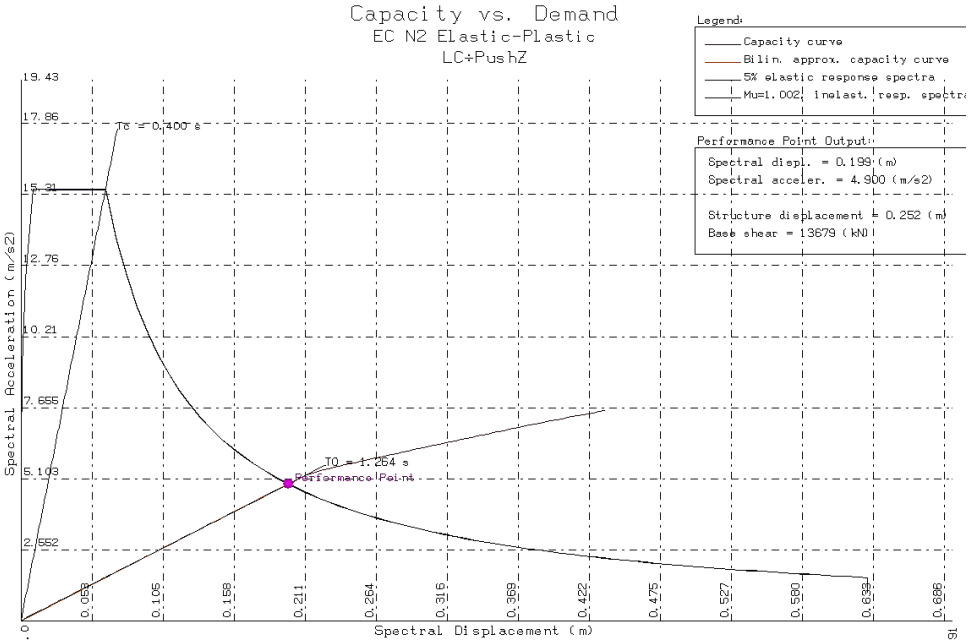

Figure 6. 29 Performance point (EC-N2) for the modal distribution.

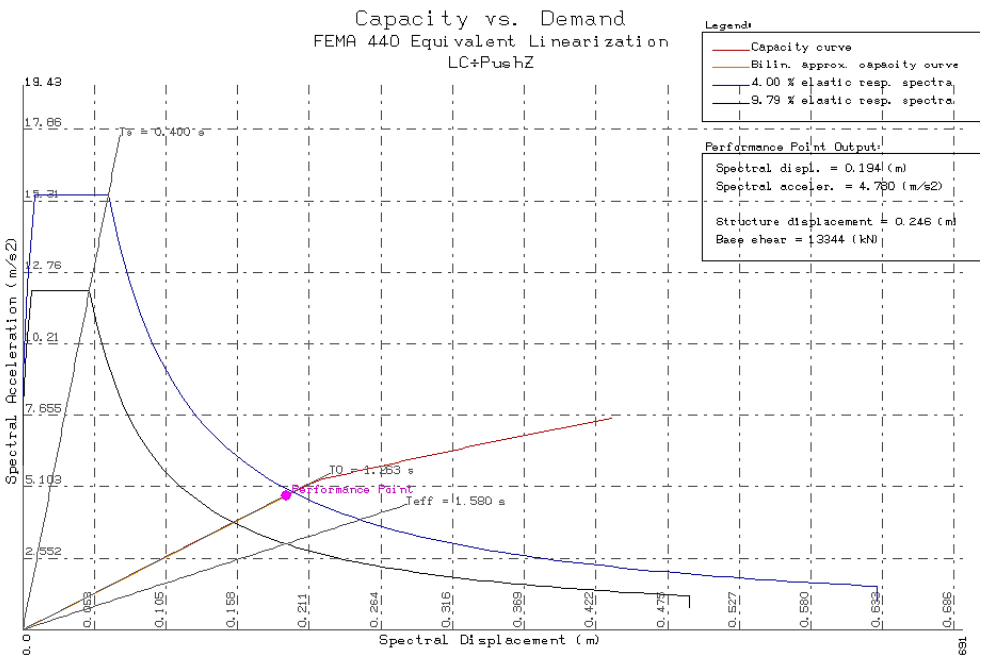

Figure 6. 30 Performance point (FEMA 440-Equivalent Linearization) for the modal distribution.

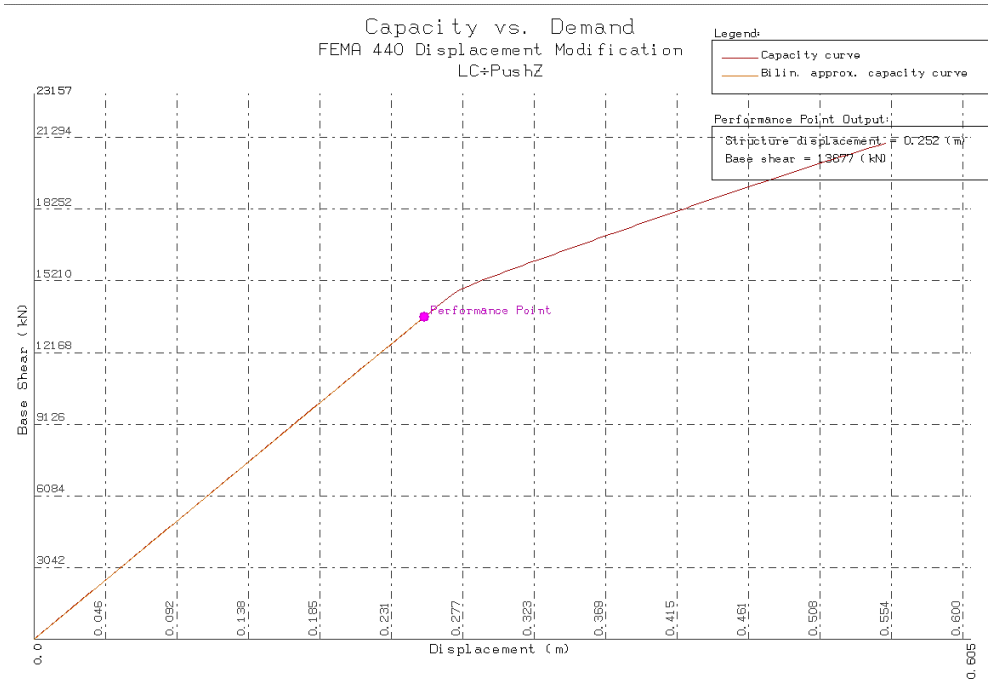

Figure 6. 31 Performance point (FEMA 440- Displacement modification) for the modal distribution.

It is possible to perceive that the structure is overdimensioned because for the design earthquake event, according to its target displacement, the structure behavior is located in the elastic response zone.

6.4.2.2 Uniform Displacement

The pushover analysis using uniform distribution loads results in the target displacement equal to 0.223 m, 0.222 m and 0.223 m with base shear of 15029 kN, 15016 kN and 15026 kN as shown in fig 6.32-6.35. The performance point obtained in the uniform load analysis has a greater displacement than in the modal load distribution.

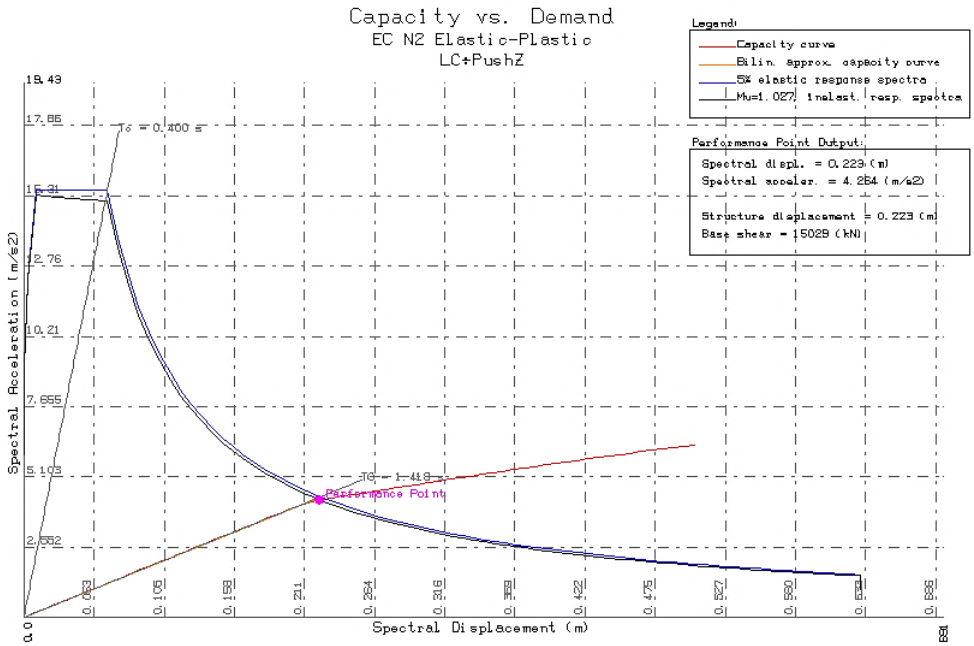

Figure 6. 32 Performance point (Uniform load, EC-N2) for the uniform distribution.

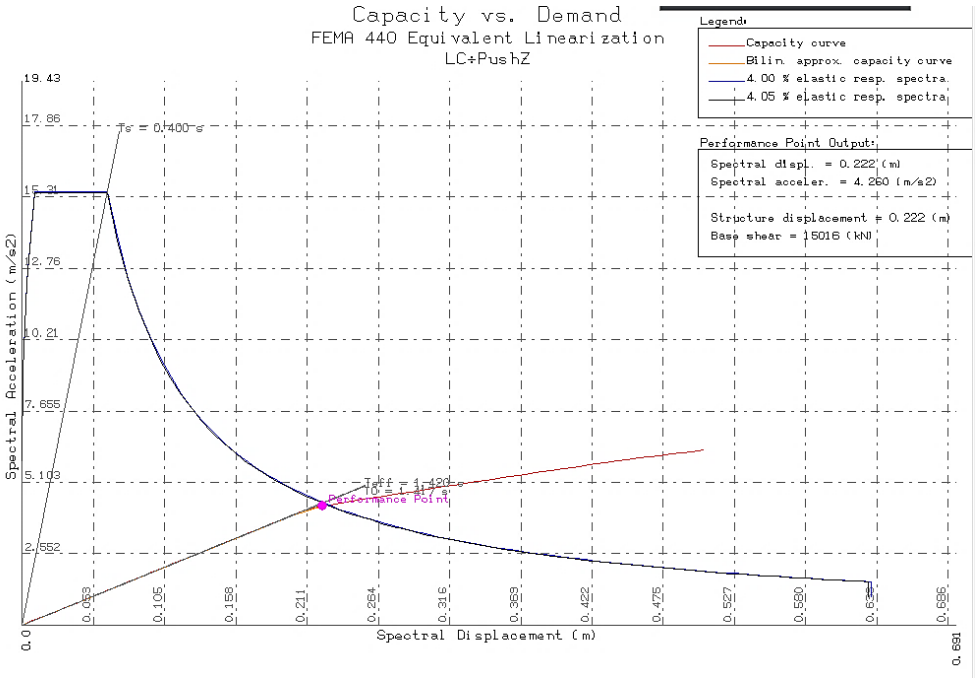

Figure 6. 33 Performance point (Uniform load, FEMA 440-Equivalent Linearization) for the uniform distribution.

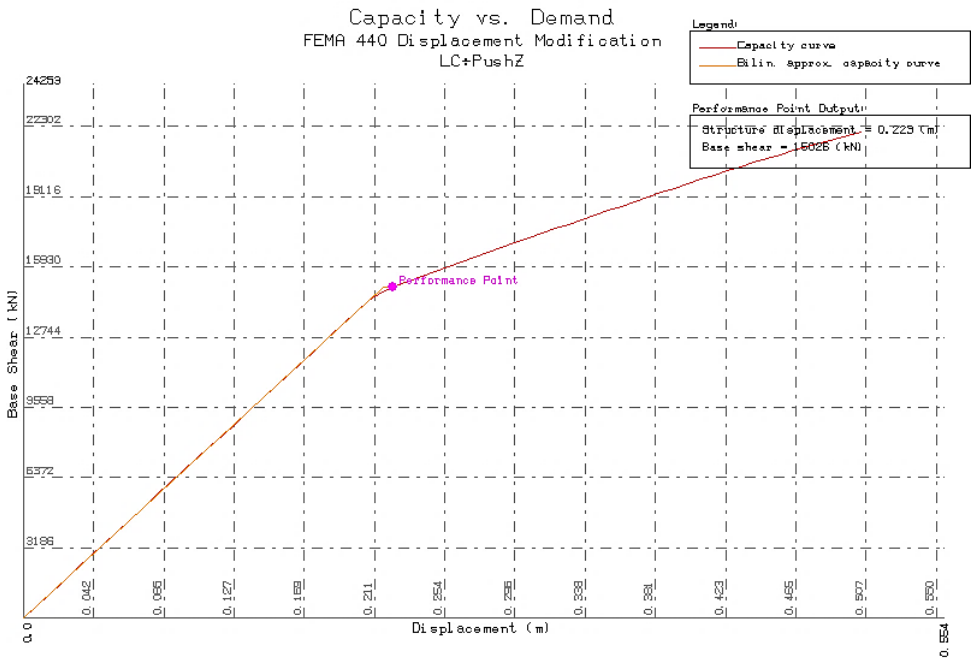

Figure 6.34 Performance point (Uniform load, FEMA 440- Displacement modification) for the uniform distribution.

6.4.2.3 Comparison of the pushover analysis results.

Table 6.4 shows the main results of the two analyzes depending on the load distribution. As we have seen before, the three methods exhibit identical results for the target displacement. The effective period is superior to the fundamental elastic period (T = 1.248 s), but very similar because the behavior of the structure is almost elastic.

Table 6.4 Main results from the two analysis (modal and uniform load distribution).

Load Distribution		**Modal**	**Uniform**
Target Displacement (m)	N2	0,25	0,22
	FEMA 440 Equivalent Linearization	0,25	0,22
	FEMA 440 Displacement Modification	0,25	0,22
Base Shear Force (kN)	N2	13678,82	15028,93
	FEMA 440 Equivalent Linearization	13344,33	15016,27
	FEMA 440 Displacement Modification	13676,76	15025,79
Effective T	N2	1,264	1,418
	FEMA 440 Equivalent Linearization	1,263	1,420
	FEMA 440 Displacement Modification	1,264	1,417

6.4.3 BEHAVIOUR FACTOR/RESPONSE MODIFICATION FACTOR

The behaviour factor in EC or the response modification factor in American regulations is a parameter used in almost all seismic design regulations, to achieve a desired structural performance using simplified procedures. This factor is a function of the material, type of the structural system and class of ductility of the structure.

Despite the empirical character of the behaviour factor, it is possible to physically determine this parameter based on the capacity curve of a structure defined in terms of its shear base (V) and horizontal (Δ) displacement [41].

The factor can be defined as:

$$q = \frac{Vel}{Vd} = \frac{Vel}{Vy} * \frac{Vy}{Vd} = q_u * \Omega \tag{62}$$

The terms q_u and Ω in the equation represents the ductility and the over-resistance component (its plastic redistribution capacity (defined in EC8 by the quotient αu / α1), the hardening of the material, the differences between the actual and calculated strength of the material, etc.) of the behaviour factor, respectively.

Where:

Vel is the maximum elastic shear base;

Vd is the design shear base;

Vy represents the lateral resistance of the structure;

$V1y$ represents the lateral force for which the first hinge in the structure is formed.

Fig.6.35 represents the variables listed above.

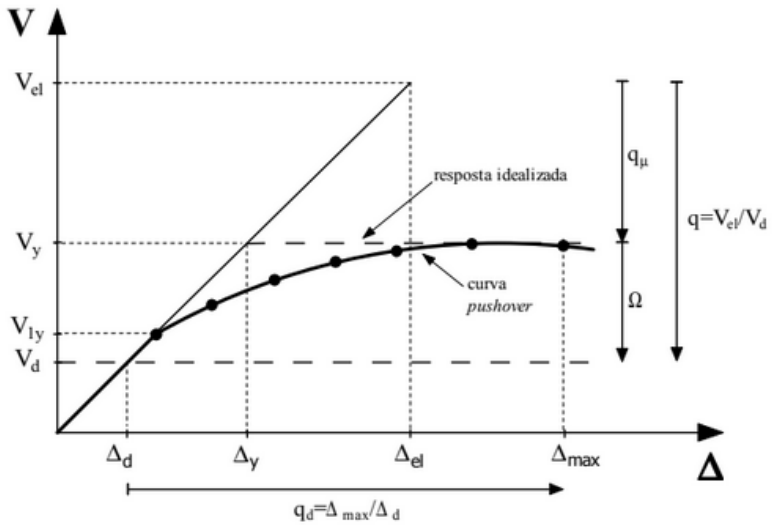

Figure 6. 35 Capacity curve and representation of behavior factor [41].

In fig.6.36, the capacity curve for the modal distribution and the initial study case are presented. The grey line shows the elastic force at which the bridge should be projected having an elastic behaviour. The blue line shows the design force based on behaviour factor of 1.5.

For the design elastic basal level, the capacity curve is in an elastic regime, that is, there is no need to take advantage of the ductility of the structure and a low behaviour factor is justifiable.

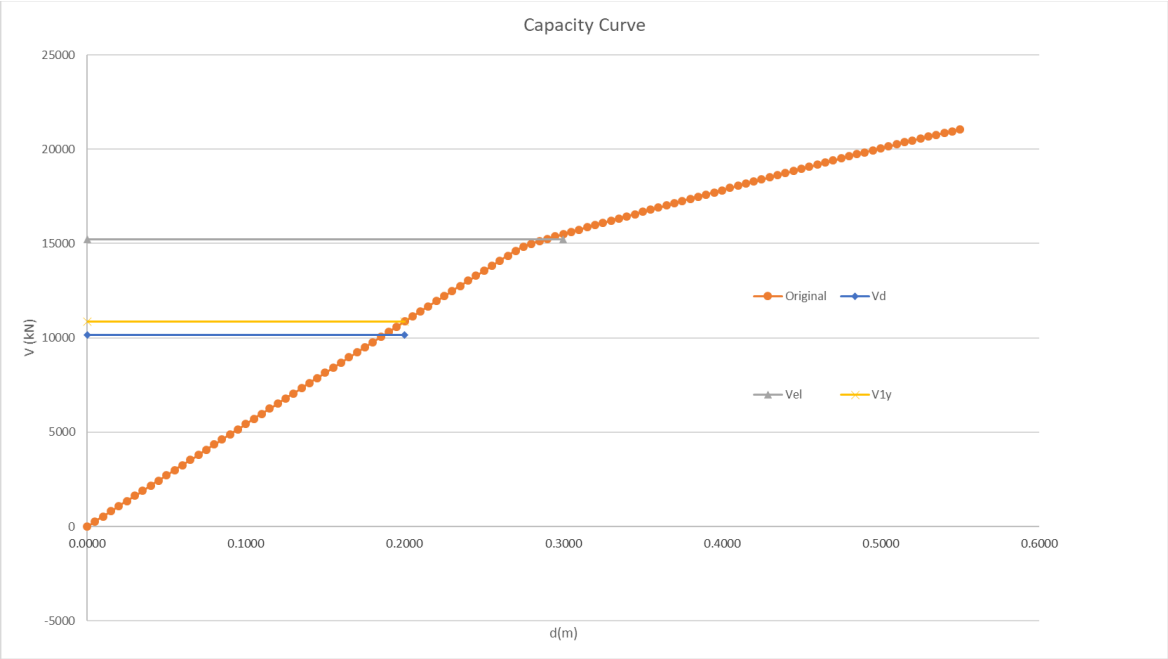

Figure 6. 36 Capacity curve and representation of the correspondent forces.

6.4.4 ANALYSIS OF A STRUCTURE CONSIDERING DIFFERENT IMPORTANCE CATEGORY

The results obtained previously refer to a structure classified as "important" according to the code of Guatemala. If the structure was classified as "essential" would the results vary significantly, or would the structure continue with an essentially elastic behavior?

According to "Normas de Seguridad Estructural de Edificaciones Y Obras de Infraestructura para la República de Guatemala";

"A structure classified as essential must remain essentially operational during and after a seismic event."

In order to answer the question posed above, another analysis was carried out classifying the structure as essential.

The level of protection of the structure, taking into account the terrain, has been altered to type E (Figure 6.37). The values referring to Fa and Fv were changed and a 0.8 value was adopted for K_d, modifying the response spectrum.

Índice de Sismicidad	Clase de obra			
	Esencial	Importante	Ordinaria	Utilitaria
Io = 5	E	E	D	C
Io = 4	E	D	D	C
Io = 3	D	C	C	B
Io = 2	C	B	B	A
Probabilidad de exceder un sismo de diseño	5% en 50 años	5% en 50 años	10% en 50 años	No aplica

a) ver clasificación de obra en Capítulo 3, norma NSE 1
b) ver índice de sismicidad en Sección 4.2.1
c) ver Sección 4.3.4, para selección de espectro sísmico de diseño según probabilidad de excederlo
d) para ciertas obras que hayan sido calificadas como "críticas" el ente estatal correspondiente puede considerar probabilidad de excedencia de 2% en 50 años (K_d = 1.00 en sección 4.3.4)
e) "esencial" e "importante" tienen la misma probabilidad de excedencia – se diferencian en el Nivel de Protección y en las deformaciones laterales permitidas

Figure 6. 37 Minimum level of seismic protection and probability of design earthquake [35].

$$S_{cd} = K_d * \frac{S_{cs}}{\eta} = 0.8 * 0.9 * \frac{1.5}{0.935} = 1.155 \tag{63}$$

$$S_{1d} = K_d * \frac{S_{1s}}{\eta} = 0.8 * 2.4 * \frac{0.55}{0.935} = 1.129 \tag{64}$$

$$T_s = \frac{S_{1d}}{S_{cd}} = 0.978\ s \tag{65}$$

In figure 6.38 is represented the spectrum used in the previous analysis and the spectrum obtained for the new analysis. For the fundamental period of the structure (T = 1.25s), it can be seen that the corresponding spectral acceleration increases considerably comparing with the original case.

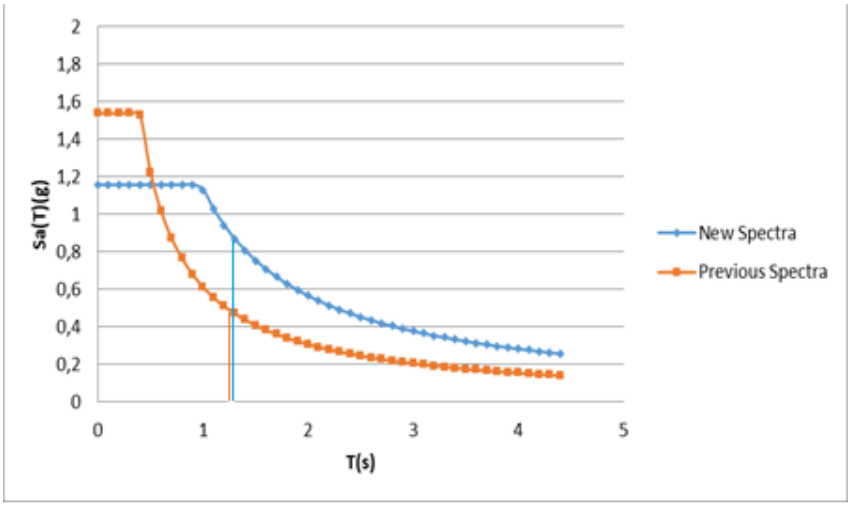

Figure 6. 38 New Response Spectrum made accordingly with Guatemalan Regulations for the case considering different importance category (essential).

As previously, the equivalent response spectrum as per the EC8 was obtained (fig.6.3) using the information of the table 6.5.

Table 6. 5 Information used for the transformation to equivalent response spectrum.

Ground Type	S	Tb(s)	Tc(s)	Td(s)	ξ (%)	η	Scd(g)
A	1	0,15	0,98	4	4	1,05	1,15

$$a_g * S * \eta * 2.5 = S_{cd} \ (=) a_g = 0.438 \tag{65}$$

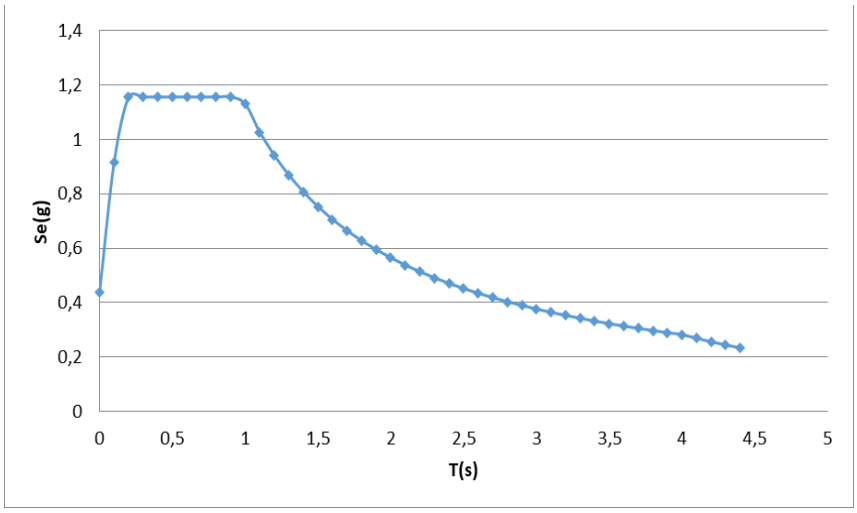

Figure 6. 39 Response Spectrum (EN) for the case considering different importance category (essential).

The capacity curve obtained is the same as from the last example because no changes were introduced to the load and stiffness of the structure. The target displacement of the MDOF system subjected to modal distribution is 0.469 m, 0.455 m and 0.453 m with maximum base shear force of 19389 kN, 18848 kN and 19031 kN respectively for EC-N2, FEMA 440 Equivalent Linearization and FEMA 440 Dispalcement Modification (fig 6.40-6.42).

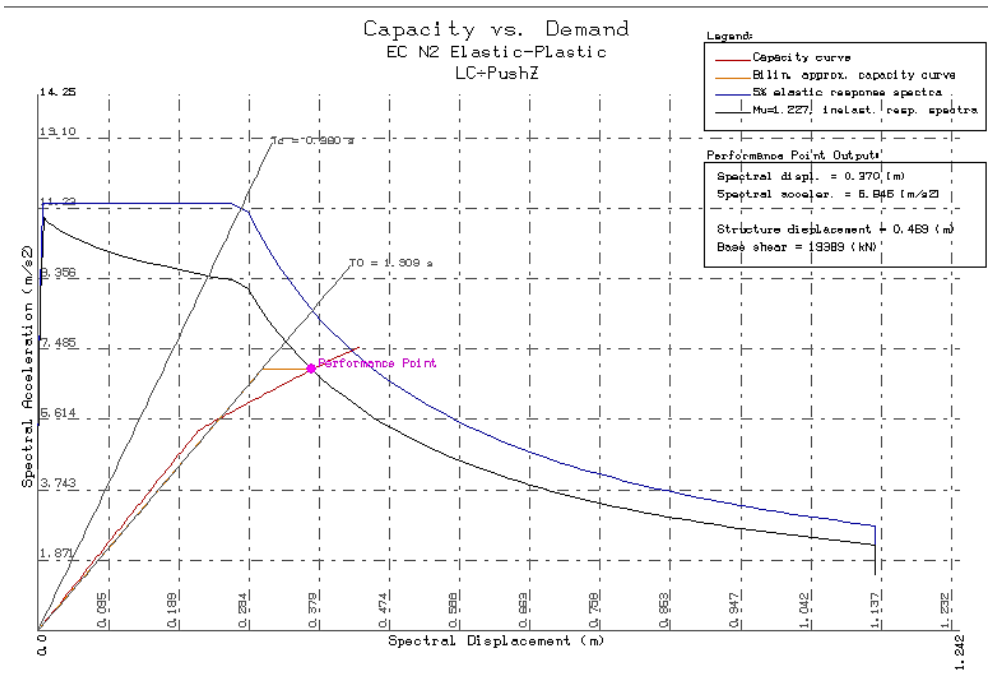

Figure 6. 40 Performance point (Modal distribution-EC N2) for the case considering different importance category (essential).

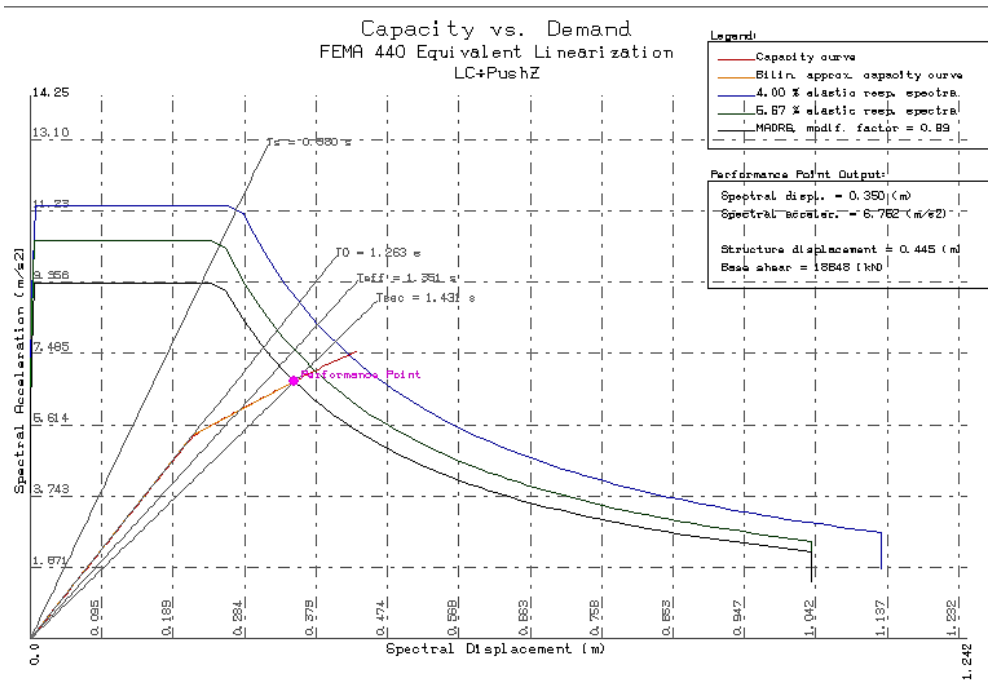

Figure 6. 41 Performance point (Modal distribution-FEMA 440 Equivalent Linearization) for the case considering different importance category (essential).

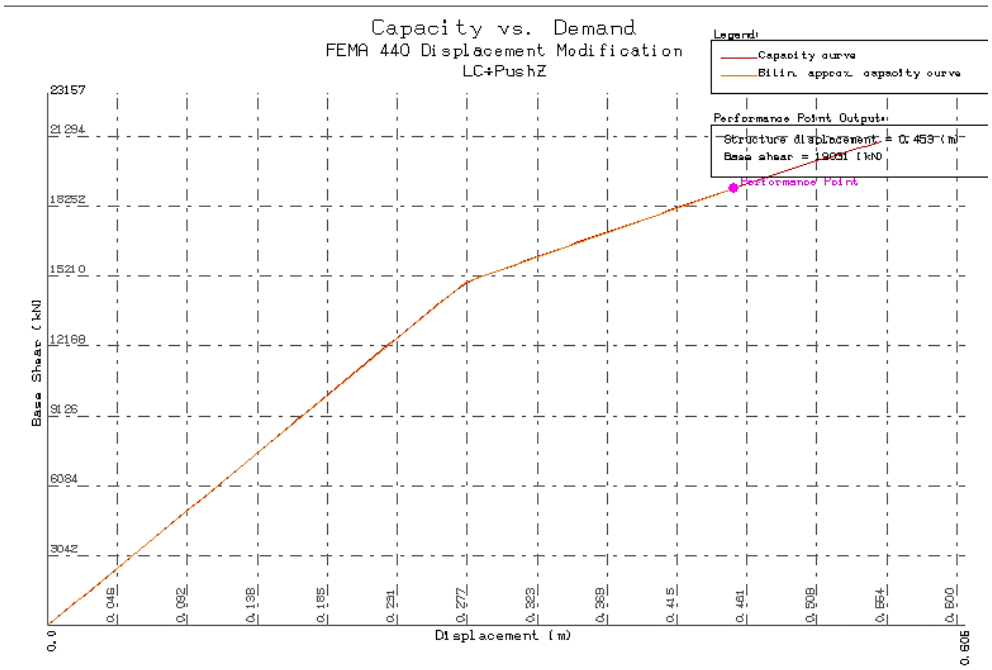

Figure 6. 42 Performance point (Modal distribution -FEMA 440- Displacement modification) for the case considering different importance category (essential).

It is possible to verify that with the change of the response spectrum the deformation and base shear increase significantly. There has been more energy dissipation, considering the position of the performance point on the capacity curve. This energy dissipation, in fact, corresponds essentially to the change in stiffness once the limit of the abutment was reached. Since the response spectrum was modified, without modifying this limit, it is reached before the performance point.

The performance point, for EC N2, falls on the iteration 74 in which the transverse elements have reached the elastic limit and the piers in the left situated near the key of the arch are close to it.

The graphs referring to a uniform load distribution will not be shown here, as they do not differ significantly from those presented, but can be seen in **Annex J.**

Table 6.6 represents the summary of the main values of this analysis.

Table 6. 6 Main results for the modal and uniform distribution for the case with different class of the structure (essential).

		Modal	Uniform
Target Displacement (m)	N2	0,47	0,42
	FEMA 440 Equivalent Linearization	0,44	0,39
	FEMA 440 Displacement Modification	0,45	0,40
Base Shear Force (kN)	N2	19388	20268
	FEMA 440 Equivalent Linearization	18847	19475
	FEMA 440 Displacement Modification	19031	19709
Effective T	N2	1,31	1,50
	FEMA 440 Equivalent Linearization	1,35	1,58
	FEMA 440 Displacement Modification	1,26	1,42

6.4.5 ANALYSIS OF A STRUCTURE WITH REDUCED SECTION

In this analysis, the stiffness of the structure will be reduced. Table 6.7 shows the sections in the original case. In order to reduce the sections an excel sheet was used that is represented in the table 6.8 and 6.9. The internal forces were extracted from the software for the structure subjected to the elastic earthquake and a spectral analysis. For these forces, the dimensions were modified, so as to obtain stresses close, but not exceeding the yield stress.

Table 6. 7 Sections in the original case.

Element	a	b	tfe	tw
Arch	2000	1500	40	40
P1	650	650	25.4	25.4
P2	650	650	40	40
Columns	650	650	30	30
Transverse Beam	650	650	30	30

Table 6. 8 Change of the section in the structure.

Element	N	My	Mz
Arch	9315	5911	10179
P1	1602	176	881
P2	1805	426	1313
Columns	1599	4003	197
Transverse Beam	6	2033	2572

Table 6. 9 Change of the sections in the structure.

Element	a	b	tfe	tw	A	Iy	Iz	σmáx
Arch	1000	1500	40	40	215200	3,29E+10	4,75E+10	294
P1	450	450	20	20	34400	1,06E+09	1,06E+09	270
P2	450	450	40	40	65600	1,86E+09	1,86E+09	238
Columns	650	650	30	30	74400	4,78E+09	4,78E+09	307
Transverse Beam	650	650	30	30	74400	4,78E+09	4,78E+09	313

With the new sections, capacity curves were obtained for the modal and uniform loading that are represented in the fig 6.43 and 6.44.

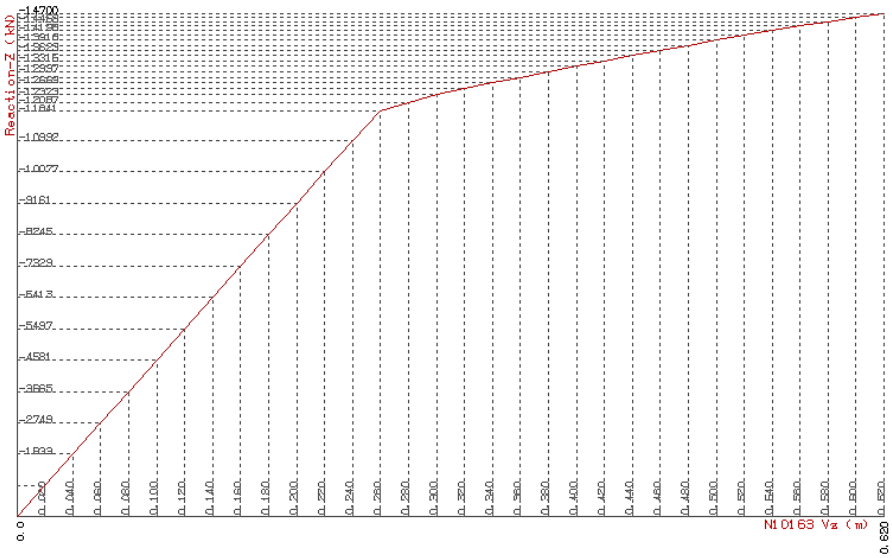

Figure 6. 43 Capacity curve for the reduced section scenario (modal).

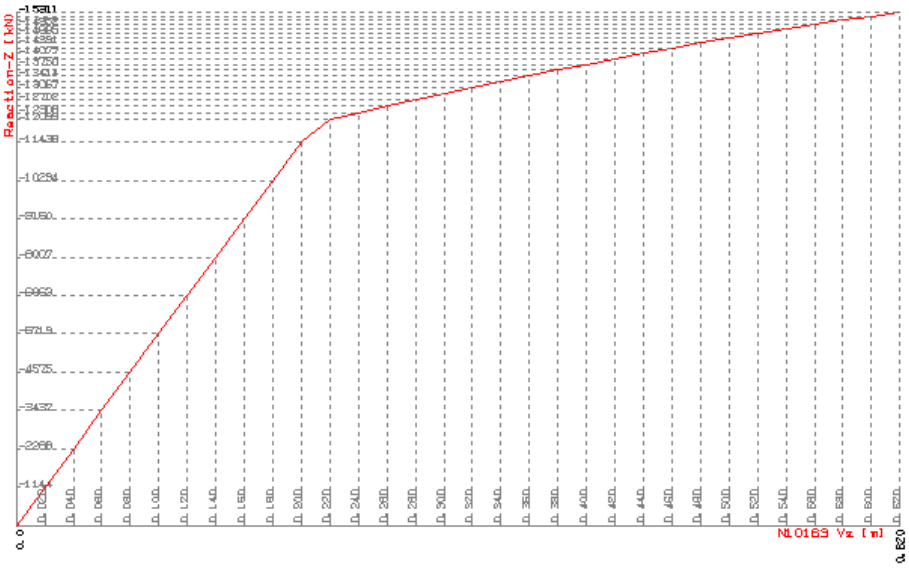

Figure 6. 44 Capacity curve for the reduced section scenario (uniform).

The two curves are very similar to each other with a maximum displacement equal to 0.62 m and a maximum base shear force equal to 14700 kN and 15311 kN for modal and uniform case. In the case of the uniform distribution, the slope change occurs sooner than in the modal distribution because this moment corresponds to the moment when the reaction limit is reached in the abutments and in the uniform distribution the increment of load, due to the load pattern, in the supports is more accentuated. This moment can correspond to the beginning of the formation of the first plastic hinge, considering the normal stresses diagram.

In fig.6.45 the capacity curves referring to the initial case and the case of the reduced section are represented, both subjected to a modal load pattern. The two curves are quite distinct, with the capacity curve of the reduced section having a lower base shear force, what was expected as there was a reduction of the section and consequent reduction of the stiffness of the structure. The curve of the reduced section presents a more horizontal branch because its stiffness is different, and it was verified that in the last iterations the elements of the arch already began to achieve its elastic limit what did not happen in the original case. This may be an indication that a ductile behavior has started and leaded to a bigger deformation of the capacity curve.

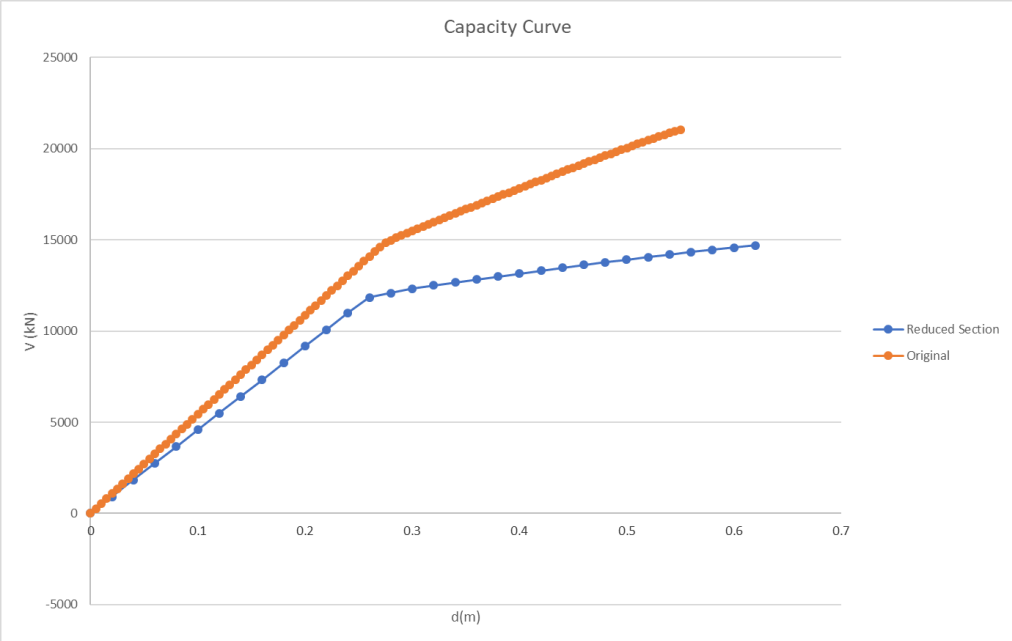

Figure 6. 45 Comparison between capacity curves in original case and in the case with reduced section.

In figures 6.46-6.49 the performance point according to the EC-N2 approach is represented, the ones obtained with the other methodologies are in the **Annex K**. The performance point is achieved for a displacement of 0.263 and 0.234 m and a base shear force of 11883 kN and 12247 kN for a modal and uniform distribution.

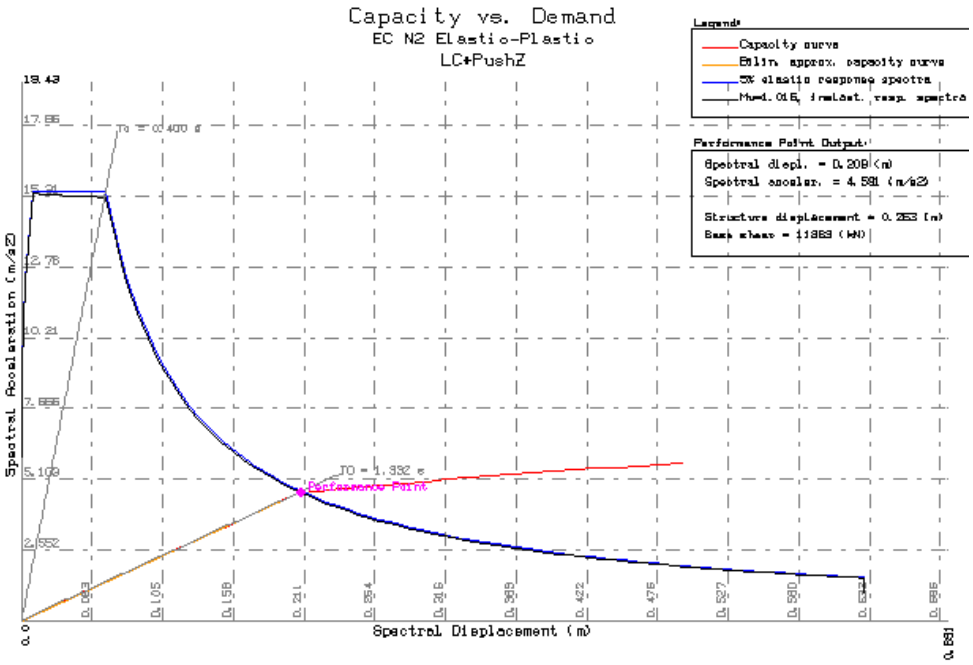

Figure 6. 46 Performance point (EC-N2- modal distribution) for the reduced section scenario.

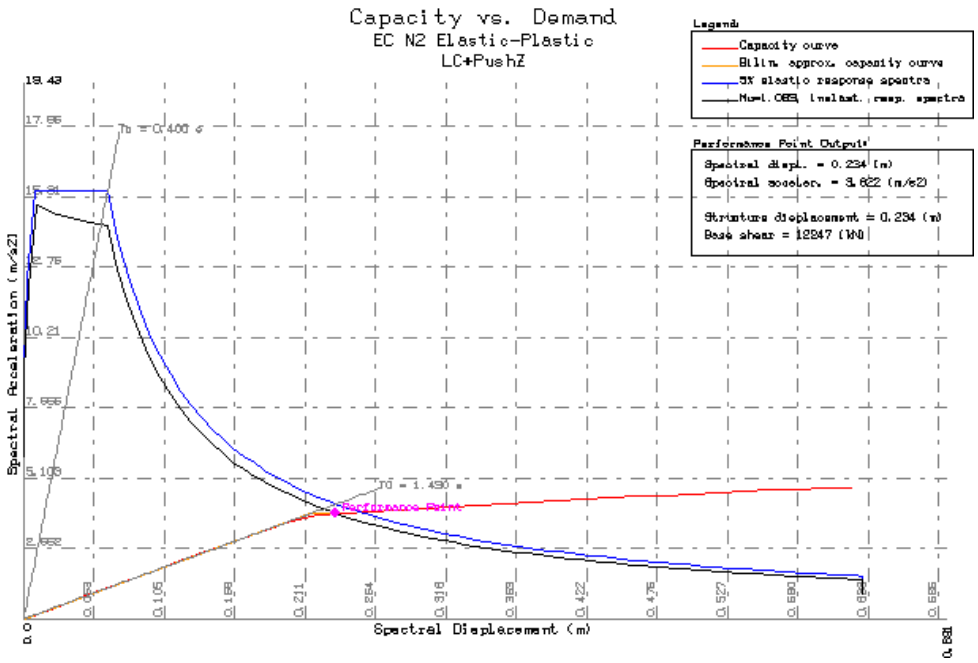

Figure 6. 47 Performance point (EC-N2 - uniform distribution) for the reduced section scenario.

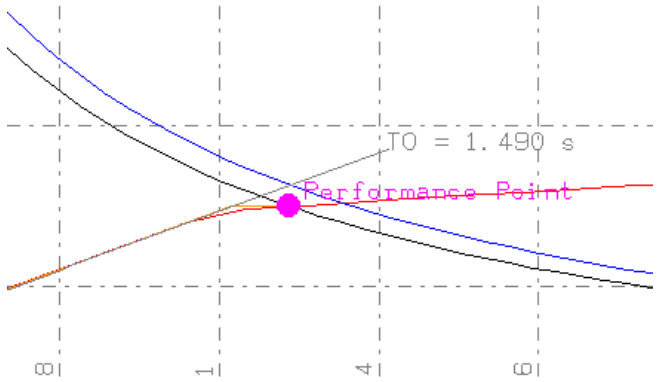

Figure 6. 48 Detail extracted from the Figure 6.47.

It is verified that the performance point in comparison with the initial analysis presents a greater displacement, but a lower shear base force reached.

When looking at the detail shown in fig 6.48, the performance point seems to be outside the elastic branch of the curve, in a zone where some dissipation of energy already occurred. In comparison to the case study analysis it can be verified an increase in the effective period, what can be seen in the table 6.10, which is due to the fact that it is inversely proportional to stiffness. In the case study the ductility factor is practically equal to one, whereas in this case, there is already a certain ductility, although reduced.

Table 6. 10 Main results for the modal and uniform distribution for the reduced section scenario.

Load Distribution		**Modal**	**Uniform**
Target Displacement (m)	N2	0,26	0,23
	FEMA 440 Equivalent Linearization	0,26	0,23
	FEMA 440 Displacement Modification	0,26	0,23
Base Shear Force (kN)	N2	11882,94	12247,36
	FEMA 440 Equivalent Linearization	11879,35	12238,66
	FEMA 440 Displacement Modification	11882,13	12242,79
Effective T	N2	1,332	1,490
	FEMA 440 Equivalent Linearization	1,333	1,487
	FEMA 440 Displacement Modification	1,331	1,487
Ductility	N2	1,015	1,089
	FEMA 440 Equivalent Linearization	1,090	1,144
	FEMA 440 Displacement Modification	1,015	1,125

6.4.6 ANALYSIS OF A STRUCTURE IN ORDER TO ANALYZE THE CAPACITY CURVE

A complementary analysis was performed in order to better understand the capacity curve and the sudden stiffness loss that occurs in the capacity curve in the original case. For this purpose, the abutments were released, and the sections modified (Table 6.11).

The section of the arch was reduced, in order to force a plastic behavior along the capacity curve, but taking into attention not to reduce too much the stiffness of the arch in transverse direction because reducing the stiffness significantly would lead to a corresponding decrease in the forces taken by the arch, leading once again to an elastic behavior. Thus, the dimensions of the arch were reduced essentially in the vertical dimension.

Since the abutments no longer could absorb the internal forces, the section of the outer piers (pier 1) was increased to withstand the increase of load. As the section of the outer pier was increased, this led to a situation where this pier, much shorter than the following one, was much stiffer. Thus, the section of pier two was increased as well.

The section of the transverse beam was increased in order to prevent from being the first element to reach the yield stress.

It should be noted that the lateral load distribution is the same as in the original case (modal), which is reasonable if the objective is to purely evaluate the capacity curve. In reality, this new configuration would lead to a modal load pattern closer to the uniform load pattern.

Table 6. 11 Sections used for the analysis of a structure in order to analyse the capacity curve.

Element	h (mm)	b (mm)	t web	t web center	t flange
Arch	1000	1500	40	2	10
Outer pier (1)	650	650	35	-	35
Pier 2	650	650	85	-	85
Transverse Beam	650	650	40	-	40

In Figure 6.12 the two capacity curves are shown and it can be seen that the new curve has a similar inclination as the curve of the original model, once the limits of the abutments are reached.

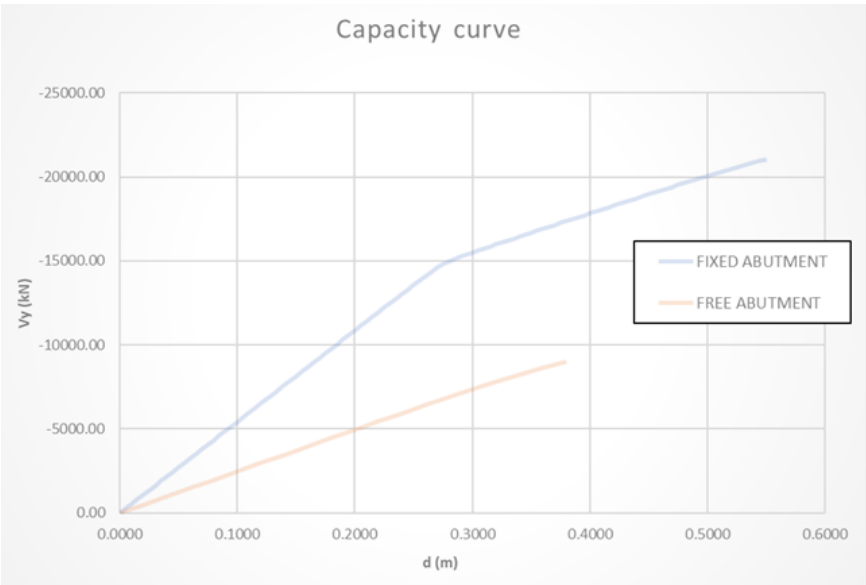

Figure 6. 49 Comparison between the capacity curve obtained for the original case and for the case with free abutments.

Figure 6.50 represents the change in stiffness that occurred in this new case. From the indicated image it is possible to clearly appreciate some inelastic (ductile) behavior that occurs in the structure and conclude that the sudden loss in stiffness is due to the abutments that reached their maximum.

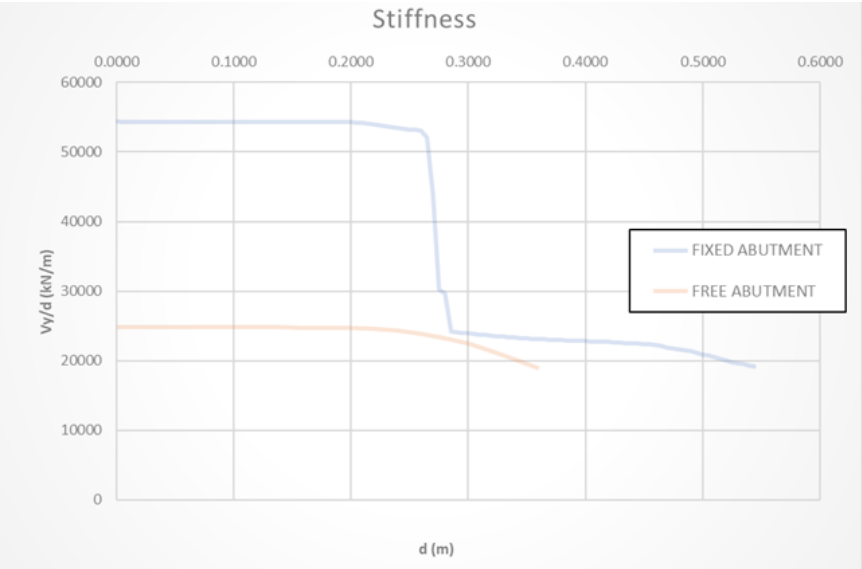

Figure 6. 50 Change in stiffness in the original case and in the case with free abutments.

7
CONCLUSIONS

7.1 DISCUSSION

Due to the fact that the case study never passed the preliminary design stage, most of the elements were defined using preliminary design strategies. The subsequent analysis showed that for the earthquake in question the structure is almost entirely in the elastic branch at the performance point and that the dimensions of some elements, based on the seismic transverse analysis, could be optimized in the detailed design stage.

The obtained capacity curve doesn't present a relevant level of plasticization, since the arch, which is the main energy-dissipating element, does not come out of its elastic domain. The capacity curves are "conditioned" by the stiffness of the abutments, "hiding" the loss of stiffness due to the plasticization of the metallic elements.

It is possible to conclude that the three proposed methods of analysis (EC-N2, FEMA 440-Linearization and FEMA 440-Displacement) led to very similar results, what was expected given their similarities. As for the application of load, which in this study was applied as a modal and uniform load pattern, it was verified that the latter one presented inferior displacements and superior base shear forces due to the fact that, in the uniform load pattern, the total mass is applied, and a greater load is concentrated near to a fixed point (abutments). Given the typology of the bridge and low mobilized mass, the longitudinal analysis was not performed because it would not allow to obtain reliable results.

Pushover analysis is a very useful tool in the design of structures, allowing to meet specific performance criteria required by codes or owner of the future project. In this case, the structure would be in the operational performance level.

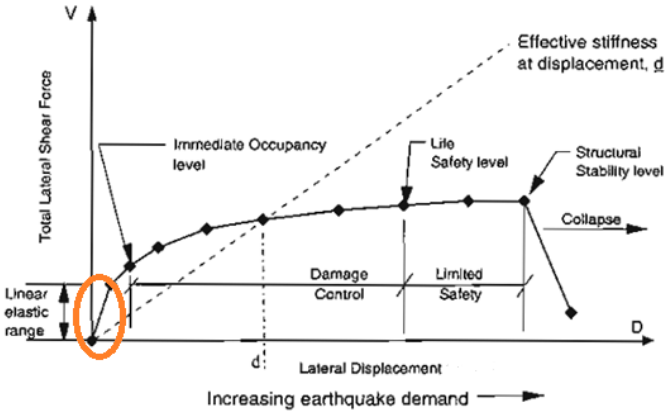

Figure 7. 1 Localization of the performance point (case study) accordingly to performance level [30].

The software used, RM Bridge, presents advantages and limitations compared to other software's in the market. Although it does not allow the visualization of the plastic hinges and the sequence of their formation it can be a relevant tool in a design office, like in the case of Pedelta, where the main goal is to assure that the performance point meets the specific demands, saving time and making this analysis more appealing to structures not only of great importance, but all the others. The software allows to perform iterations very easily by having all the geometry and loads introduced in a parametric way and allows to define the models with the help of text files with programming routines. The main problem is to analyse the capacity curve, in particular in the ductile branch, but for an analysis where the main concern is to find performance point, it is very practical. According, to information provided by the developers of the software, improvements are envisaged, primarily in the detection of the elements that fail when the capacity curve ends.

In order to circumvent the constraint imposed by the software in knowing which of the elements led to the rupture of the capacity curve, another software, FAGUS, was used. Using the forces extracted from RM Bridge for the last iteration, moment-curvature curves were obtained, and the corresponding curvatures of the most relevant elements were positioned in these curves. The conclusion reached is that the transverse beam connecting both arches near the foundations, with great probability, was responsible for the termination of the capacity curve. As this element is secondary, the structure could possibly still be able to withstand more force increments.

Also, it was concluded that for the design elastic basal level, the capacity curve remains in the elastic regime, which means that, no advantage is taken from the ductility of the structure, which leads to a behaviour factor close to 1.0.

The two additional analyses, that consisted in the change of the seimic importance class and the cross section, still led to a performance point just outside the elastic branch.

Finally, the third analysis allowed to confirm that the sudden change in stiffness, that occurred in all the cases shown previously, was, essentially, due to the abutments reaching their maximum. In the case of this third analysis, all the dissipated energy in the capacity curve, was entirely due to the ductile behavior of the steel elements.

7.2 Recommendations for Future Developments

During the analysis of the case study, some of the topics were treated briefly due to lack of time and that should be taken into account in future analyzes:

- The comparison of the obtained results with those from a time-history analysis, where interaction with higher vibration modes is accurately captured.
- The analysis in the longitudinal direction followed by a comparison of results with those from a time-history analysis.
- The modeling of the deck considering its non-linear behavior.
- The determination of capacity curves with a software allowing the identification of plastic hinges and of the failing elements.
- The consideration of the soil-structure nonlinear behavior.

REFERENCES

[1] "Cambridge Dictionary," Cambridge University Press, Available: https://dictionary.cambridge.org/dictionary/english-spanish/bridge. [04 /2019].

[2] "Visit Portugal,". Available: https://www.visitportugal.com/pt-pt/content/aqueduto-das-%C3%A1guas-livres-1. [04 /2019]

[3] L. F. Troyano, Bridge Engineering: A Global Perspective, Thomas Telford Ltd, 2003.

[4] J. Sobrino, "PEDELTA:Projects," Available: https://pedelta.com/portfolio_page/lleida-gfrp-pedestrian-bridge/. [05/ 2019].

[5] BERD, "BERD FEUP WIBEPRIZE,". Available: https://paginas.fe.up.pt/~wibe/.[04 /2019]

[6] S. J. S. R. H.-L. D. F. &. S. A. L. De Waal, "BERD WIBE Prize,". Available: https://paginas.fe.up.pt/~wibe/wp-content/uploads/WIBE-Prize-Ceremony-Press_low.pdf. [05 /2019]

[7] N. P. Walsh, "Arch Daily : World's Largest 3D-Printed Concrete Pedestrian Bridge Completed in China,". Available: https://www.archdaily.com/909534/worlds-largest-3d-printed-concrete-pedestrian-bridge-completed-in-china. [05 /2019]

[8] P. Pacheco, "Disciplina de Pontes," 2018.

[9] A. d. Fonseca, "Contemporary Concrete Arch Bridges," em *8th International Conference on Arch Bridges*, Wroclaw, 2016.

[10] "Way Marking," Available: http://www.waymarking.com/gallery/image.aspx?f=1&guid=13fbc7b3-9b43-41b5-b9ea-f906aa06518e&gid=3.

[11] "Highest Bridges : Danhe Bridge," Available: http://www.highestbridges.com/wiki/index.php?title=Danhe_Bridge. [05 /2019]

[12] P. Tomkins, "Visit Scotland,". Available: https://www.visitscotland.com/info/towns-villages/craigellachie-bridge-p1457971 .

[13] G. M. López, "Poleni´s Manuscripts about the Dome of Saint Peter's,"

[14] M. A. Jean-Paul Lebet, Steel Bridges: Conceptual and Structural Design of Steel and Steel-Concrete Composite Bridges, EPFL Press, 2013.

[15] "Wikipedia,". Available: https://en.wikipedia.org/wiki/Garabit_viaduct. [04 /2019]

[16] D. Frieder, "Untapped Cities,". Available: https://untappedcities.com/2018/03/09/the-top-10-secrets-of-hell-gate-bridge-in-nyc/.[04 /2019]

[17] "New Steel Construction," Available: https://www.newsteelconstruction.com/wp/ssda-2005-river-usk-crossing-newport-southern-distributor-road/ . [04 /2019]

[18] J. Manterola, Puentes: Tomo VI, 2000.

[19] L. F. Troyano, "PROCEDURES FOR THE CONSTRUCTION OF LARGE CONCRETE ARCHES," em *ARCH´04*, Madrid, 2004.

[20] J. Appleton, A. Costa, N. Travassos e P. França, "Ponte sobre o Rio Cávado EN304 - km 76+626 (Inspecçao, Reabilitaçao e Reforço)," em *ASCP'09 – 1º Congresso de Segurança e Conservação de Pontes ASCP* , Lisbon, 2009.

[21] A. F. e. Abreu, Evolução da Construção de Pontes na obra da J.A.E, Ministério das Obras Públicas, 1953.

[22] S. P.-F. Martínez, "ARCHES: EVOLUTION AND FUTURE TRENDS," em *ARCH´04*, 2004.

[23] "Adif Alta Velocidad," Available: http://www.adifaltavelocidad.es/es_ES/comunicacion_y_prensa/fichas_de_actualidad/ficha_actualidad_00074.shtml. [05/2019]

[24] PROIN3D, "Proceso constructivo del viaducto del río Tajo, embalse de Alcántara, en el Tramo Talayuela - Cáceres de la Línea de Alta Velocidad a Extremadura," PROIN3D, 2013. Available: https://www.youtube.com/watch?v=y17zGG0oZkU. [04/2019]

[25] "Structurae," Available: https://structurae.net/structures/lussia-bridge/photos. [05/2019]

[26] J. S. J.A.Llomabrt, "Bridge over the river Tagus at Alcántara Reservoir,". Available: https://www.researchgate.net/publication/26524677_Puente_sobre_el_rio_Tajo_en_el_Embalse_de_Alcantara_Arcos_de_Alconetar/fulltext/03c4ee360cf2d448b67ada88/26524677_Puente_sobre_el_rio_Tajo_en_el_Embalse_de_Alcantara_Arcos_de_Alconetar.pdf. [05 /2019]

[27] I. G. E. K. M.Lee Marsh, "LRFD Seismic Analysis and Dedign of Bridges," 2014.

[28] R. Ribeiro, "Análise Pushover de Pontes em Betão Armado," FEUP, Porto, 2008.

[29] W.-F. C. a. L. Duan, Bridge Engineering Handbook,Second Edition. Seismic Design, Florida: Taylor & Francis Group, 2014.

[30] Applied Technology Council, ATC-40 : Seismic Evaluation and Retrofit of Concrete Buildings,Volume 1, California, 1996.

[31] S. R.Bento, "Non-Linear Static Procedures in Performance Based Seismic Design," em *13th World Conference on Eartquake Engineering*, Vancouver, 2004.

[32] Applied Technology Counci, FEMA 440 : IMPROVEMENT OF NONLINEAR STATICSEISMIC ANALYSIS PROCEDURES, California, 2005.

[33] E. C. f. Standardization, Eurocode 8: Design of structures for earthquake resistance - Part 1 EN 1998-1, Brussels: CEN, 2004.

[34] AMERICAN SOCIETY OF CIVIL ENGINEERS, FEMA 356, Virginia, 2000.

[35] Associacion Guatemalteca de Ingenieria Estructural y Sismica, Normas de Seguridad Estructural de Edificaciones y Obras de Infraestrutura para La República de Guatemala, Guatemala, 2010.

[36] U. T. G. Zheng Y, “Ductility of thin-walled steel box stub-columns.,” *Journal of Structural Engineering,* 2000.

[37] Z. L. G. Tsutomu Usami, Seismic performance evaluation of steel arch bridges against major earthquakes. Part 1: Dynamic analysis approach, Japão: John Wiley & Sons, Ltd, 2004.

[38] A. M. R. R. W. Gregory G. Deierlein, Nonlinear Structural Analysis For Seismic Design, National Institute of Standards and Technology.

[39] B. D.-S. Svetlana Kostic, “Fiber element formulation for inelastic frame analysis,” *Gradjevinski materijali i konstrukcije,* 2016.

[40] F. Marmo, A fiber-free approach to the inelastic analysis of reinforced concrete structures, Napoli, 2007.

[41] A. V. A. Y. José Miguel Castro, “Nova Metodologia de Dimensionamento Sísmico de Pórticos Metálicos,” em *VII Congresso de Construção Metálica e Mista*.

ANNEX A - CALCULATING T_{eff} and β_{eff} (FEMA 440)

Effective Period :

For 1.0 < μ < 4.0

$$T_{eff} = [G(\mu - 1)^2 + H(\mu - 1)^3 + 1]T_0 \tag{A.1}$$

For 4.0 ≤ μ ≤ 6.5

$$T_{eff} = [I + J(\mu - 1) + 1]T_0 \tag{A.2}$$

For μ > 6.5

$$T_{eff} = \left\{ K \left[\sqrt{\frac{(\mu - 1)}{1 + L(\mu - 2)}} - 1 \right] + 1 \right\} T_0 \tag{A.3}$$

Effective damping

For 1.0 < μ < 4.0

$$\beta_{eff} = A(\mu - 1)^2 + B(\mu - 1)^3 + \beta_0 \tag{A.4}$$

For 4.0 ≤ μ ≤ 6.5

$$\beta_{eff} = C + D(\mu - 1) + \beta_0 \tag{A.5}$$

For μ > 6.5

$$\beta_{eff} = E \left[\frac{F(\mu - 1) - 1}{[F(\mu - 1)]^2} \right] \left(\frac{T_{eff}}{T_0} \right)^2 + \beta_0 \tag{A.6}$$

Where:

- A through L are coefficients that depend on the energy dissipation hysteretic behavior and on the characteristics of the capacity curve for the oscillator in terms of basic hysteretic and post-elastic stiffness, α (slope of the post-yielding branch of the bilinear representation of the capacity curve). In the FEMA440 three different types of hysteretic behavior are proposed:
    - BLH - Bilinear Hysteretic (Type A in the ATC40)
        - structures with reasonably full hysteretic loops (similar to an elastoplastic Perfectly plastic behavior - EPP)

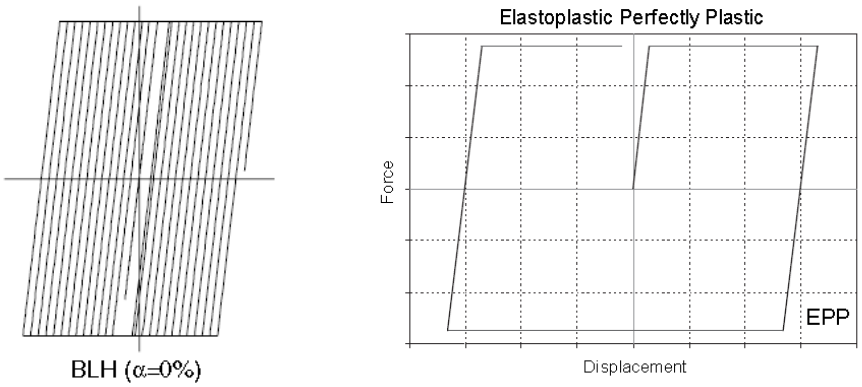

Figure A.1 Types of inelastic behavior considered, BLH=Bilinear Hysteretic [25].

- STDG – Stiffness degrading model (Type B in the ATC40)
  - structures with a hysteretic behavior between stiffness degrading and stiffness and strength degrading models.

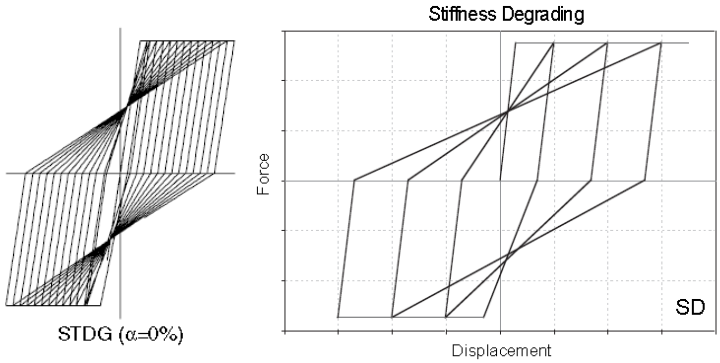

Figure A.2 Types of inelastic behavior considered, STDG = Stiffness Degrading [25].

- STRDG - Strength degrading model (different from Type C in ATC40)
  - Structures with severely degraded hysteretic loops (strength and stiffness degrading systems - SSD)

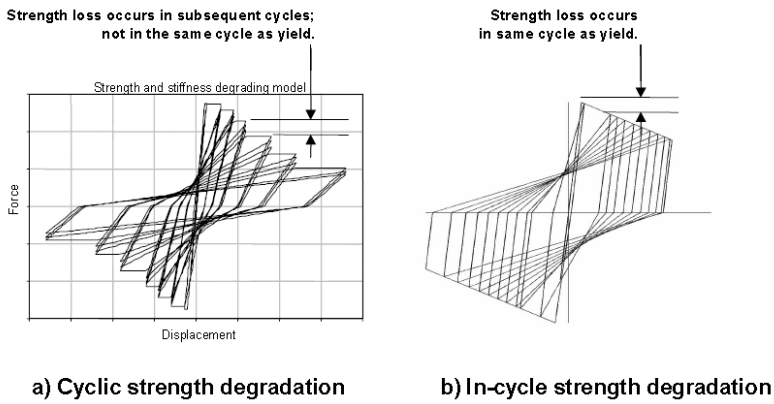

Figure A.3 Types of inelastic behavior considered, STRDG=Strength Degrading [25].

ANNEX B-SIMPLIFIED EQUATIONS FOR CALCULATING T_{eff} and β_{eff} (FEMA 440)

The FEMA440 also proposes the following simplified equations, in case of doubts on which model to use, that are independent on the hysteretic model or α value.

Effective Period

For 1.0 < μ < 4.0

$$T_{eff} = [0.20(\mu - 1)^2 - 0.038(\mu - 1)^3 + 1]T_0 \tag{B.1}$$

For 4.0 ≤ μ ≤ 6.5

$$T_{eff} = [0.28 + 0.13(\mu - 1) + 1]T_0 \tag{B.2}$$

For μ > 6.5

$$T_{eff} = \left\{0.89\left[\sqrt{\frac{(\mu - 1)}{1 + 0.05(\mu - 2)}} - 1\right] + 1\right\}T_0 \tag{B.3}$$

Effective damping

For 1.0 < μ < 4.0

$$\beta_{eff} = 4.9(\mu - 1)^2 - 1.1(\mu - 1)^3 + \beta_0 \tag{B.4}$$

For 4.0 ≤ μ ≤ 6.5

$$\beta_{eff} = 14 + 0.32(\mu - 1) + \beta_0 \tag{B.5}$$

For μ > 6.5

$$\beta_{eff} = 19\left[\frac{0.64(\mu - 1) - 1}{[0.64(\mu - 1)]^2}\right]\left(\frac{T_{eff}}{T_0}\right)^2 + \beta_0 \tag{B.6}$$

ANNEX C – SPECIFIC RULES FOR THE PUSHOVER ANALYSIS OF BRIDGES (EUROCODE EN 1998-2:2005)

- The analysis should be made for each horizontal direction
- The control node should be the center of mass of the deformed deck
- The analysis should be carried out until a target displacement equal to the elastic deformation calculated using effective stiffness of ductile members and the multi-modal response spectrum analysis with the two horizontal directions combined with $E_1+0.3E_2$ (E1 longitudinal earthquake and E2 transversal earthquake) and $E_2+0.3E_1$.
- The horizontal load increments are given by:
    - $\Delta F_{i,j} = \Delta\alpha_j g M_i \zeta_i$, where:
    - $\Delta\alpha_j$ is the horizontal force increment, normalized to weight gM_i applied in step j
    - ζ_i is a shape factor defining the load distribution along the whole structure. Unless a better approximation is used, the following distributions should be investigated:
        - Constant along the deck (*Uniform* pattern)
            - $\zeta_i = 1$ (deck)
            - $\zeta_i = \frac{z_i}{z_p}$ for the piers, where z_i is the height of each point and z_p is the pier total height
        - Proportional to the first mode shape (*Modal* pattern)
            - ζ_i is proportional to the component, in the considered direction, of the modal displacement at point i. The mode with largest mass contribution in each direction should be used. For piers, the following expression can be used:
                - $\zeta_i = \zeta_{T,P}\frac{z_i}{z_p}$, where $\zeta_{T,P}$ is the value of ζ at the joint Pier-Deck

ANNEX D – TRANSFORMATION OF THE RESPONSE SPECTRUM IN THE FORMAT (Sa, T) to format (Sa, Sd).

T (s)	Se(T) (m/s2)	Sd(T)
0,00	6,180	0,0000000000
0,05	9,270	0,0005870581
0,10	12,361	0,0031309766
0,13	14,215	0,0060850529
0,14	14,833	0,0073640569
0,20	15,451	0,0156548828
0,30	15,451	0,0352234863
0,40	15,451	0,0626195311
0,50	12,361	0,0782744139
0,60	10,301	0,0939292967
0,70	8,829	0,1095841795
0,80	7,725	0,1252390623
0,90	6,867	0,1408939450
1,00	6,180	0,1565488278
1,10	5,618	0,1722037106
1,20	5,150	0,1878585934
1,30	4,754	0,2035134762
1,40	4,415	0,2191683589
1,50	4,120	0,2348232417
1,60	3,863	0,2504781245
1,70	3,635	0,2661330073
1,80	3,434	0,2817878901
1,90	3,253	0,2974427729
2,00	3,090	0,3130976556
2,10	2,803	0,3130976556
2,20	2,554	0,3130976556
2,30	2,337	0,3130976556
2,40	2,146	0,3130976556
2,50	1,978	0,3130976556
2,60	1,828	0,3130976556
2,70	1,696	0,3130976556
2,80	1,577	0,3130976556
2,90	1,470	0,3130976556
3,00	1,373	0,3130976556
3,10	1,286	0,3130976556
3,20	1,207	0,3130976556
3,30	1,135	0,3130976556
3,40	1,069	0,3130976556
3,50	1,009	0,3130976556
3,60	0,954	0,3130976556
3,70	0,903	0,3130976556
3,80	0,856	0,3130976556
3,90	0,813	0,3130976556
4,00	0,773	0,3130976556
1,71	3,613	0,2677572523

ANNEX E – INELASTIC RESPONSE SPECTRUM FOR THE CANTILEVER EXAMPLE

Sd(T)	Se*(T) (m/s2)=Se(t)/Ru
0,000	4,091063482
0,001	6,136595223
0,003	8,182126964
0,006	9,409446008
0,007	9,818552357
0,016	10,2276587
0,035	10,2276587
0,063	10,2276587
0,078	8,182126964
0,094	6,818439136
0,110	5,844376403
0,125	5,113829352
0,141	4,545626091
0,157	4,091063482
0,172	3,71914862
0,188	3,409219568
0,204	3,146971909
0,219	2,922188201
0,235	2,727375655
0,250	2,556914676
0,266	2,406507931
0,282	2,272813045
0,297	2,153191306
0,313	2,045531741
0,313	1,855357588
0,313	1,6905221
0,313	1,546715872
0,313	1,420508153
0,313	1,309140314
0,313	1,210373811
0,313	1,122376813
0,313	1,043638643
0,313	0,972904514
0,313	0,909125218
0,313	0,851417998
0,313	0,799035836
0,313	0,751343156
0,313	0,70779645
0,313	0,667928732
0,313	0,631336957
0,313	0,597671802
0,313	0,566629291
0,313	0,537943916
0,313	0,511382935

ANNEX F – MANUAL CLASSIFICATION OF THE SECTION ACCORDINGLY TO EN 1993-1-1:2005

Componentes internos comprimidos				
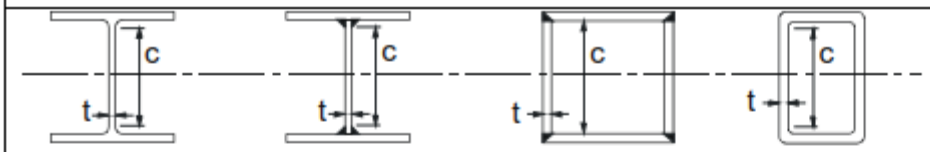				Eixo de flexão
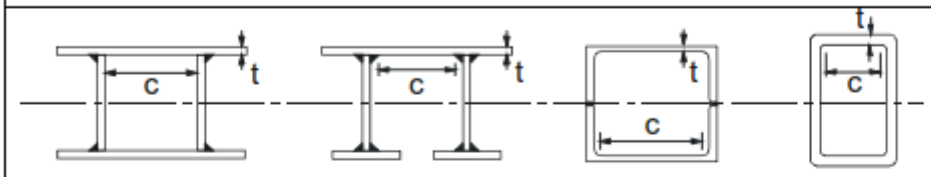				Eixo de flexão
Classe	Componente solicitado à flexão	Componente solicitado à compressão	Componente solicitado à flexão e à compressão	
Distribuição das tensões nos componentes (compressão positiva)	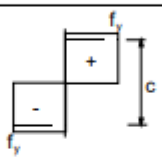	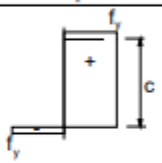	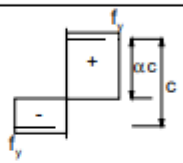	
1	$c/t \le 72\varepsilon$	$c/t \le 33\varepsilon$	quando $\alpha > 0{,}5$: $c/t \le \frac{396\,\varepsilon}{13\,\alpha - 1}$ quando $\alpha \le 0{,}5$: $c/t \le \frac{36\,\varepsilon}{\alpha}$	
2	$c/t \le 83\varepsilon$	$c/t \le 38\varepsilon$	quando $\alpha > 0{,}5$: $c/t \le \frac{456\,\varepsilon}{13\,\alpha - 1}$ quando $\alpha \le 0{,}5$: $c/t \le \frac{41{,}5\,\varepsilon}{\alpha}$	
Distribuição das tensões nos componentes (compressão positiva)	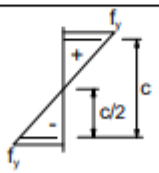	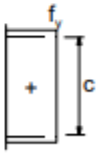	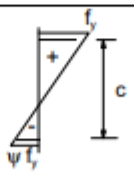	
3	$c/t \le 124\varepsilon$	$c/t \le 42\varepsilon$	quando $\psi > -1$: $c/t \le \frac{42\varepsilon}{0{,}67 + 0{,}33\psi}$ quando $\psi \le -1$ *): $c/t \le 62\varepsilon(1-\psi)\sqrt{(-\psi)}$	

$\varepsilon = \sqrt{235/f_y}$	f_y	235	275	355	420	460
	ε	1,00	0,92	0,81	0,75	0,71

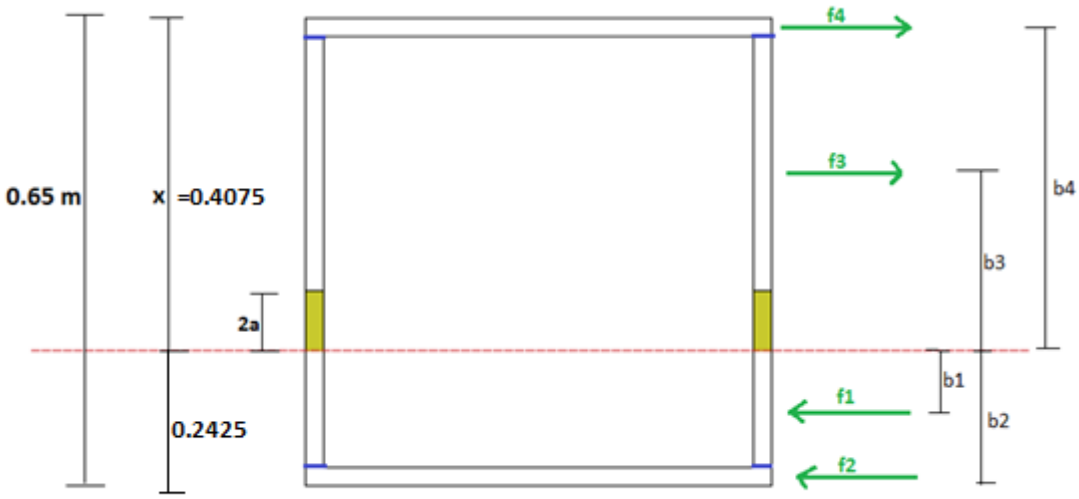

$$N = 2at_w f_y \ (=)\ 2a = \frac{2974}{0.0254 * 2 * 355 * 10^3} = 0.165\ m$$

$$f1 = (0.65 - x - 0.0254) * 0.0254 * 2 * 355 * 10^3$$
$$f2 = 0.0254 * 0.65 * 355 * 10^3$$
$$f3 = (x - 0.0254 - 0.165) * 0.0254 * 2 * 355 * 10^3$$
$$f4 = 0.0254 * 0.65 * 355 * 10^3$$

$$b1 = \frac{0.65 - x - 0.0254}{2}$$
$$b2 = 0.65 - x - \frac{0.0254}{2}$$
$$b3 = \frac{x - 0.0254 - 0.165}{2} + 0.165$$
$$b4 = x - 0.0254/2$$

$$f1 + f2 = f3 + f4\ (=)x = 0.4075\ m$$

Web Classification:

$$\alpha = \frac{0.4075 - 0.0254}{0.599} = 0.638$$
$$\frac{c}{t} = \frac{0.5992}{0.0254} = 23.6 \leq \frac{396\varepsilon}{13\alpha - 1} = \frac{396 * 0.81}{13 * 0.638 - 1} = 43.97$$

Class 1.

Classification top flange:

$$\frac{c}{t} = \frac{23.6}{0.0254} = 23.6 \leq 33\varepsilon = 33 * 0.81 = 26.7$$

Class 1

Classification bottom flange:

Class 1 because it is in tension.

Therefore, the cross-section is Class 1.

ANNEX G – MODIFICATION OF THE MATERIAL CURVE TAKING INTO ACCOUNT LOCAL BUCKLING

FAILURE CRITERIA UNSTIFFENED ELEMENTS N/Ny<0.5						
	SHS650*25,4	SHS650*50,8	SHS650*38,1	Arch long	Arch long	
Material						
v	0,3	0,3	0,3	0,3	0,3	
E	200000	200000	200000	200000	200000	MPa
Fy	345	345	345	345	345	MPa
Section						
width	650	650	650	1500	1500	mm
n cells	1	1	1	2	2	
depth	650	650	650	2000	2000	mm
t flanges	25,4	50,8	38,1	25	44,5	mm
t walls	25,4	50,8	38,1	19	38,1	mm
t webs	0	0	0	19	38,1	mm
direction	transv	transv	transv	long	long	
B	599,2	548,4	573,8	731	711,9	mm
t	25,4	50,8	38,1	25	44,5	
A	63459,36	121757,44	93253,56	186150	351927,3	mm2
n	1	1	1	1	1	
Rf	0,52	0,24	0,33	0,64	0,35	
Ultimate strength						
Ny	21882538	41985324	32156400	64221750	121354241	N
N	1500000	1500000	1500000	7500000	7500000	N
N/Ny	0,1	0,0	0,0	0,1	0,1	
εu/εy	**8**	**17**	**17**	**5**	**17**	
εy	1,72	1,72	1,72	1,72	1,72	**‰**
εu	17,2	17,2	17,2	17,2	17,2	**‰**
εu'	13,2	17,2	17,2	7,9	17,2	**‰**
fu	448	448	448	448	448	MPa
fu'	**422**	**448**	**448**	**386**	**448**	**MPa**

FAILURE CRITERIA STIFFENED ELEMENTS N/Ny<0.5					
	Arch transv	Arch transv	Arch transv	Arch transv	
Material					
ν	0,3	0,3	0,3	0,3	
E	200000	200000	200000	200000	MPa
Fy	345	345	345	345	MPa
Section					
width	1500	1500	1500	1500	mm
n cells	1	1	1	1	
depth	2000	2000	2000	2000	mm
t flanges	25	38	38	44,5	mm
t walls	19	19	25	38,1	mm
t webs	19	19	25	38,1	mm
direction	transv	transv	transv	transv	
B	1950	1924	1924	1911	mm
t	25	38	38	44,5	
A	186150	223668	258300	351927,3	mm2
Rf	0,57	0,37	0,37	0,31	
Stiffeners					
number	2	2	2	2	
stiff. Depth	100	100	100	100	mm
stiff. Thick	10	10	10	10	mm
n subpanels	3	3	3	3	
subpanel width	650	641,3333333	641,3333333	637	mm
a	100	100	100	100	mm
β	1,623	1,358	1,358	1,284	
Q	0,898	1,000	1,000	1,000	
Eq. "T" stiff+subpanel					
A	17250	25370,66667	25370,66667	29346,5	mm2
COG	16	22	22	25	mm
I	5359488	8339279	8339279	10553282	mm4
rs	17,63	18,13	18,13	18,96	mm
λs	0,08	0,07	0,07	0,07	
Ultimate strength					
Ny	64189655	77126897	89068966	121354241	N
N	7500000	7500000	7500000	7500000	N
N/Ny	0,1	0,1	0,1	0,1	
εu/εy	**8,1685**	**17,2000**	**17,2000**	**17,2000**	
εy	1,72	1,72	1,72	1,72	**‰**
εu	17,2	17,2	17,2	17,2	**‰**
εu'	14,0	17,2	17,2	17,2	**‰**
fu	448	448	448	448	MPa
fu'	**427**	**448**	**448**	**448**	**MPa**

ANNEX H – CALCULATION OF COMPOSED STRESSES USING - VON MISES

Stresses measured at the extreme points of a section.

	LC_PushZ#110				LC_PushZ#110			
	SP:SP01				SP:SP02			
	σ	τy	τz	VonMises	σ	τy	τz	VonMises
40101	-371971	-5966	14554	372,9674	-371970	5962	14549	372,9656
	-371971	-5966	14554	372,9674	-371970	5962	14549	372,9656
40102	-347629	-5966	14552	348,6947	-347629	5961	14548	348,6939
	-347629	-5966	14552	348,6947	-347629	5961	14548	348,6939
31101	-353962	-6307	15393	355,1327	-353961	6313	15399	355,1328
	-353962	-6307	15393	355,1327	-353961	6313	15399	355,1328
801	-362133	8756	16922	363,6336	-75682	28019	31326	105,0091
	-362133	8756	16922	363,6336	-75682	28019	31326	105,0091
901	-389695	15189	13023	391,2328	-55824	35039	36694	104,1099
	-389695	15189	13023	391,2328	-55824	35039	36694	104,1099

	LC_PushZ#110				LC_PushZ#110			
	SP:SP03				SP:SP04			
	σ	τy	τz	VonMises	σ	τy	τz	VonMises
40101	357632	-5962	14549	358,6674	357631	5966	14554	358,6672
	357632	-5962	14549	358,6674	357631	5966	14554	358,6672
40102	295885	-5961	14548	297,1354	295873	5966	14552	297,1244
	295885	-5961	14548	297,1354	295873	5966	14552	297,1244
31101	353696	-6313	15399	354,8687	353696	6307	15393	354,8676
	353696	-6313	15399	354,8687	353696	6307	15393	354,8676
801	362294	9220	16458	363,7644	80512	28483	31790	109,3062
	362294	9220	16458	363,7644	80512	28483	31790	109,3062
901	389652	9169	19043	391,3679	54531	29019	30674	91,22839
	389652	9169	19043	391,3679	54531	29019	30674	91,22839

Stresses measured in the middle of the web and flange of a section.

	LC_PushZ#110				LC_PushZ#110			
	SP:SP01				SP:SP02			
	σ	τy	τz	VonMises	σ	τy	τz	VonMises
40101	-369266	-2	-3865	369,3267	-214424	0	16017	216,2112
	-369266	-2	-3865	369,3267	-214424	0	16017	216,2112
40102	-346430	-2	-3864	346,4946	-63877	0	16015	69,63987
	-346430	-2	-3864	346,4946	-63877	0	16015	69,63987
31101	-352118	3	-4089	352,1892	-3998	0	16952	29,63267
	-352118	3	-4089	352,1892	-3998	0	16952	29,63267
801	-347380	20662	-6544	349,4025	345187	-5051	26831	348,4111
	-347380	20662	-6544	349,4025	345187	-5051	26831	348,4111
901	-359512	27489	-6743	362,8391	357806	-5996	30576	361,8531
	-359512	27489	-6743	362,8391	357806	-5996	30576	361,8531

	LC_PushZ#110				LC_PushZ#110			
	SP:SP03				SP:SP04			
	σ	τy	τz	VonMises	σ	τy	τz	VonMises
40101	354923	2	-3865	354,9861	-214454	0	16021	216,2418
	354923	2	-3865	354,9861	-214454	0	16021	216,2418
40102	267574	2	-3864	267,6577	-63888	0	16019	69,65272
	267574	2	-3864	267,6577	-63888	0	16019	69,65272
31101	351850	-2	-4089	351,9213	-4020	0	16947	29,62706
	351850	-2	-4089	351,9213	-4020	0	16947	29,62706
801	347542	21077	-6544	349,6379	-345026	-5051	27246	348,3483
	347542	21077	-6544	349,6379	-345026	-5051	27246	348,3483
901	359469	22061	-6743	361,6828	-357849	-5996	25148	360,6397
	359469	22061	-6743	361,6828	-357849	-5996	25148	360,6397

ANNEX I –REPRESENTATION OF MOMENT CURVATURE FOR THE ORIGINAL CASE STUDY

			N (kN)	Mlong (kNm)	Mtransv (kNm)	χ (km^{-1})	Composite stresses
Composite stresses not calculated because Mtran very big	Arch	Right	-2078	4675	-34172	1,6	
	(begin)	Left	-16543	4372	-33618	1,6	
	Pier1	Right	58	0	-5398	19,2	
	(base)	Left	-2974	0	-5183	15,3	
	Pier2	Right	426	-1	-5917	3,9	
	(base)	Left	-3199	0	-5774	3,8	
Have composite stresses	Column1	Right	-143	-880	-4471	3,6 (y)	**4556,779674**
	(base)	Left	-2869	948	-4537	3,6(y)	**4634,983603**
Have composite stresses	Column2	Right	-632	-908	-2276	1,9	**2450,436696**
	(base)	Left	-2185	2994	-2331	3	**3794,416556**
The section has not been rotated to be subjected to simple bending because curvature at y very small	Column3	Right	-1212	-170	989	1,1	**1003,50436**
	(base)	Left	-1258	3789	927	4,4(y)	**3900,749928**
The calculation was only made for beam 1 because it is the one that is subject to greater efforts.	Transv.Beam1		**-9**	**4187**	**4816**	**22,2**	**6381,600505**
	Transv.Beam2		72	3444	4718		5841,289241
	Transv.Beam3		42	1944	2056		2829,535651

Transverse Beam 1:

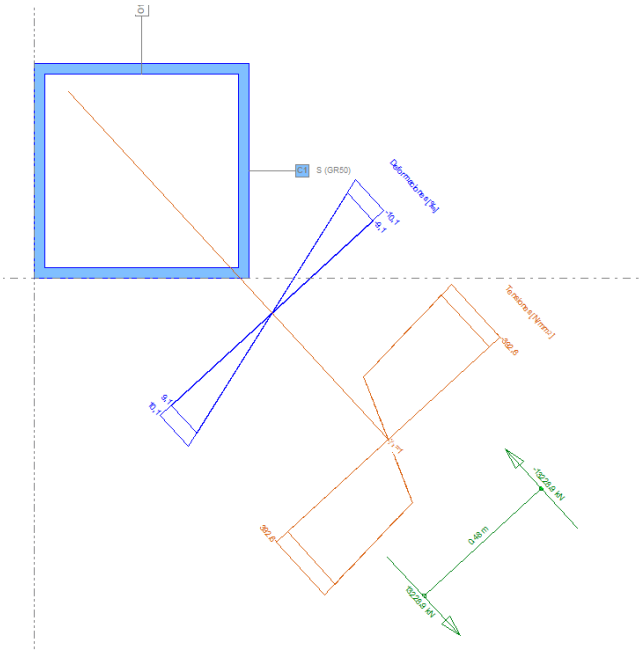

Esfuerzos			Deformación y curvatura			Valores rigidez		
N [kN]	M_y [kNm]	M_z [kNm]	ε_x [‰]	χ_y [km^{-1}]	χ_z [km^{-1}]	N/ε_x [kN]	M_y/χ_y [kNm^2]	M_z/χ_z [kNm^2]
-0,0	4186,9	4815,9	0,0	14,9	16,3	98,53	2,810E+5	2,963E+5

Transverse Beam 1 (rotated):

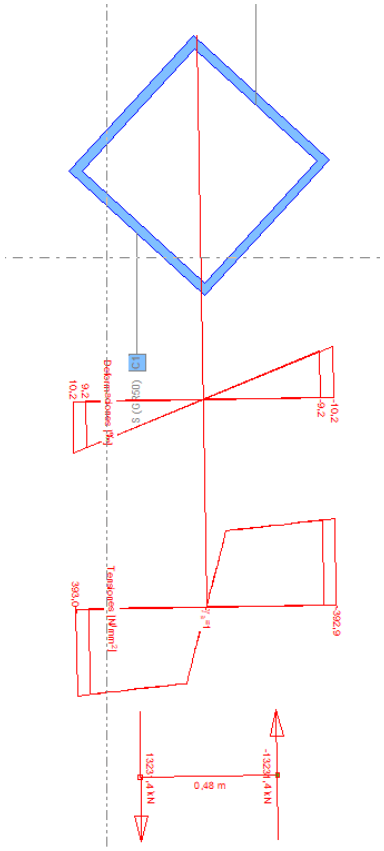

Esfuerzos			Deformación y curvatura			Valores rigidez		
N [kN]	M_y [kNm]	M_z [kNm]	ε_κ [‰]	χ_y [km-1]	χ_z [km-1]	N/ε_κ [kN]	M_y/χ_y [kNm2]	M_z/χ_z [kNm2]
-0,0	-0,0	6381,9	0,0	0,3	22,2	99,98	6,19	2,877E+5

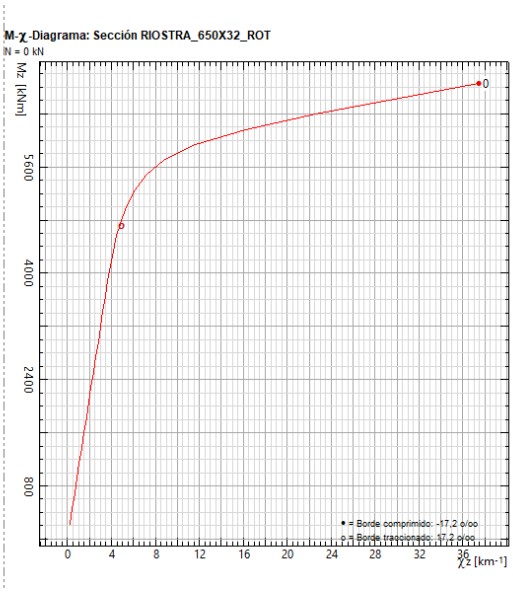

ANNEX J– PERFORMANCE POINT OF A STRUCTURE CONSIDERING DIFFERENT CLASS (UNIFORM DISTRIBUTION)

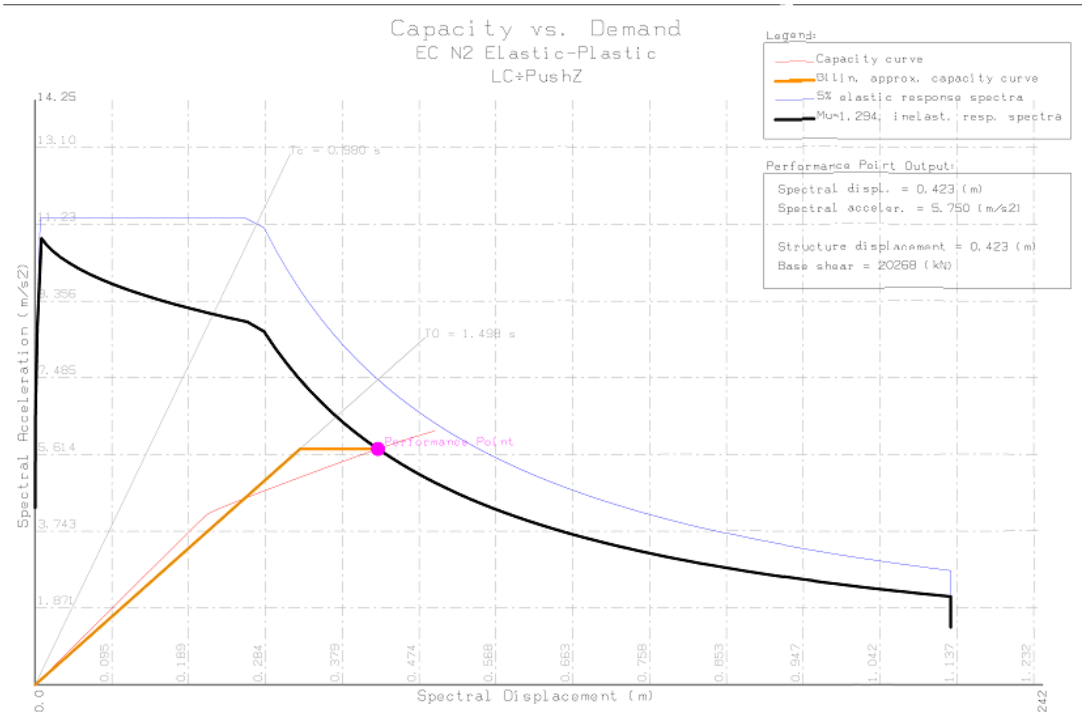
Capacity vs. Demand
EC N2 Elastic-Plastic
LC+PushZ
Legend:
Capacity curve
Bilin. approx. capacity curve
5% elastic response spectra
Mu=1.294, inelast. resp. spectra
Performance Point Output:
Spectral displ. = 0.423 (m)
Spectral acceler. = 5.750 (m/s2)
Structure displacement = 0.423 (m)
Base shear = 20268 (kN)
Ts = 0.380 s
T0 = 1.498 s
Performance Point
Spectral Acceleration (m/s2)
Spectral Displacement (m)
14.25
13.10
11.23
9.356
7.485
5.614
3.743
1.871
0.0
0.095
0.189
0.284
0.379
0.474
0.568
0.663
0.758
0.853
0.947
1.042
1.137
1.232
1.242

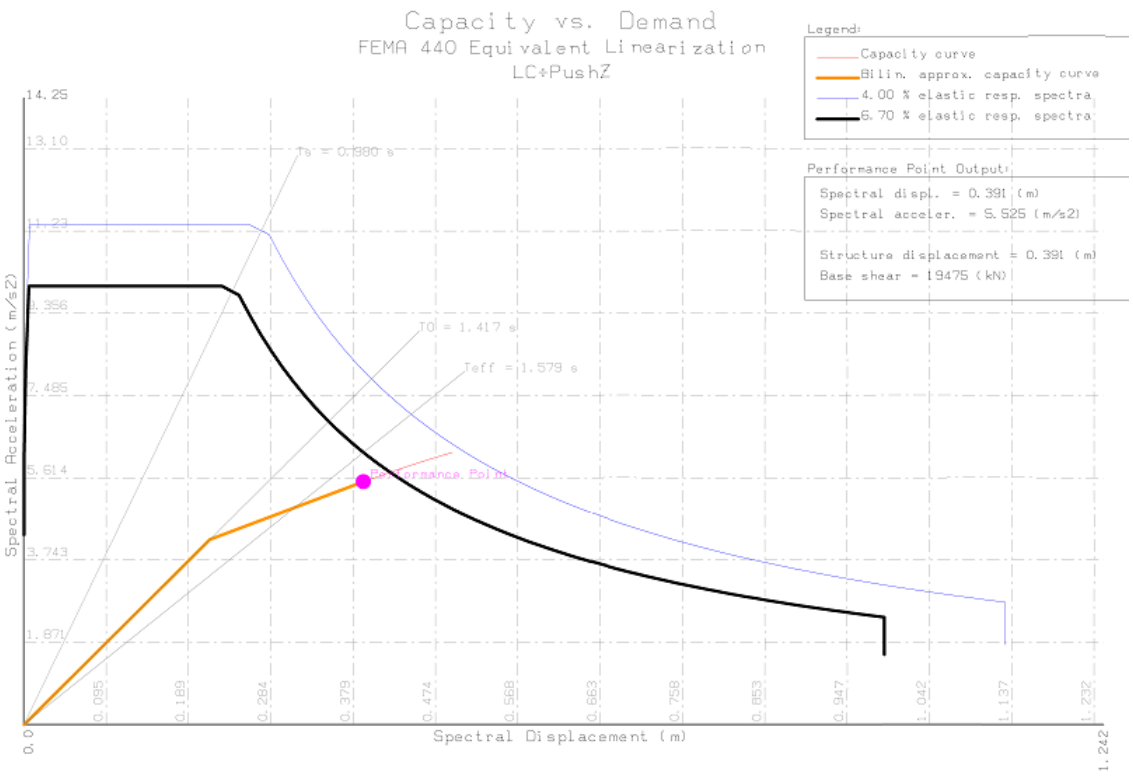
Capacity vs. Demand
FEMA 440 Equivalent Linearization
LC+PushZ
Legend:
Capacity curve
Bilin. approx. capacity curve
4.00 % elastic resp. spectra
5.70 % elastic resp. spectra
Performance Point Output:
Spectral displ. = 0.391 (m)
Spectral acceler. = 5.525 (m/s2)
Structure displacement = 0.391 (m)
Base shear = 19475 (kN)
Ts = 0.380 s
T0 = 1.417 s
Teff = 1.579 s
Performance Point
Spectral Acceleration (m/s2)
Spectral Displacement (m)
14.25
13.10
11.23
9.356
7.485
5.614
3.743
1.871
0.0
0.095
0.189
0.284
0.379
0.474
0.568
0.663
0.758
0.853
0.947
1.042
1.137
1.232
1.242

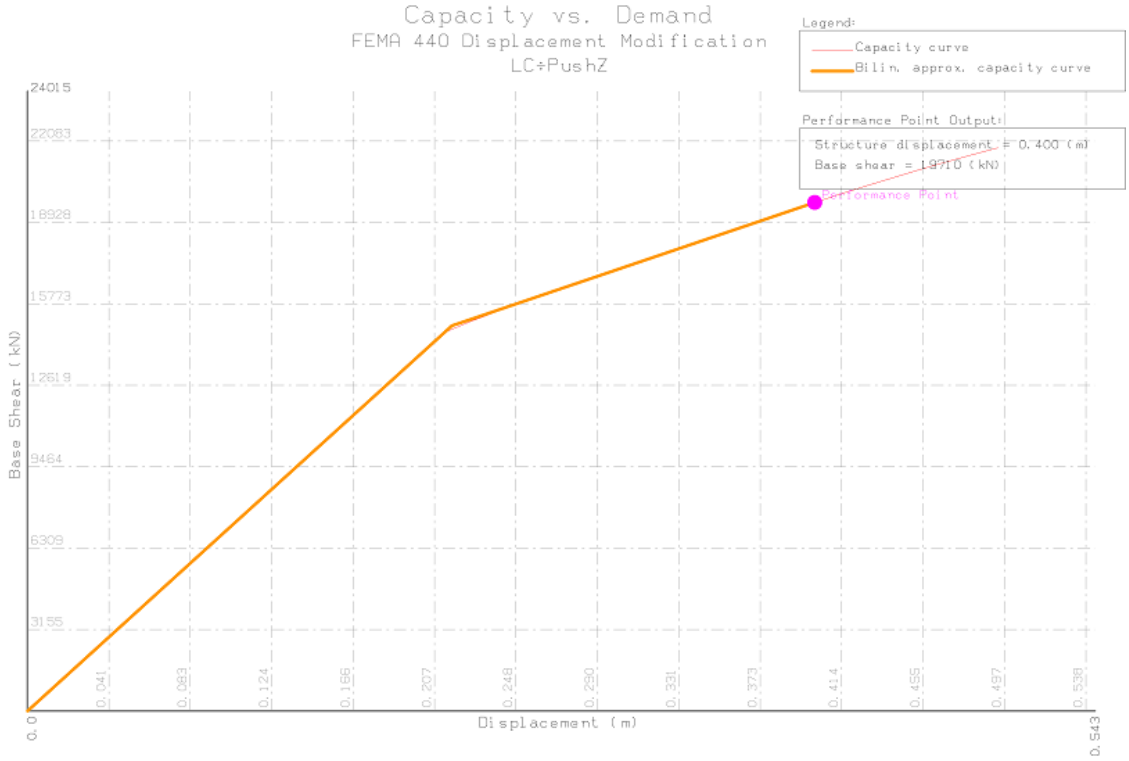
Capacity vs. Demand
FEMA 440 Displacement Modification
LC+PushZ
Legend:
Capacity curve
Bilin. approx. capacity curve
Performance Point Output:
Structure displacement = 0.400 (m)
Base shear = 19710 (kN)
Performance Point
Base Shear (kN)
24015
22083
18928
15773
12619
9464
6309
3155
0.0
0.041
0.083
0.124
0.166
0.207
0.248
0.290
0.331
0.373
0.414
0.455
0.497
0.538
0.543
Displacement (m)

ANNEX K – PERFORMANCE POINT OF A STRUCTURE CONSIDERING REDUCED SECTION (MODAL AND UNIFORM DISTRIBUTION)

MODAL DISTRIBUTION

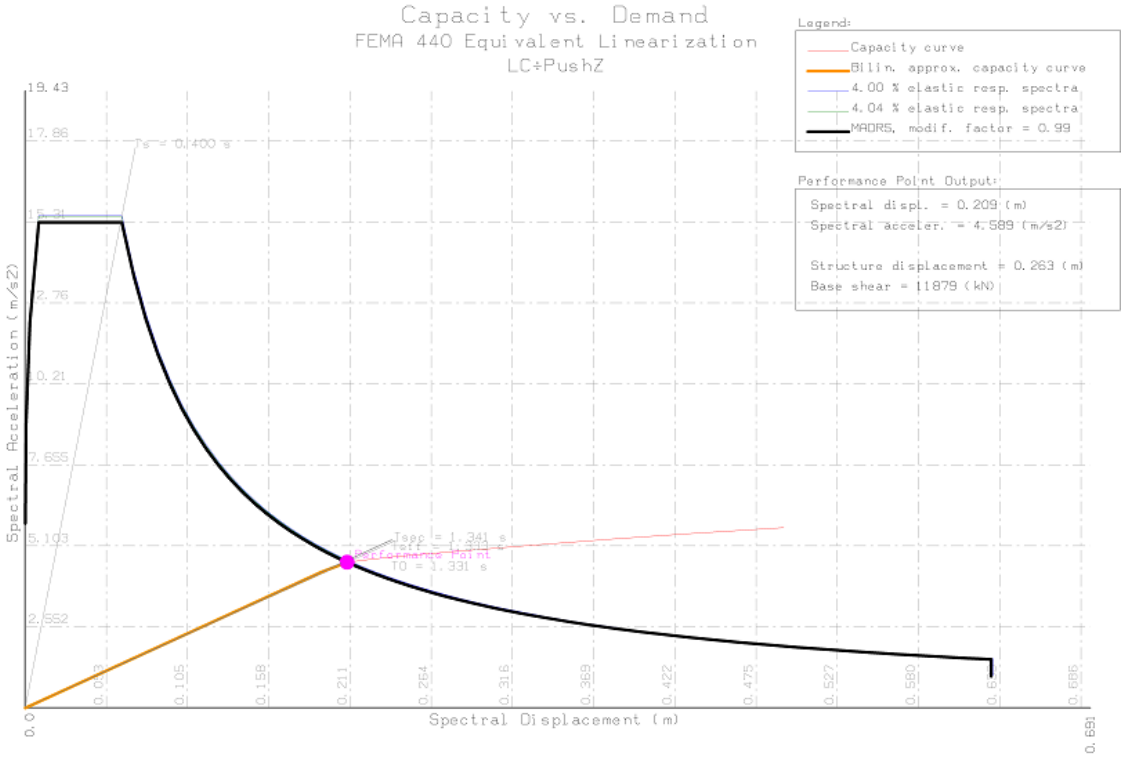

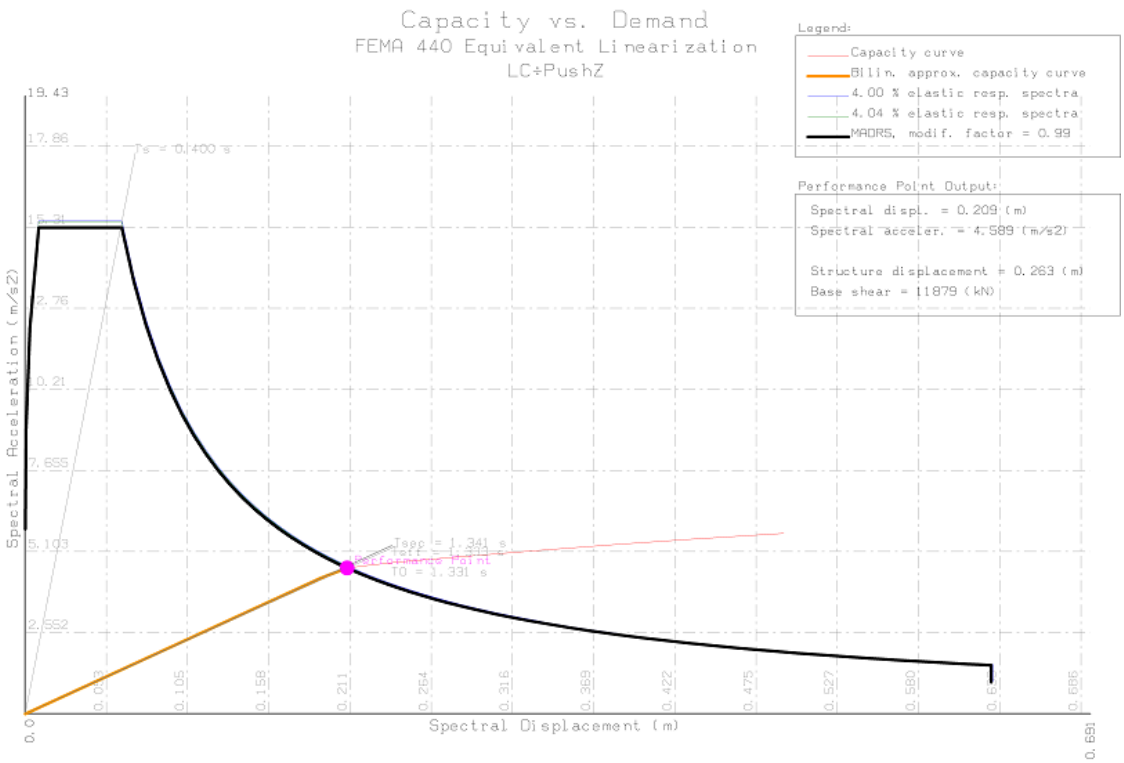

UNIFORM DISTRIBUTION

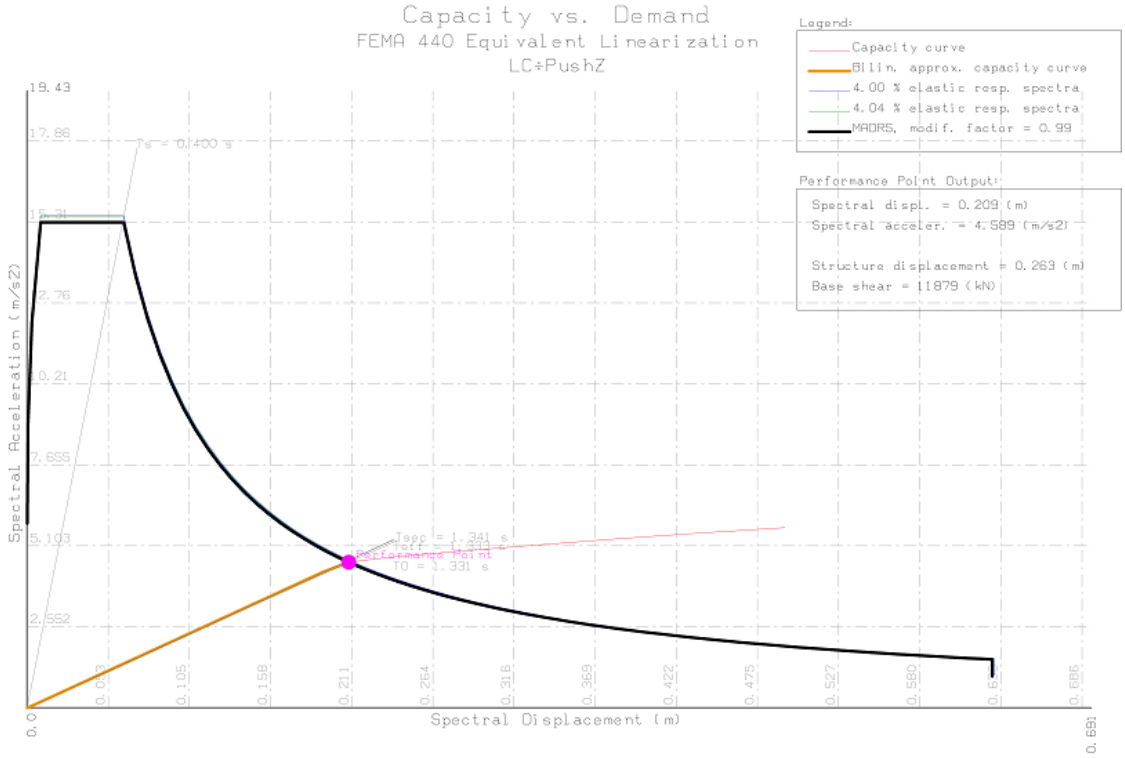
Capacity vs. Demand
FEMA 440 Equivalent Linearization
LC÷PushZ
Legend:
Capacity curve
Bilin. approx. capacity curve
4.00 % elastic resp. spectra
4.04 % elastic resp. spectra
MADRS, modif. factor = 0.99
Performance Point Output:
Spectral displ. = 0.209 (m)
Spectral acceler. = 4.589 (m/s2)
Structure displacement = 0.263 (m)
Base shear = 11879 (kN)
Ts = 0.400 s
Tsec = 1.341 s
Performance Point
T0 = 3.331 s
Spectral Acceleration (m/s2)
Spectral Displacement (m)
19.43
17.86
15.31
12.76
10.21
7.655
5.103
2.552
0.0
0.053
0.105
0.158
0.211
0.264
0.316
0.369
0.422
0.475
0.527
0.580
0.633
0.686
0.691

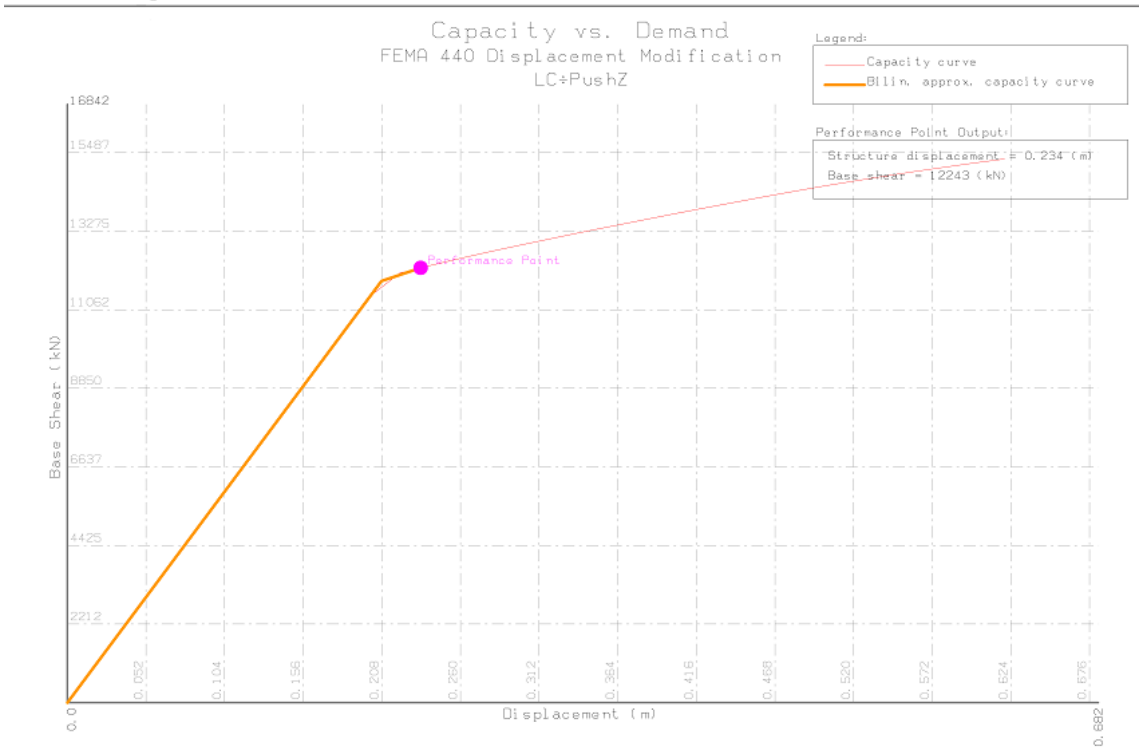
Capacity vs. Demand
FEMA 440 Displacement Modification
LC÷PushZ
Legend:
Capacity curve
Bilin. approx. capacity curve
Performance Point Output:
Structure displacement = 0.234 (m)
Base shear = 12243 (kN)
Performance Point
Base Shear (kN)
Displacement (m)
16842
15487
13275
11062
8850
6637
4425
2212
0.0
0.052
0.104
0.156
0.208
0.260
0.312
0.364
0.416
0.468
0.520
0.572
0.624
0.676
0.682

H2